

AD-A013 925

LANDING GEAR/SOIL INTERACTION DEVELOPMENT OF CRITERIA
FOR AIRCRAFT OPERATION ON SOIL DURING TURNING AND HIGH
SPEED STRAIGHT ROLL

David C. Kraft, et al

Dayton University

Prepared for:

Air Force Flight Dynamics Laboratory

January 1974

DISTRIBUTED BY:

NTIS

National Technical Information Service
U. S. DEPARTMENT OF COMMERCE

245097

AFFDL-TR-74-6

AD A013925

**LANDING GEAR/SOIL INTERACTION DEVELOPMENT
OF CRITERIA FOR AIRCRAFT OPERATION
ON SOIL DURING TURNING AND HIGH
SPEED STRAIGHT ROLL**

*UNIVERSITY OF DAYTON
SCHOOL OF ENGINEERING
DAYTON, OHIO*

TECHNICAL REPORT AFFDL-TR-74-6

JANUARY 1974



Approved for public release; distribution unlimited.

Reproduced by
NATIONAL TECHNICAL
INFORMATION SERVICE
US Department of Commerce
Springfield, VA. 22151

Best Available Copy


AIR FORCE FLIGHT DYNAMICS LABORATORY
AIR FORCE SYSTEMS COMMAND
WRIGHT-PATTERSON AIR FORCE BASE, OHIO 45433

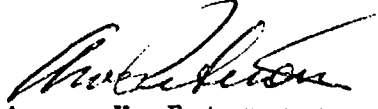
NOTICE


When Government drawings, specifications, or other data are used for any purpose other than in connection with a definitely related Government procurement operation, the United States Government thereby incurs no responsibility nor any obligation whatsoever; and the fact that the government may have formulated, furnished, or in any way supplied the said drawings, specifications, or other data, is not to be regarded by implication or otherwise as in any manner licensing the holder or any other person or corporation, or conveying any rights or permission to manufacture, use, or sell any patented invention that may in any way be related thereto.

This report has been reviewed and cleared for open publication and/or public release by the appropriate Office of Information (OI) in accordance with AFR 190-17 and DODD 5230.9. There is no objection to unlimited distribution of this report to the public at large or by DDC to the National Technical Information Service (NTIS).

Publication of this technical report does not constitute Air Force approval of the report's finding or conclusions. It is published only for the exchange and stimulation of ideas.

ACCESSION for		
NTIS	White Section	<input checked="" type="checkbox"/>
DDC	Buff Section	<input type="checkbox"/>
UNANNOUNCED		<input type="checkbox"/>
JUSTIFICATION		
BY		
DISTRIBUTION/AVAILABILITY CODES		
Dist.	A, AIL, and/or SPECIAL	
		


Aivars V. Petersons
Acting Chief, Mechanical Branch
Vehicle Equipment Division
Air Force Flight Dynamics Laboratory


George J. Sperry
Project Engineer, Mechanical Branch
Vehicle Equipment Division
Air Force Flight Dynamics Laboratory

Copies of this report should not be returned unless return is required by security considerations, contractual obligations, or notice on a specific document.

UNCLASSIFIED

SECURITY CLASSIFICATION OF THIS PAGE (When Data Entered)

REPORT DOCUMENTATION PAGE		READ INSTRUCTIONS BEFORE COMPLETING FORM
1. REPORT NUMBER AFFDL-TR-74-6	2. GOVT ACCESSION NO.	3. RECIPIENT'S CATALOG NUMBER
4. TITLE (and Subtitle) LANDING GEAR/SOIL INTERACTION DEVELOPMENT OF CRITERIA FOR AIRCRAFT OPERATION ON SOIL DURING TURNING AND HIGH SPEED STRAIGHT ROLL		5. TYPE OF REPORT & PERIOD COVERED Final Report
7. AUTHOR(s) David C. Kraft, Donald A. Kahle, Henry Luming		6. PERFORMING ORG. REPORT NUMBER
9. PERFORMING ORGANIZATION NAME AND ADDRESS University of Dayton School of Engineering 300 College Park Ave., Dayton, Ohio 45469		8. CONTRACT OR GRANT NUMBER(s) F33615-73-C-3023
11. CONTROLLING OFFICE NAME AND ADDRESS United States Air Force Air Force Systems Command, 4950th Test Wing, 4950/PMNA Wright-Patterson AFB, Ohio 45433		10. PROGRAM ELEMENT, PROJECT, TASK AREA & WORK UNIT NUMBERS Project No. 1369
14. MONITORING AGENCY NAME & ADDRESS (if different from Controlling Office) Air Force Flight Dynamics Laboratory (FY1456) Wright-Patterson AFB, Ohio 45433 Attn: Mr. George J. Sperry, 4950/PMNA		12. REPORT DATE January 1974
		13. NUMBER OF PAGES 22 179
		15. SECURITY CLASS. (of this report) Unclassified
		15a. DECLASSIFICATION/DOWNGRADING SCHEDULE
16. DISTRIBUTION STATEMENT (of this Report) Approved for public release; distribution unlimited.		
17. DISTRIBUTION STATEMENT (of the abstract entered in Block 20, if different from Report)		
18. SUPPLEMENTARY NOTES		
19. KEY WORDS (Continue on reverse side if necessary and identify by block number) Aircraft flotation, Aircraft tire sinkage Aircraft high speed ground surface drag Aircraft tire drag Aircraft turning operations Soil mechanics aircraft tire turning side loads		
20. ABSTRACT (Continue on reverse side if necessary and identify by block number) The continuing design and operational requirements for military air- craft to operate on unimproved runways has led to the need to investigate those landing gear/soil runway parameters which most significantly influence per- formance. This report summarized those activities accomplished during the first year of a two-year research effort concerned with the development of criteria for turning, operation at high speed, and multi-pass operation.		

DD FORM 1 JAN 73 1473

EDITION OF 1 NOV 65 IS OBSOLETE

UNCLASSIFIED

1. SECURITY CLASSIFICATION OF THIS PAGE (When Data Entered)

UNCLASSIFIED

SECURITY CLASSIFICATION OF THIS PAGE(When Data Entered)

The work accomplished consisted primarily of a comprehensive investigation of the turned aircraft tire/soil interaction effects and how these effects should influence future criteria for aircraft turning operations on soil runways. Two turned tire test programs were conducted in both clay and sand type soils with tire diameters ranging from 14" to 29" and turn angles up to 20°. The first test program conducted in April 1973 used the University of Dayton's Linear Tire/Soil Interaction Test Track. The second test program was conducted in July 1973 at the Army Engineers Waterways Experiment Station under supervision by the University of Dayton.

Dimensionless analysis techniques were then used to interpret these test results leading to the establishment of procedures and criteria for predicting turned tire lateral loads. An analytical study of aircraft turning operations on soil was also made leading to the development of a computer program, which when fully implemented, will permit the prediction of drag and side loads of tricycle-type landing gear aircraft undergoing variable turning operations on soil runways.

Also accomplished was the further development of high speed rolling drag for aircraft in the takeoff mode of operation. These further efforts resulted in the development of a predictive computer program for rolling high speed drag ratios.

UNCLASSIFIED

SECURITY CLASSIFICATION OF THIS PAGE(When Data Entered)

FOREWORD

This report was prepared by the Aerospace Mechanics Group of the University of Dayton under USAF Contract F33615-73-C-3023. This work was accomplished under the direction of the Vehicle Equipment Division, Air Force Flight Dynamics Laboratory, Wright-Patterson Air Force Base, Ohio, Mr. George J. Sperry (AFFDL/FEM) Project Engineer.

This report covers work conducted from October 8, 1972 to November 15, 1973.

The authors wish to thank Mr. Sperry for his support and assistance in the accomplishment of the research activities and in the successful conduction of the training sessions.

Publication of this technical report does not constitute Air Force approval of the reported findings or conclusions. It is published only for the exchange and stimulation of ideas.

ABSTRACT

The continuing design and operational requirements for military aircraft to operate on unimproved runways has led to the need to investigate those landing gear/soil runway parameters which most significantly influence performance. This report summarizes those activities accomplished during the first year of a two-year research effort concerned with the development of criteria for turning, operation at high speed, and multipass operation.

The work accomplished consisted primarily of a comprehensive investigation of the turned aircraft tire/soil interaction effects and how these effects should influence future criteria for aircraft turning operations on soil runways. Two turned tire test programs were conducted in both clay and sand type soils with tire diameters ranging from 14" to 29" and turn angles up to 20° . The first test program conducted in April 1973 used the University of Dayton's Linear Tire/Soil Interaction Test Track. The second test program was conducted in July 1973 at the Army Engineers Waterways Experiment Station under supervision by the University of Dayton.

Dimensionless analysis techniques were then used to interpret these test results leading to the establishment of procedures and criteria for predicting turned tire lateral loads. An analytical study of aircraft turning operations on soil was also made leading to the development of a computer program, which when fully implemented, will permit the prediction of drag and side loads of tricycle-type landing gear aircraft undergoing variable turning operations on soil runways.

Also accomplished was the further development of high speed rolling drag for aircraft in the takeoff mode of operation. These further efforts resulted in the development of a predictive computer program for rolling high speed drag ratios.

TABLE OF CONTENTS

Section		Page
I	INTRODUCTION AND SUMMARY	1
II	TURNED TIRE/SOIL INTERACTION ANALYSIS	4
	A. General and Definitions	4
	B. Turned Tire Test Programs	5
	C. Comparative Summary Analysis of Turned Tire Tests	40
	D. Aircraft Turning Operation Predictive Computer Program	43
III	ROLLING HIGH SPEED DRAG RATIO PREDICTION TECHNIQUE AND COMPUTER PROGRAM	50
	A. General	50
	B. High Speed Drag Ratio Analysis	57
	C. High Speed Drag Ratio Prediction Computer Program and Comparative Study	64
IV	ADDITIONAL STUDIES IN TIRE/SOIL INTERACTION	76
	A. Aircraft Takeoff Length Prediction Computer Program	76
	B. Training Session - Short Course on Landing Gear/Soil Interaction and Flotation System Design	76
	C. Integrated Flotation Design System	77
V	APPLICATIONS TO CURRENT MILITARY SPECIFICATIONS	80
VI	CONCLUSIONS AND RECOMMENDATIONS	82
	REFERENCES	84

TABLE OF CONTENTS

Section		Page
APPENDIX I	1. University of Dayton Linear Tire/Soil Test Track and Turned Tire Test Program	86
	A. Test Setup and Instrumentation	87
	B. Soil and Test Tire Property Data	95
	C. Test Results	100
	2. UD (AEWES) Turned Tire Test Program	108
	A. Soil Preparation, Test Procedure, and Tire/Loads Geometry	109
	B. Soil and Test Tires Property Data	112
	C. Test Results	112
APPENDIX II	Aircraft Turning Operation Predictive Computer Program	136
APPENDIX III	Rolling High Speed Drag Ratio Prediction Technique and Computer Program	145
APPENDIX IV	AFFDL/FEM Approved List of Symbols on Aircraft Landing Gear/Surface Interaction Computer Programs	156

LIST OF ILLUSTRATIONS

Figure		Page
1	Aircraft Turning Geometry	6
2	Turned Tire Geometry/Loads Definition	7
3	UD-Linear Tire/Soil Interaction Test Track	9
4	UD-Test Track Carriage	12
5	Sand Test Bed Surface -20° Turned Tire (UD Tests)	14
6	Summary Results - UD Turned Tire Test Program, Riverwash Sand	16
7	Clayey Silt Test Bed Surface -15° Turned Tire (UD Tests)	18
8	Clayey Silt Test Bed Surface -20° Turned Tire (UD Tests)	19
9	Summary Results - UD Turned Tire Test Program, Clayey Silt	21
10	Tire/Soil Test System UD (AEWES)	26
11	Tire/Soil Carriage UD (AEWES)	27
12	Tire/Soil Turned Tire Mount UD (AEWES)	28
13	Turned Tire Rut Profile, 8:50-10 Tire, d = 35%, Sand UD (AEWES)	31
14	Rutting From 8:50-10 Tire, 15° Turn Test, Sand UD (AEWES)	32
15	Summary Results - UD (AEWES) Turned Tire Test Program, Sand	33
16	Turned Tire Rut Profile, 8:50-10 Tire, d = 35%, Clay UD (AEWES)	36
17	Rutting From 8:50-10 Tire, 15° Turn Test, Clay UD (AEWES)	37
18	Summary Results - UD (AEWES) Turned Tire Test Program, Clay	38
19	Comparative Turned Tire Test Results - Influence of Sinkage Ratio (Z/D)	41

LIST OF ILLUSTRATIONS (Continued)

Figure		Page
20	Aircraft Turning Geometry and Force System	45
21	General Flow Chart of Computer Program for Turning Operation	47
22	Boeing-High Speed Rolling Drag Tests ⁽⁸⁾	51
23	Typical Drag Ratio vs. Horizontal Velocity Relationship in Soil	56
24	Tire/Soil Interaction at High Speed	58
25	Drag Ratio-Sinkage Ratio, Single Wheels on Soil	60
26	Sinkage Characteristic vs. Load-Strength Ratio, Cohesive Soils	61
27	Sinkage Characteristic vs. Load-Strength Ratio, Cohesionless Soils	62
28	Rolling-High Speed Drag Ratio Prediction Computer Program Flow Chart	66
29	Experimental-Predicted, High Speed Lockheed/Langley Tests, Case No. 1	67
30	Experimental-Predicted, High Speed Lockheed/Langley Tests, Case No. 2	68
31	Experimental-Predicted, High Speed Lockheed/Langley Tests, Case No. 3	69
32	Experimental-Predicted, High Speed Lockheed/Langley Tests, Case No. 4	70
33	Experimental-Predicted, High Speed Lockheed/Langley Tests, Case No. 5	71
34	Experimental-Predicted, High Speed Lockheed/Langley Tests, Case No. 6	72
35	Examples of High Speed Rolling Drag Ratio Determinations Using Predictive Computer Program	74
36	Load Measuring Test Fixture, UD Linear Test Track	90
37	Typical Force Member Calibration, UD Test Carriage	93

LIST OF ILLUSTRATIONS (Continued)

Figure		Page
38	Typical Oscillographic Data Recording, 0° Turn Angle	94
39	Grain Size Distribution - Riverwash Sand	98
40	Grain Size Distribution - Clayey Silt	99
41	In-Line Drag Ratio (R/P) vs. Tire Turn Angle, Sand (UD Tests)	101
42	Side Load Ratio (S/P) vs. Tire Turn Angle, Sand (UD Tests)	102
43	Lateral Load Ratio (L/P) vs. Turn Angle, Sand (UD Tests)	103
44	In-Line Drag Ratio (R/P) vs. Tire Turn Angle, Clayey Silt (UD Tests)	104
45	Side Load Ratio (S/P) vs. Tire Turn Angle, Clayey Silt (UD Tests)	105
46	Lateral Load Ratio (L/P) vs. Tire Turn Angle, Clayey Silt (UD Tests)	106
47	Drag Ratio vs. Sinkage Ratio, 0° Turned Tire (UD Tests)	107
48	Turned Tire/Soil Test UD (AEWES)	110
49	Turned Tire - Load/Geometry Relationships UD (AEWES)	111
50	Turned Tire Rut Profile, 8:50-10 Tire, d = 35%, Sand UD (AEWES)	115
51	Turned Tire Rut Profile, 8:50-10 Tire, d = 40%, Sand UD (AEWES)	116
52	Turned Tire Rut Profile, 7:00-6 Tire, d = 35%, Sand UD (AEWES)	117
53	Turned Tire Rut Profile, 7:00-6 Tire, d = 40%, Sand UD (AEWES)	118
54	Turned Tire Rut Profile, 8:50-10 Tire, d = 35%, Clay UD (AEWES)	119

LIST OF ILLUSTRATIONS (Continued)

Figure		Page
55	Turned Tire Rut Profile, 8:50-10 Tire, $d = 40\%$, Clay UD (AEWES)	120
56	Turned Tire Rut Profile, 7:00-6 Tire, $d = 35\%$, Clay UD (AEWES)	121
57	Turned Tire Rut Profile, 7:00-6 Tire, $d = 40\%$, Clay UD (AEWES)	122
58	In-Line Drag Ratio (R/P) vs. Turn Angle, 8:50-10 Tire, Sand UD (AEWES)	123
59	Side Load Ratio (S/P) vs. Turn Angle, 8:50-10 Tire, Sand UD (AEWES)	124
60	Lateral Load Ratio (L/P) vs. Turn Angle, 8:50-10 Tire, Sand UD (AEWES)	125
61	In-Line Drag Ratio (R/P) vs. Turn Angle, 7:00-6 Tire, Sand UD (AEWES)	126
62	Side Load Ratio (S/P) vs. Turn Angle, 7:00-6 Tire, Sand UD (AEWES)	127
63	Lateral Load Ratio (L/P) vs. Turn Angle, 7:00-6 Tire, Sand UD (AEWES)	128
64	In-Line Drag Ratio (R/P) vs. Turn Angle, 8:50-10 Tire, Clay UD (AEWES)	129
65	Side Load Ratio (S/P) vs. Turn Angle, 8:50-10 Tire, Clay UD (AEWES)	130
66	Lateral Load Ratio (L/P) vs. Turn Angle, 8:50-10 Tire, Clay UD (AEWES)	131
67	In-Line Drag Ratio (R/P) vs. Turn Angle, 7:00-6 Tire, Clay UD (AEWES)	132
68	Side Load Ratio (S/P) vs. Turn Angle, 7:00-6 Tire, Clay UD (AEWES)	133
69	Lateral Load Ratio (L/P) vs. Turn Angle, 7:00-6 Tire, Clay UD (AEWES)	134
70	Drag Ratio vs. Sinkage Ratio, 0° Turned Tire Tests UD (AEWES)	135

LIST OF TABLES

Table		Page
I	Quick Reference - Tires on Soil Flotation Guide	3
II	UD-Turned Tire Test Program (Design) - Sand Tests	10
III	UD-Turned Tire Test Program (Design) - Clayey Silt Tests	10
IV	Turned Tire Test Results - Sand (UD Tests)	13
V	Turned Tire Test Results - Clayey Silt (UD Tests)	17
VI	Turned Tire Test Program (Design), Buckshot Clay Soil UD (AEWES)	23
VII	Turned Tire Test Program (Design), Mortar Sand UD (AEWES)	24
VIII	Turned Tire Test Results, Sand UD (AEWES)	30
IX	Turned Tire Test Results, Clay UD (AEWES)	35
X	Aircraft Parameters for Turning Analysis	49
XI	Lockheed/Langley High Speed Test Program Summary Results	53
XII	Test Case Input Data Lockheed/Langley Test Program	65
XIII	Soil Test Bed - Average Soil Strength Results (UD Tests)	96
XIV	Moisture- Density Summary (UD Tests)	96
XV	Clayey Silt Soils Data (UD Turned Tire Test Program)	97
XVI	5:00-5 Tire Test Data	97
XVII	Moisture-Density Summary UD (AEWES)	112
XVIII	Turned Tire Test Program - Tire Data UD (AEWES)	114

LIST OF SYMBOLS

The following is a list of symbols and definitions used in the text of this report. A complete listing of symbols related to landing gear/surface interaction is given in Appendix IV.

Symbol	Definition	Page Defined
A	Rigid surface contact area	8
a	Moment arm in turned tire test carriage	111
B, b	Tire section width	3
CBR	California bearing ratio	51
C_{DI}	Soil inertia drag coefficient	55
C. G. (c. g.)	Center of gravity	6
CI	Mobility cone penetration test or resistance	32
CI_{avg}	Average cone index of soil over 0" to 6" depth	10
D	Tire outside diameter	8
d	Tire deflection in per cent	31
FL	Front lateral load in turned tire test carriage	22, 111
f_1, f_2	Functional expressions	63
h	Mechanical trail distance	44
K_1, K_2	Constants in high speed drag ratio equations	59
L.	Lateral load - the vector sum of the side and drag loads	7
L/P	Lateral load ratio	3
l	Tire footprint length (rigid surface)	55

LIST OF SYMBOLS (Continued)

Symbol	Definition	Page Defined
ΔL	Incremental change in the hydrodynamic lift	59
M	Turned tire restoring torque	25
MSTOL	Medium short takeoff and landing aircraft	1
O	Instantaneous center of rotation for turning aircraft	4
P	Tire vertical load	8
P'	Total vertical load minus lift	59
PR	Tire ply rating	22
p	Tire inflation pressure	67
R	Resistance to motion encountered in-line with the tire longitudinal axis	7
R'	Longitudinal drag for turned tire	22
RL	Rear lateral load for turned tire	22, 111
RMI	Relative merit index	1
R/P	Rolling drag ratio	3
R_b/P	Braked drag ratio (R_b = braked drag)	3
R_s/P	High speed drag ratio (R_s = high speed rolling drag)	67
r	Pneumatic trail distance for turned tire	7
$\Delta R, \Delta R_{\text{Inertia}}$	High speed inertia drag term	59

LIST OF SYMBOLS (Continued)

Symbol	Definition	Page Defined
S	Side load for turned tire	7
S/P	Side load ratio for turned tire	15
STOL	Short takeoff and landing aircraft	46
TL	Total lateral load for turned tire	111
V	Aircraft forward velocity	44
W	Total weight of the aircraft	43
x_c	Distance from the main gear axis (y-axis) to the instantaneous center of rotation	6
y_c	Distance from the aircraft axis (x-axis) to the instantaneous center of rotation	6
Z	Instantaneous soil sinkage	8
Z_o	Low speed (Region II) rolling sinkage	63
Z/D	Sinkage ratio	8
Z_{rut}	Rut depth	58
$\Delta Z_{inertia\ drag}$	Incremental sinkage due to high speed inertia drag	59
ΔZ_{lift}	Incremental sinkage due to lift	59
α/CI	Load strength ratio, where α = Vertical Load/Tire Contact Area	61
β	Nose gear steering angle	4
θ, θ_v	Angle defining equivalent plane of contact for high speed aircraft tire (angle of attack)	59

LIST OF SYMBOLS (continued)

Symbol	Definition	Page Defined
μ_o	Coefficient of rolling friction on rigid surface	52
ζ	Instantaneous radius of turn	6
ρ	Soil density	55
ψ	Direction of resultant lateral load for turned tire	111
ϕ	Tire turn angle - the angle between the direction of motion and tire longitudinal axis	5, 7

SECTION I

INTRODUCTION AND SUMMARY

The continuing design and operational requirement for aircraft to operate on unimproved runways, as evidenced by the current design requirements on the MSTOL aircraft currently under development, has resulted in continuing efforts to identify and analyze the primary and secondary variables which influence aircraft flotation/operation performance on soil runways. These flotation/operation variables have been defined previously ⁽¹⁻⁵⁾. These variables include drag, sinkage, braking, turning, multipass, high speed, soil strength, etc.

The current research effort is a part of a long range research program sponsored by the United States Air Force Flight Dynamics Laboratory. The objective of this continuing research program is : (1) to identify and analytically define landing gear/soil interaction; (2) to develop criteria for establishing working range conditions for aircraft in their landing, takeoff, braking, and turning modes of operation; (3) to develop systematic design procedures for optimizing the flotation and surface operations capability of existing and future aircraft. Phase I ⁽⁵⁾ of this program included a survey of the flotation problem, establishment of the critical parameters, and an investigation of available flotation data leading to the development of a flotation analysis equation. Phase II ⁽⁴⁾ included the development of an empirical sinkage prediction equation, development of a lumped parameter simulation prediction technique, conducting the Rolling Single Wheel Verification Tests, and the development of the Single Wheel Relative Merit Index (RMI) system for defining comparative flotation capacity. Phase III - Part I ⁽³⁾ consisted of the development of the multiwheel sinkage-drag analysis equations, conducting the Multiwheel Verification Tests, and the development of a lumped parameter iteration technique for simulating the interaction of dual tires on soil.

Phase III - Part II⁽¹⁾ included the Braked Wheel Verification Tests, the development of a lumped parameter braking simulation technique computer program, the development of the braking analysis equations for defining braking drag ratios, and preliminary studies of multipass and high speed effects of aircraft tire operation on soil.

The current two-year research program is aimed at developing analysis techniques, conducting necessary verification tests, and developing predictive equations for the landing gear/soil interaction variables of turning, high speed, and multipass. More specifically, the first year described herein included:

- Turned Tire Test Program at UD and AEWS
- Development of Aircraft Turning Operation Predictive Computer Program
- High Speed Drag Ratio Analysis and Prediction Technique
- Aircraft Takeoff Length Prediction Computer Program
- Landing Gear/Soil Interaction Training Sessions

The results of the numerous tire/soil interaction studies conducted to date⁽¹⁻¹⁰⁾, were used to update a previous Aircraft Flotation/Operation Summary Guide as shown in Table I. Reference to Table I indicates considerable advancements have been made to date (1973) in establishing interaction phenomena and developing criteria related to aircraft operation on soil runways.

TABLE I
QUICK REFERENCE - TIRES ON SOIL FLotation GUIDE

FLotation VARIABLE	SINKAGE AND DRAG	VELOCITY
Single Wheel	<ul style="list-style-type: none"> - Drag Ratio (R/P) correlates with sinkage ratio (Z/D) $R/P = 0.018 + 3.23 (Z/D)$, all soils, Region II velocity range - Sinkage prediction techniques available for sand and clay, Region II velocity range by UD - High speed (Region III) sinkage/drag theory preliminary defined - Low speed (Region I) sinkage/drag relationship not important - Flotation performance improves with increasing tire diameter - Increasing tire deflection - Increasing soil strength - decreasing tire load 	<p>3 Regions of sinkage/drag variance.</p> <p><u>Approximate</u></p> <p>0 \leq Region I \leq 5 knots 5 knots \leq Region II \leq 40 knots 40 knots \leq Region III</p>
<p><u>Multiple Wheel</u></p> <p>Twin</p> <p>Tandem-Tracking</p> <p>Tandem-Nontracking</p>	<p>Optimum spacing based on drag minimization (Region II velocity range)</p> <ul style="list-style-type: none"> - 1.75 b to 2.5 b, sand - 2.5 b to 3.5 b, clay - $\leq 1.75 D$ or $\leq 2.5 D$, sand - 1.5 D to 2.5 D, clay - $> 1.25 b$ all soils - $> 1.25 D$ 	<p>Velocity influence on optimum multiple wheel spacing is not known. Very likely optimum spacing not influenced by Region I and III velocities.</p>
Braked Wheel	<ul style="list-style-type: none"> - Braking drag ratio (R_B/P) analysis equations available for low speed range - Braking drag ratio (R_B/P) independent of initial sand soil strength - Sinkages increase markedly for braking in sand - Sinkages increase moderately for braking in clay - Braking drag ratio increases with: <ul style="list-style-type: none"> increasing sinkage, sand and clay increasing slip, sand and clay 	<p>Velocity is known not to affect the R_B/P for clay soils in the 3 to 15 knot range. Velocity does affect the braked sinkage in sand in the 3 to 15 knot speed range. The effects of higher speeds on braking has not been established as of 12-73.</p>
Turned Wheel	<ul style="list-style-type: none"> - Lateral load ratio, L/P (where L = resultant lateral load and P = vertical load). Increase with increasing turn angle at least through 0° to 20° turn angle range in both sand and clay type soils - Lateral load ratio may exceed 0.5 for relatively large turn angles - Sinkages increase moderately for turning in clay - Sinkages increase markedly for turning in sand 	<p>Velocity influence on lateral load buildup in turning operation is not known.</p>
<p>Multipasses</p> <p>(Preliminary)</p>	<ul style="list-style-type: none"> - Subsequent pass rolling drag ratio generally decreases with increasing passes in clay type soil - Decreasing rate of increase in accumulative rut depth with increasing passes in clay type soil 	

SECTION II

TURNED TIRE/SOIL INTERACTION ANALYSIS

A. GENERAL AND DEFINITIONS

Aircraft turning operation is an important consideration in the flotation analysis of aircraft operating on unprepared runways. Landing gear failures due to high side loads brought about by turning either in a high sinkage condition or out of accumulated ruts as well as problems related to runway deterioration and steering torque design are just a few of the considerations. Excessively high lateral loads in a turning operation may prevent the use of a soil runway even when the longitudinal rolling drag loads are acceptable for takeoff. The turning design criteria presently used by the Air Force was developed primarily for paved runways and its application to turning operations on soil runways is uncertain. For example, the C-130 operations manual merely indicates that the nose gear steering angle should not exceed 20 degrees on unimproved runways. Such criteria also provides very little rational explanation for the nature of the development of lateral loads in turning.

Most military aircraft use the castered-steerable nose wheel for turning operations. This method of turning leads to the development of longitudinal and side loads on the aircraft tires which involves such variables as steering angle, braking tire slip, and driving tire slip. A review of existing literature ⁽¹⁰⁻¹³⁾ indicates very little is known either analytically or experimentally about side loads on tires for aircraft turning on paved runways, and essentially nothing is known about turning phenomena for aircraft on soil runways. Some investigations were conducted on the side forces on tires for turning of agricultural tractor tires ^(12, 13), but tractor tire geometry, loads, and conditions are substantially different from aircraft tires. As a nose gear tire is turned through some steer angle, θ , the aircraft undergoes a rotation about some instantaneous center

of rotation, O . As indicated in Figure 1, the steer angle and the turn angle, ϕ , are not the same for the nosegear tires. In the case of main gear tires which are not castered, a turn angle is formed by relationship with the direction of motion of the aircraft and the instantaneous center of rotation as shown in Figure 1. In conducting the turned tire test programs, detailed below, the tire was kept at a constant turn angle, ϕ , with respect to the forward motion of the carriage as it moved down a linear test track. Figure 2 shows the turned tire geometry and loads definitions used in the test program.

B. TURNED TIRE TEST PROGRAMS

Two series of turned tire/soil interaction tests were conducted. The purpose of both test programs was to obtain experimental data to permit further studies of the variables that influence the performance of aircraft tires while operating in a turned (yawed) mode. The test program using the University of Dayton Linear Tire/Soil Test Track was conducted first (March 1973) and the results were used primarily to design the test program conducted at the Army Engineers Waterways Experiment Station (AEWES) under supervision by the University of Dayton during the June-July, 1973 time period. Although the turned tire tests did not fully simulate an actual aircraft tire in its turning operation (i.e., variable radius of turn), the results did permit the establishment of some preliminary relationships between those variables that influence turning performance. The more specific objectives of the turned tire tests included:

1. Establishment of relationships between in-line drag (see Figure 2), side load, and lateral load as a function of turn angle. Such information was necessary for the complete development of the "Aircraft Turning Operation Predictive Computer Program" described in Section II-D.
2. Determine the variations in per cent slip (negative) with increasing turn angle.

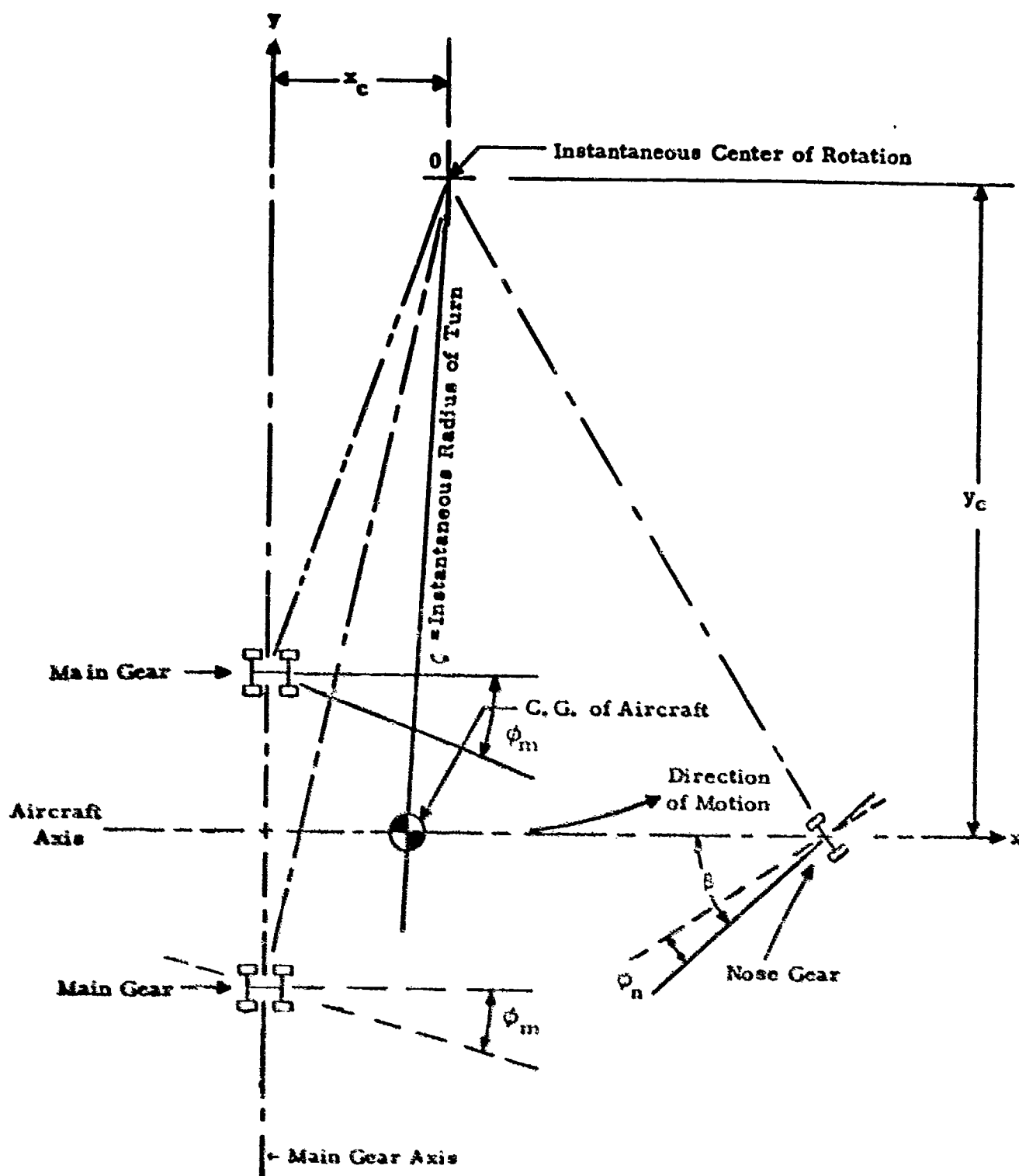
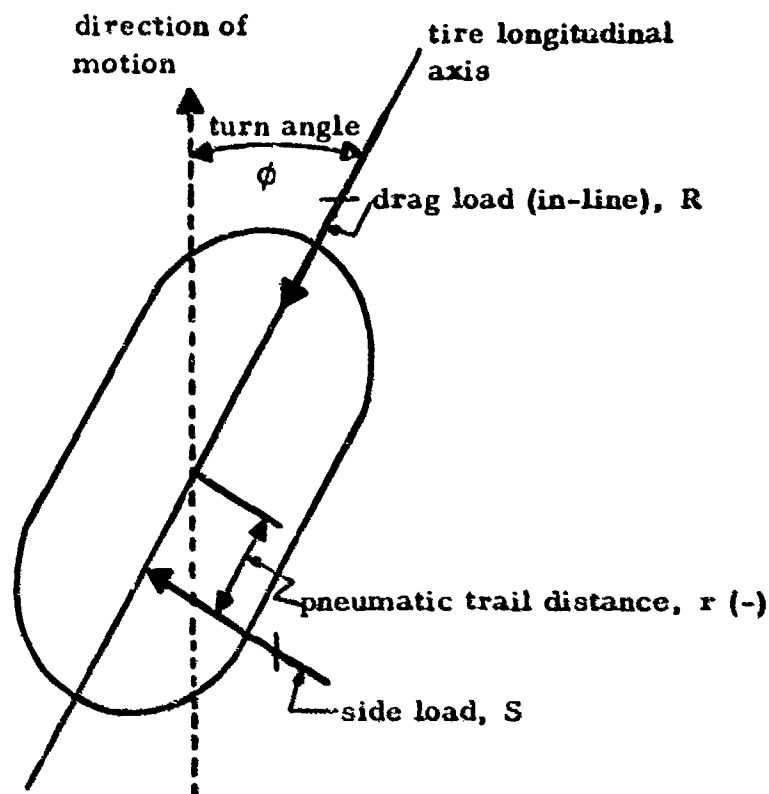


Figure 1. Aircraft Turning Geometry



Turn Angle, ϕ , angle distance between direction of motion (as determined by the instantaneous center of rotation of aircraft) and tire longitudinal axis.

Drag Load, R , resistance to motion encountered in-line with the tire longitudinal axis.

Side Load, S , force acting on tire at right angle to the tire longitudinal axis.

Lateral Load, L , resultant (lateral) load on tire (vector sum of drag load and side load).

Pneumatic Trail - Distance from c. g. of tire to location of side load (the product of the side load and pneumatic trail gives the tire restoring moment).

Figure 2. Turned Tire Geometry/Loads Definition

3. To determine the influence of increasing turn angle on the resultant sinkage and rut depth.
4. To establish, on a preliminary basis, some guide lines for turning operations of aircraft on soil runways.

UNIVERSITY OF DAYTON TEST PROGRAM

Test Program

A series of 45 tests were conducted in the Linear Tire/Soil Test Track shown in Figure 3 for turn angles ranging from 0° to 20° in both a sand and a clayey silt type soil. The test program design is summarized in Tables II and III. The tire, tire loads, and soil parameters were selected to provide an initial rolling sinkage of the non-turned tire of approximately 1/2 inch in both the sand and clayey silt. For the 5.00-5, Type III test tire, used in the test program, these sinkages give a Z/D (Z = sinkage, D = tire diameter) ratio of 0.03 to 0.04 in a non-turned mode which is typical for aircraft under operational conditions on soil runways. The following parameters were measured and evaluated in the program:

- vertical load, P
- drag load (in-line drag), R
- side load (perpendicular to plane of wheel), S
- resultant lateral force (determined from R and S above), L
- horizontal carriage velocity
- turn angle, ϕ
- tire deflection, d
- tire contact geometry (rigid surface contact area, A)
- soil properties (moisture, density, classification properties, Cone Index, CI_{avg})
- permanent rut depth (instantaneous sinkages were determined from rut depth and rebound measurements)

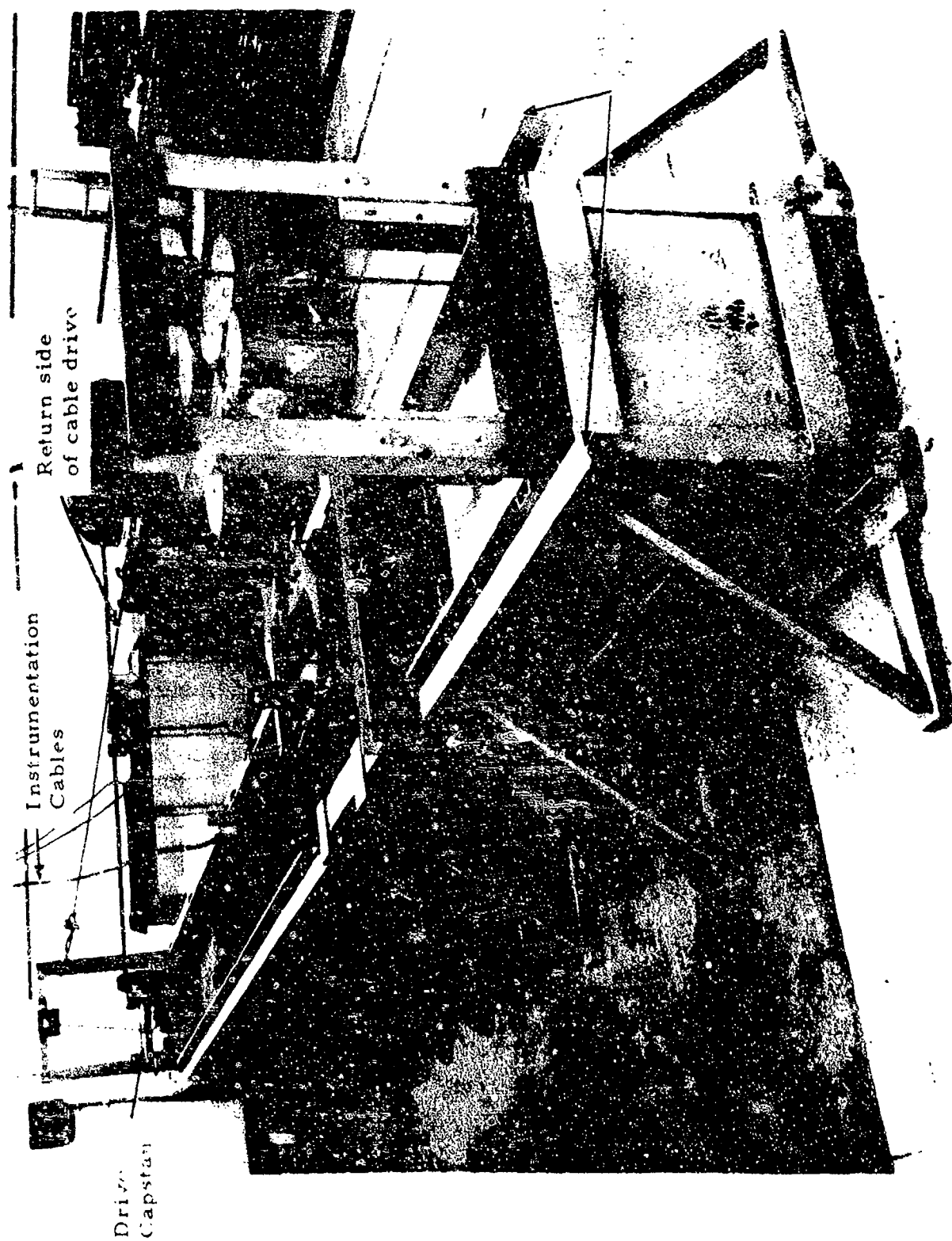


Figure 3. UD-Linear Tire/Soil Interaction Test Track

TABLE II
UD-TURNED TIRE TEST PROGRAM (DESIGN) - SAND TESTS

Turn Angle *	Tire Type	Tire Deflection %	Vertical Load, lbs.	Soil Strength Cone Index CI _{avg} **
0°	5.00-5, Type III	17	115	70-80
0°	5.00-5, Type III	17	145	70-80
5°	5.00-5, Type III	17	115	70-80
10°	5.00-5, Type III	17	115	70-80
10°	5.00-5, Type III	17	145	70-80
15°	5.00-5, Type III	17	115	70-80
20°	5.00-5, Type III	17	115	70-80
20°	5.00-5, Type III	17	145	70-80

TABLE III
UD-TURNED TIRE TEST PROGRAM (DESIGN) - CLAYEY SILT TESTS

Turn Angle *	Tire Type	Tire Deflection %	Vertical Load lbs	Soil Strength Cone Index CI _{avg} **
0°	5.00-5, Type III	17	115	30-40
0°	5.00-5, Type III	17	145	30-40
5°	5.00-5, Type III	17	115	30-40
10°	5.00-5, Type III	17	115	30-40
10°	5.00-5, Type III	17	145	30-40
15°	5.00-5, Type III	17	115	30-40
20°	5.00-5, Type III	17	115	30-40
20°	5.00-5, Type III	17	145	30-40

* Replicate tests were run for each test condition.

** Average penetration resistance over 0" to 6" depth, psi.

All tests were conducted with a forward carriage velocity of 6 fps and sufficient repetitive tests were conducted for each test variable investigated to insure the accuracy of the test results.

Test Equipment and Setup

All tests were conducted in the Linear Tire/Soil Test Track shown in Figure 3 using the carriage/dynamometer system, shown in Figure 4. The test facility consists of a linear test track with a powered carriage for moving the tire over the soil bed, the required force and velocity sensing devices, and a data recorder. A complete description of the Test Track and instrumentation is given in Appendix I.

Turned Tire Test Results - Riverwash Sand

A total of 22 turned tire tests were conducted on the riverwash sand soil using the 5.00-5 tire. Since only five turn angles were used (0° , 5° , 10° , 15° , and 20°), many of these tests were replicates and were conducted to insure consistency of test results. The complete results of the turned tire/soil interaction tests are given in Table IV. Previous tire/soil interaction studies have indicated that rut depths and sinkages are nearly identical for tires operating on granular type soils.

Reference to Table IV shows the effect of a turned tire performance on sand in terms of sinkage. For the range of turning angles tested in sand, the sinkage increases for each increase in the turn angle. In going from a 0° turn to a 20° turn, sinkages in sand increased from approximately 0.3" to 0.8" for the 115 lb vertical load, and from 0.5" to 1.1" for the 145 lb vertical load. This order of magnitude of sinkage change of approximately 2 to 3 would significantly influence the deterioration of a sand (or frictional soil) by an unsurfaced runway when subjected to turning motions of aircraft. Figure 5 very clearly shows a buildup of sand away from the direction of turn.

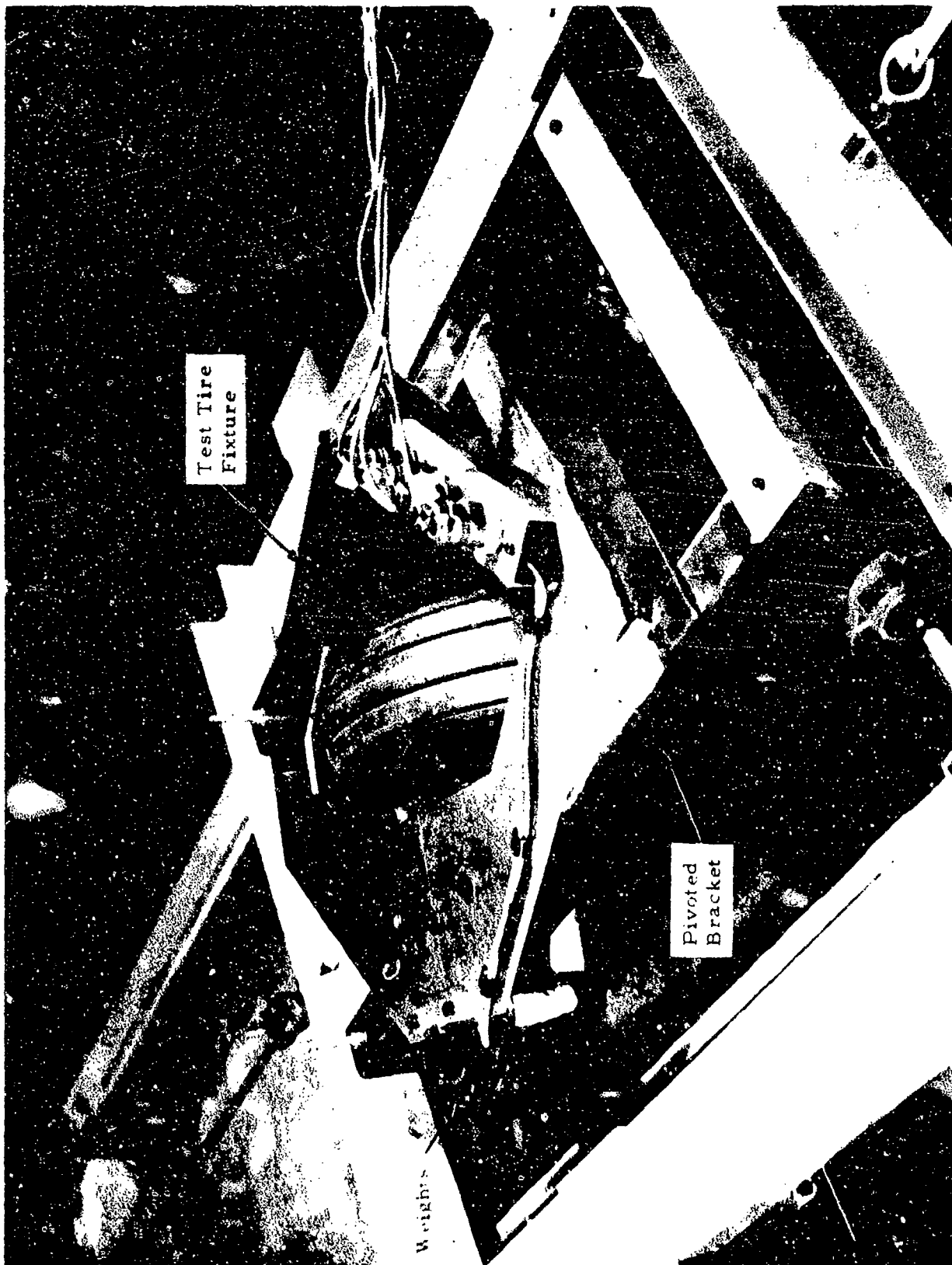


Figure 4. UD-Test Track Carriage

TABLE IV
TURNED TIRE TEST RESULTS - SAND (UD TESTS)

Test Number and Turn Angle	Vertical Load, P (lbs)	In-Line Drag, R (lbs)	Side Load, S (lbs)	Rut Depth (Sinkage) (in)
0° - A	121	14	4	0.30
0° - B	121	12	-5	0.35
0° - C	122	14	-4	0.30
0° - D	150	18	2	0.55
0° - E	149	19	-1	0.45
5° - A	117	17	15	0.50
5° - B	117	17	14	0.45
5° - C	116	17	16	0.45
10° - A	118	23	24	0.65
10° - B	118	16	36	0.25
10° - C	120	20	34	0.40
10° - D	114	18	29	0.50
10° - E	145	29	34	0.60
10° - F	146	30	32	0.60
15° - A	111	26	31	0.80
15° - B	111	25	31	0.75
15° - C	112	25	33	0.70
20° - A	112	28	38	0.85
20° - B	112	28	38	0.75
20° - C	112	27	39	0.70
20° - D	139	41	43	1.05
20° - E	138	40	42	1.10



Figure 5. Sand Test Bed Surface -20° Turned Tire (UD Tests)

The detailed results showing the variation of the in-line drag load and side load with turn angle are given in Appendix I. Figure 6 presents a summary picture of the results in order to examine trends. The buildup of tire side load and resultant lateral load with increasing turn angle is evident by reference to Figure 6. Figure 6 also shows that the ratio of the resultant lateral load to vertical load acting on the 5.00-5 tire turned at an angle of 20° on sand approaches one-half. Further, the results indicate that the tire encountered both an increasing drag load (in-line drag) and an increasing side load with increasing tire turn angle.

Turned Tire Test Results - Clayey Silt

Using the 5.00-5 tire, a total of 23 tests were conducted on the clayey silt soil with many of the tests being replicates to insure the same consistency of results from the clayey silt tests as for the sand tests. The complete results of the turned tire tests in the clayey silt are given in Table V. Previous tire/soil interaction studies have indicated that tire performance parameters on soil correlates more closely with sinkage rather than rut depth, and that clayey-silt type soils exhibit a rebound (difference between sinkage and rut depth) phenomena. Plate tests conducted on this clayey silt soil indicated soil rebounds of approximately 20% to 35%. The sinkage values shown in Table V then are measured rut depths adjusted to indicated true sinkage.

The variation of sinkage with increasing turn angles for the tests conducted on the clayey silt was quite different than that for sand as shown in Table V. Reference to Table V indicates a lesser increase in the magnitude of the sinkage with variation in the degree of turn. Although some evidence of soil shoving (away from the direction of turn) was seen in the clayey silt tests as shown in Figures 7 and 8, the extent of shoving was far less than that exhibited in sand.

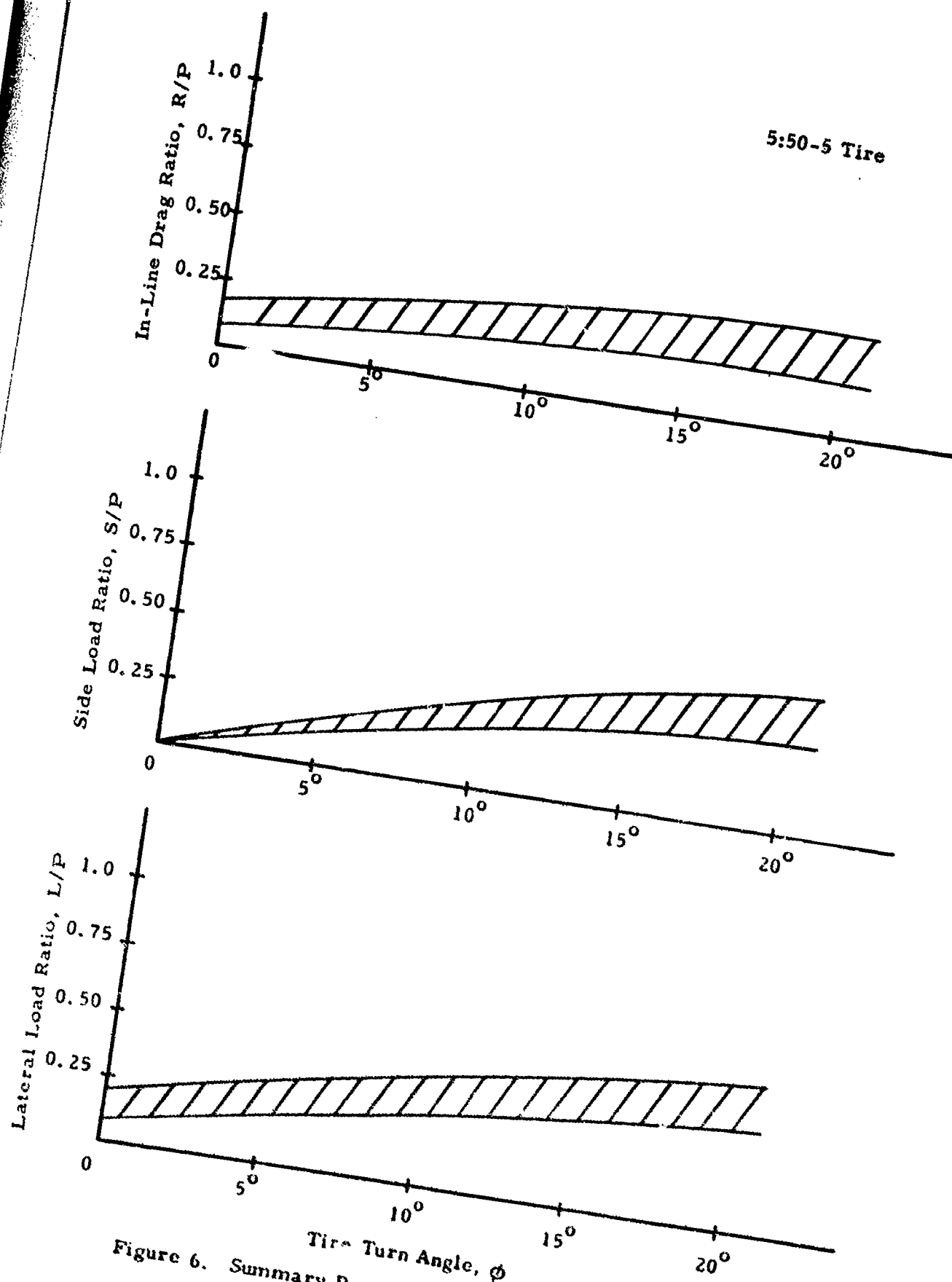


Figure 6. Summary Results - UD Turned Tire Test Program,
Riverwash Sand 16

TABLE V
TURNED TIRE TEST RESULTS - CLAYEY SILT (UD TESTS)

Test Number and Turn Angle	Vertical Load, P (lbs)	In-Line Drag, R (lbs)	Side Load, S (lbs)	Rut Depth (in)	Sinkage (in)
0° - A'	117	16	3	0.15	0.30
0° - B'	118	23	1	0.25	0.40
0° - C'	116	18	1	0.25	0.40
0° - D	148	28	3	0.40	0.55
0° - E	144	31	1	0.45	0.65
0° - E'	148	27	1	0.30	0.50
0° - F'	149	28	3	0.40	0.55
5° - A	115	20	37	0.70	0.90
5° - B	113	20	35	0.60	0.80
5° - C	112	19	35	0.50	0.70
10° - A	111	22	67	0.45	0.65
10° - B	110	22	67	0.55	0.75
10° - C	111	22	61	0.45	0.65
10° - D	138	31	84	0.50	0.70
10° - E	139	30	85	0.55	0.75
15° - A	106	21	81	0.40	0.60
15° - B	108	20	72	0.45	0.65
15° - C	107	18	78	0.55	0.75
20° - A	103	18	75	0.35	0.50
20° - B	101	19	81	0.35	0.50
20° - C	106	17	61	0.55	0.75
20° - D	126	27	105	0.55	0.75
20° - E	125	25	103	0.40	0.60



Figure 7. Clayey Silt Test Bed Surface - 15° Turned Tire (UD Tests)

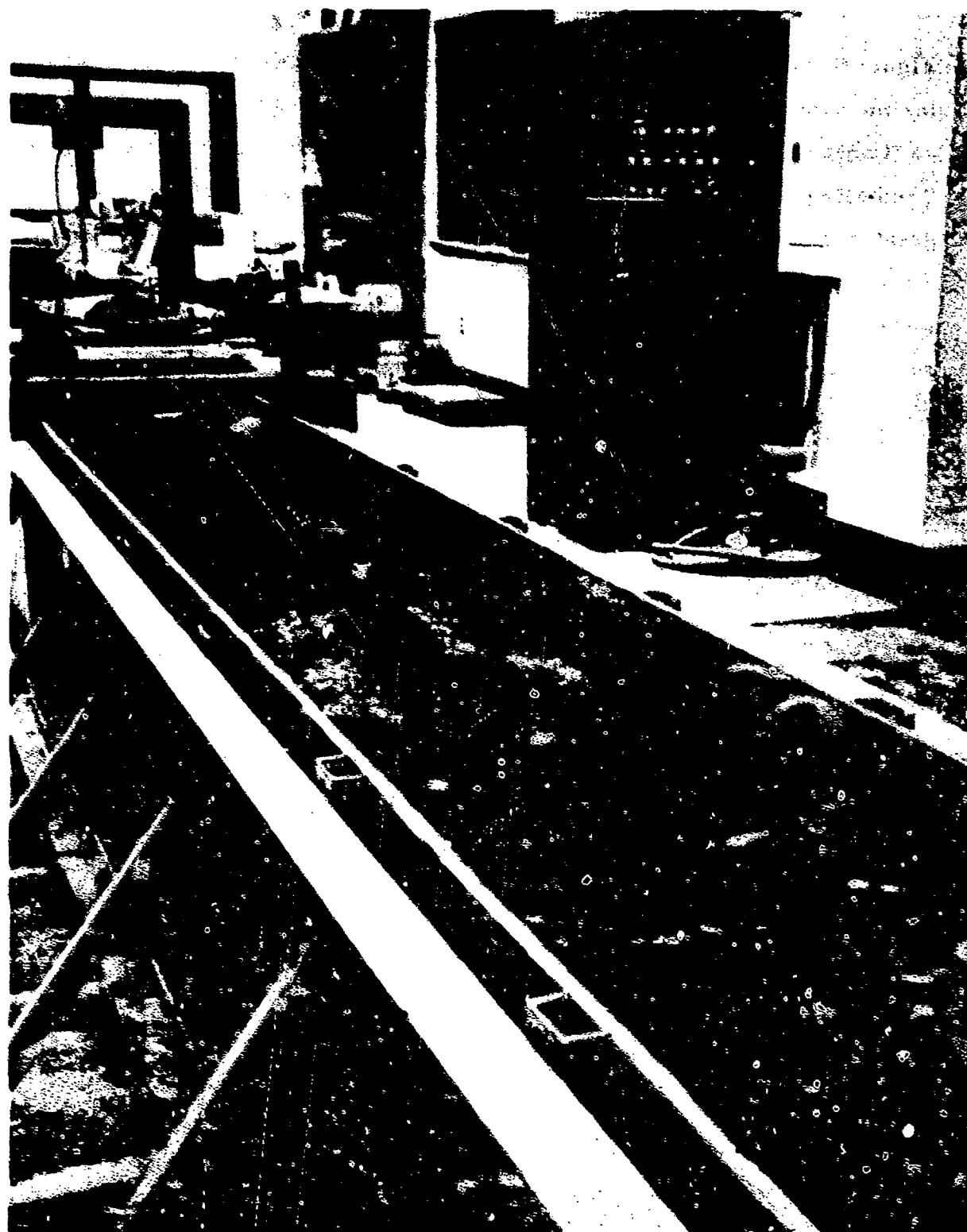


Figure 8. Clayey Silt Test Bed Surface - 30° Turned Tire (UD Tests)

The detailed results of the clayey silt tests are given in Appendix I. Figure 9 gives a summary look of the results and shows the variation of in-line drag load, side load, and resultant lateral load on the 5.00-5 tire as it operates in a turned mode on the clayey silt soil. Reference to Figure 9 indicates that the increase in side load with turn angle is significantly greater in the clayey silt than in the sand. This phenomena was true even though no significant increase in sinkage occurred in the clayey silt with increasing turn angle. Figure 9 also shows that the in-line drag load remained relatively constant with all turn angles.

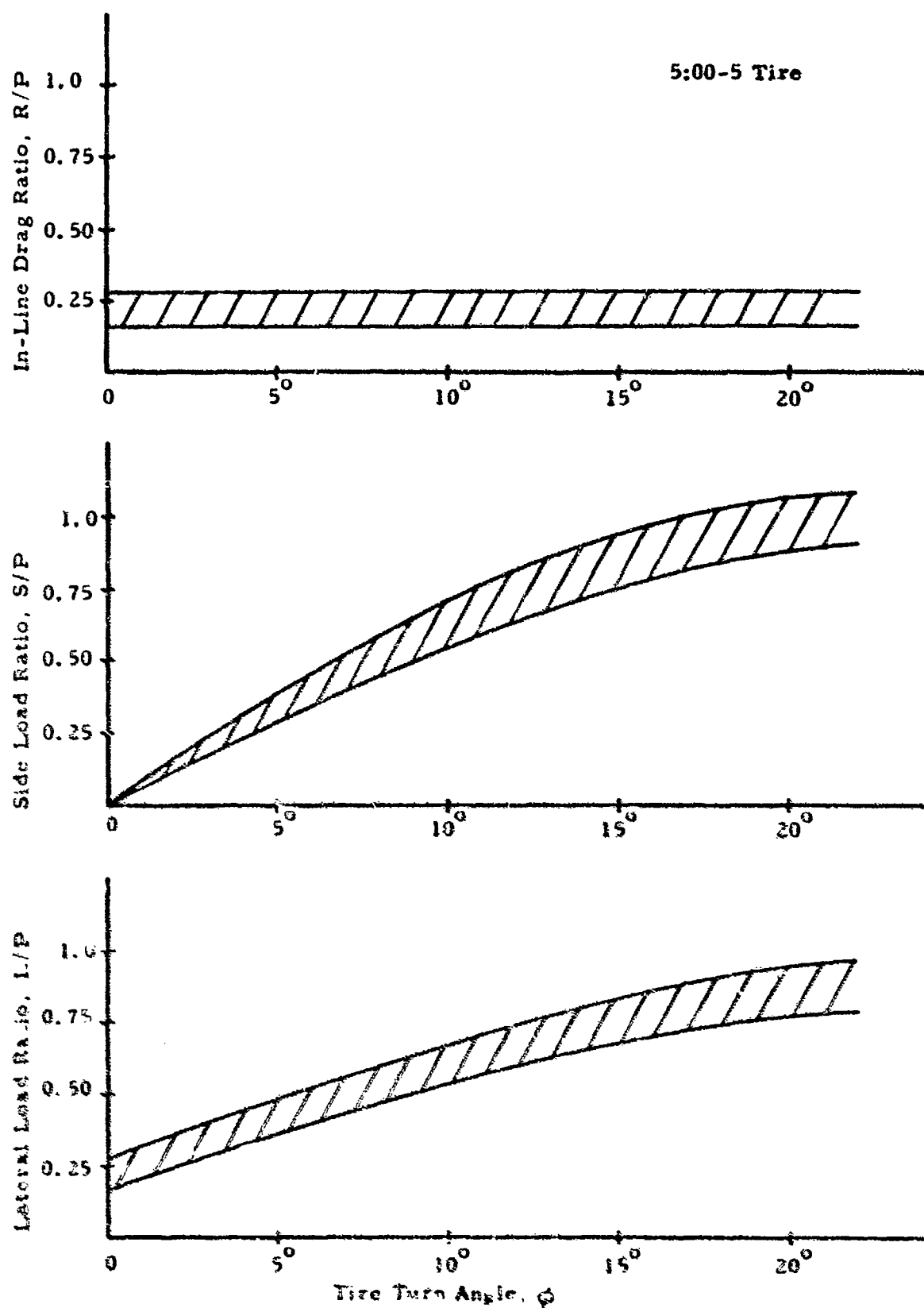


Figure 9. Summary Results - UD Turned Tire Test Program, Clayey Silt

TEST PROGRAM AT AEWES

Test Program

A series of turned tire tests were also conducted at the Army Engineers Waterways Experiment Station (AEWES) under supervision by the University of Dayton. The turned tire/soil tests at AEWES were conducted using larger tire diameters and tire loads than the tests conducted at UD. A total of 44 tests were conducted in mortar sand and buckshot clay with turn angles ranging from 0° to 20°. The vertical loads and soil strength combinations were selected to give a non-turned tire sinkage ratio (Z/D) of about 0.03. The test program, which is summarized in Tables VI and VII for the sand and clay type soil was conducted with a 7:00-6, 6 PR and an 8:50-10, 8 PR aircraft tire. Both tires are Type III and have been used in previous programs conducted at WES. All tests were conducted at a forward carriage speed of 10 fps. The following parameters were measured and data reduction made for each test:

-Measurement

Vertical Load, P

Drag Force (longitudinal direction of track), R'

Side Force (perpendicular to longitudinal axis of track), FL, RL

Turn Angle (or yaw).

Tire Slip (both by standard definition and by measuring wheel rotations)

Wheel Axle Vertical Movement

Rut Depth (measured from initial soil surface)

Rut Profile (measured from initial soil surface profiles)

Sinkage (insertion of pins in clay and washers in sand)

Soil strength (cone index profile before and after), CI_{avg}

Carriage Forward Velocity

TABLE VI
TURNED TIRE TEST PROGRAM (DESIGN), BUCKSHOT CLAY SOIL
UD (AEWES)

Tire Designation	Tire Deflection %	Soil Type	Soil Strength CI ¹ _{avg}	Vertical Load, lb.	Turn Angle deg.	Predicted Rolling Sinkage in.
7.00-6	35	Clay	70	1200 to 1300	0	≈ 1/2
7.00-6	35	Clay	70	1200 to 1300	5	
7.00-6	35	Clay	70	1200 to 1300	10	
7.00-6	35	Clay	70	1200 to 1300	15	
7.00-6	35	Clay	70	1200 to 1300	20	
7.00-6	40	Clay	70	1500 to 1600	0	≈ 1/2
7.00-6	40	Clay	70	1500 to 1600	5	
7.00-6	40	Clay	70	1500 to 1600	10	
7.00-6	40	Clay	70	1500 to 1600	15	
7.00-6	40	Clay	70	1500 to 1600	20	
8.50-10	35	Clay	40	1300 to 1400	0	≈ 3/4
8.50-10	35	Clay	40	1300 to 1400	5	
8.50-10	35	Clay	40	1300 to 1400	10	
8.50-10	35	Clay	40	1300 to 1400	15	
8.50-10	35	Clay	40	1300 to 1400	20	
8.50-10	40	Clay	40	1400 to 1500	0	≈ 3/4
8.50-10	40	Clay	40	1400 to 1500	5	
8.50-10	40	Clay	40	1400 to 1500	10	
8.50-10	40	Clay	40	1400 to 1500	15	
8.50-10	40	Clay	40	1400 to 1500	20	

¹ Average cone index over 0- to 6-in. penetration.

TABLE VII
TURNED TIRE TEST PROGRAM (DESIGN), MORTAR SAND SOIL
UD (AEWES)

Tire Designation	Tire Deflection %	Soil Type	Soil Strength CI _{avg} ¹	Vertical Load, lb.	Turn Angle deg.	Predicted Rolling Sinkage in.
7.00-6	35	Sand	40	550 to 660	0	≈ 1/2
7.00-6	35	Sand	40	550 to 660	5	
7.00-6	35	Sand	40	550 to 660	10	
7.00-6	35	Sand	40	550 to 660	15	
7.00-6	35	Sand	40	550 to 660	20	
7.00-6	40	Sand	40	600 to 700	0	≈ 1/2
7.00-6	40	Sand	40	600 to 700	5	
7.00-6	40	Sand	40	600 to 700	10	
7.00-6	40	Sand	40	600 to 700	15	
7.00-6	40	Sand	40	600 to 700	20	
8.50-10	35	Sand	40	900 to 1000	0	≈ 3/4
8.50-10	35	Sand	40	900 to 1000	5	
8.50-10	35	Sand	40	900 to 1000	10	
8.50-10	35	Sand	40	900 to 1000	15	
8.50-10	35	Sand	40	900 to 1000	20	
8.50-10	40	Sand	40	1000 to 1100	0	≈ 3/4
8.50-10	40	Sand	40	1000 to 1100	5	
8.50-10	40	Sand	40	1000 to 1100	10	
8.50-10	40	Sand	40	1000 to 1100	15	
8.50-10	40	Sand	40	1000 to 1100	20	

¹ Average cone index over 0- to 6-in. penetration.

This measured data was then converted to the same format as used in the UD Turned Tire tests as given below:

drag load (in-line drag), R
side load (perpendicular to plane of wheel), S
resultant lateral force, L
restoring moment (torque), M
pneumatic trail, r

The turned tire load-geometry relationships are given in Figure 49 of Appendix I.

Test Equipment and Setup

All turned tire tests in the program were conducted at the U. S. Army Waterways Experiment Station (AEWES), Vicksburg, Mississippi, at the small scale wheel facility of the Mobility and Environmental Systems Laboratory (MESL) between the dates of June 2 and July 13, 1973. A full description of this test facility has been given previously ⁽⁴⁾. The basic carriage and dynamometer was modified to accommodate the 8:50-10 and 7:00-6 tires for turned angles ranging from 0° to 20° in 5 degree increments. The basic layout of the test track and the modified dynamometer/carriage are shown in Figures 10, 11, and 12.

Test Tire

Complete sets of tire data were taken on the 7:00-6 and the 8:50-10, PR, Type III tires. This test data is summarized in Table XVIII of Appendix I.

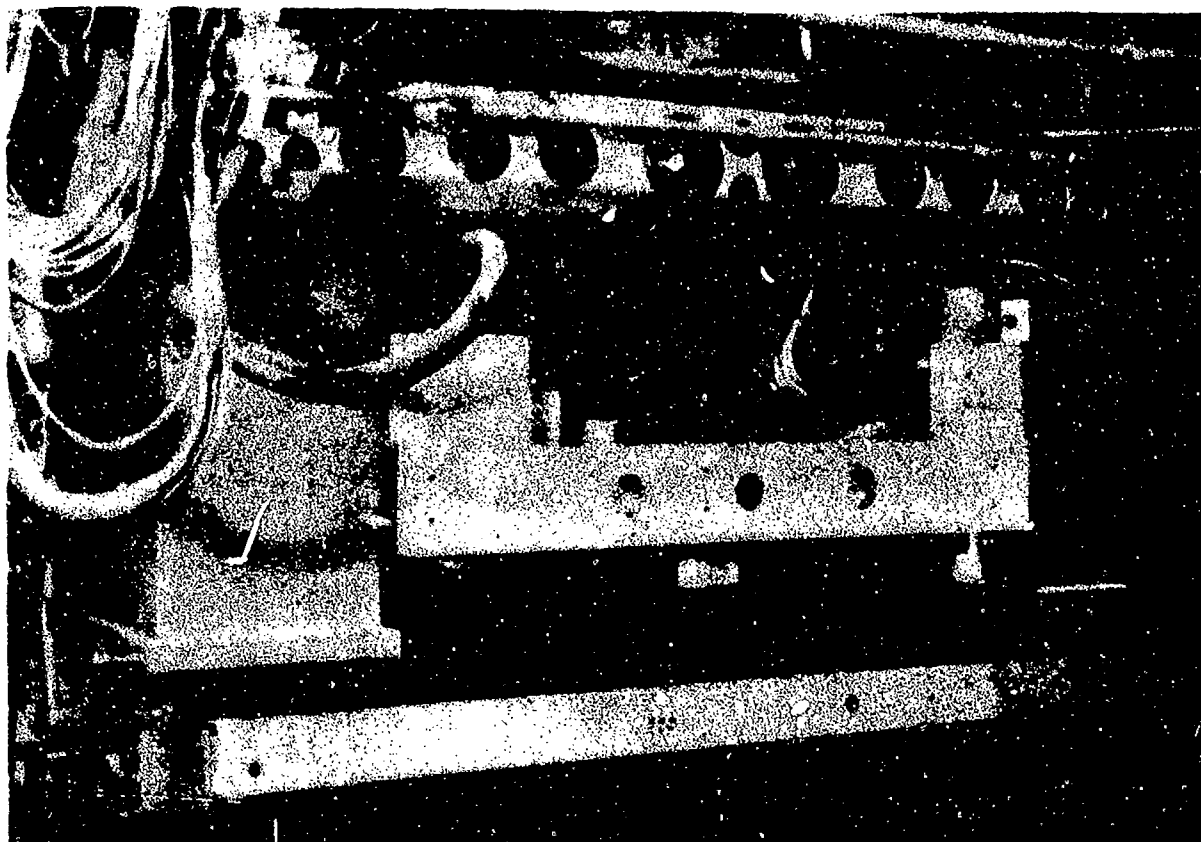
Soil Preparation and Test Procedures

As in previous testing programs conducted at AEWES under UD supervision, a set procedure was followed in preparing the soil test beds and in conducting each test. A summary of this procedure and the soils information is given in Appendix I.



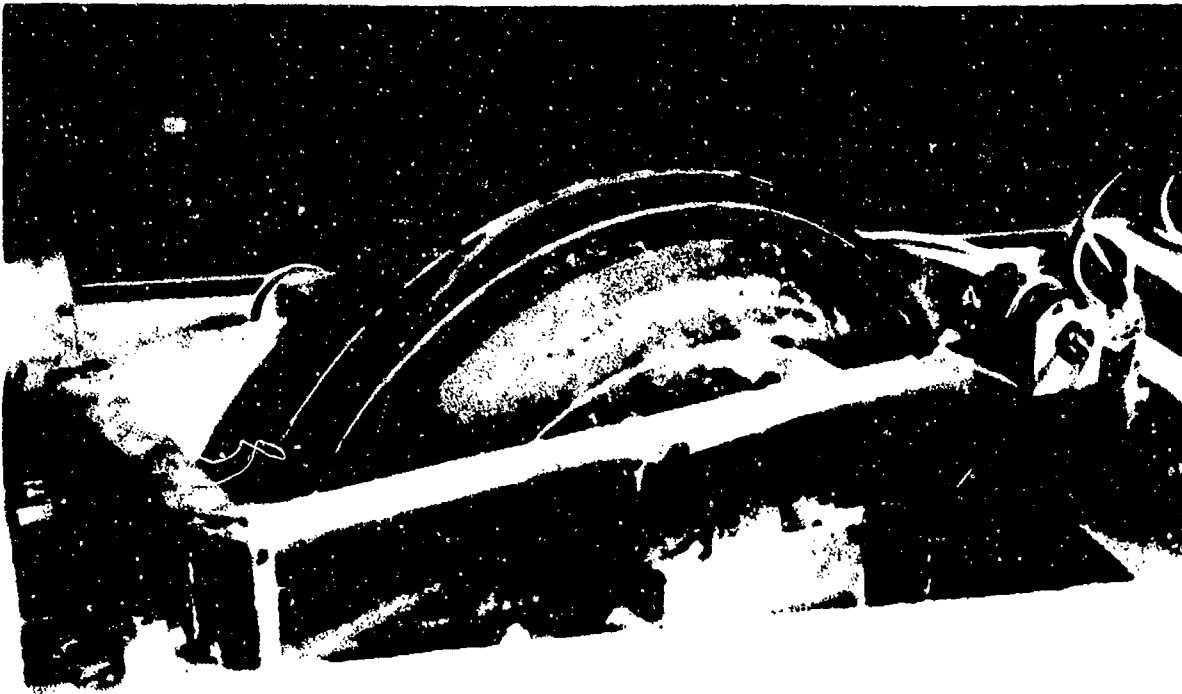
The tests were conducted in the Small-Scale Facility of the Mobility Systems Division. The main equipment consisted of soil bins (64 in. wide, 32 in. deep, and 54 ft. long) in which the soil was prepared to the desired consistencies, and a dynamometer system to which the tire was mounted.

Figure 10. Tire/Soil Test System UD (AEWES) Tests



The dynamometer system, or test carriage, is supported by solid rubber-tired rollers on a pair of overhead rails that are in turn suspended from cantilever columns and crossarms. It is towed by an endless steel cable that is fastened fore and aft to the carriage, passes over pulleys at the ends of the track system and is driven by sheaves mounted on a platform above the overhead rails. The speed of the towing cable can be varied continuously from zero to about 30 ft/sec. Test carriage and cable can be shifted transversely across the width of the soil bins. The carriage consists of the main structure that contains the pneumatic loading system, and the lower frame assembly to which under normal circumstances the test wheel is mounted. The system is instrumented to continuously measure carriage velocity, wheel load, pull or drag force, wheel hub movement (sinkage), and if necessary, torque applied to the wheel and the RPM of the latter.

Figure 11. Tire/Soil Carriage UD (AEWES)



The support frame with the wheel inserted into the main carriage. The support frame was bolted to the inner frame of the lower frame assembly at the desired turn angle. Turn angles could be varied from 0 to 20 degrees in 5-degree intervals.

Figure 12. Tire/Soil Turned Tire Mount UD (AEWES)

Turned Tire Test Results - Mortar Sand

A total of 21 turned tire tests were conducted in sand with turn angles ranging from 0° to 20° . The complete results of these tests are given in Table VIII. As indicated previously, the dynamometer was instrumented to measure the longitudinal (R') and lateral (TL) loads acting on the tire and consequently the in-line drag (R) and side load (S) shown in Table VIII were calculated using R' and TL as shown in Figure 49 of Appendix I. Previous experience with tire tests conducted in sand have shown that rut depth and instantaneous sinkage are approximately equal. When a tire is turned and moving through the soil, the maximum rut depth does not occur directly beneath the vertical centerline of the wheel (See Figure 13 for typical result.) Consequently, some adjustments were made to centerline rut depths using the results of rut depth profiles to determine the values for instantaneous sinkage listed in Table VIII. A complete set of rut profiles is given in Appendix I for the sand tests.

Examination of the results given in Table VIII and as shown in Figure 13 shows the influence of increasing turn angle on the resulting sinkage. In general, for a turned tire operating in sand, the sinkage increases with increasing turn angle. The ratio of the 20° turn sinkage to 0° turn sinkage ranged from about 2-1/2 to 3. Reference to Figure 13 shows a significant buildup of sand away from the direction of the turn. Also noted in the rut depth profiles is the variable depth rut which increasingly occurs as the turn angle increases. Figure 14 shows a typical resulting rut from a turned tire test in sand.

The detailed results showing the variation of the in-line drag load and side load with turn angle are given in Appendix I. Figure 15 gives a summary picture of the results. These results indicate an increasing in-line drag force and side load throughout the 20° turn range. As indicated in Figure 15, the total lateral load on both the 8:50-10 and 7:00-6 tire exceeded one-half the vertical load at the 20° turn angle.

TABLE VIII - TURNED TIRE TEST RESULTS, SAND, UD (AEWES)

Test Number	Turn Per Cent Angle (Deg- rate)	Cone Index CI Avg.	Vertical Load, P (lbs)	Wheel Speed (fps)	Carriage Speed (fps)	Per Cent Slip (%)	Forward		Rear		Total Lateral, RL (lbs)	Side Load, S (lbs)	In-Line Drag, R (lbs)	Resultant Lateral Load, L (lbs)	Pneumatic Trail, r (in)	Axle Movement (in)	Rut Depth (in)	Instantaneous Sinkage, Z (in)
							FL (lbs)	RL (lbs)	FL (lbs)	RL (lbs)								
0:50 - 10 Tire, Sand																		
A-73	-001-2	0	35.5	913.7	9.40	10.17	-8.2	-0.89	-2.2	-1.6	-142.4	-3.1	142.7	142.7	—	0.43	0.55	0.70
	-002-2	15	38.1	904.7	9.18	10.30	-12.2	168.4	127.4	298.1	-311.8	368.4	431.8	3.09	0.84	1.10	1.50	
	-003-2	20	39.9	916.7	7.95	10.17	-27.7	167.3	104.2	271.6	-445.8	406.4	520.4	5.32	1.28	1.45	2.00	
	-004-2	5	38.8	915.7	9.69	10.28	-6.0	74.3	69.0	144.9	-146.1	157.1	133.8	0.80	0.43	0.45	0.70	
	-005-2	10	38.2	917.9	9.71	10.41	-7.2	120.9	111.1	234.8	-217.8	266.4	174.4	0.92	0.71	0.95	1.15	
	-006-2	0	37.4	1022.5	9.50	10.28	-8.2	-4.2	-4.2	-6.61	-154.8	-8.2	154.7	154.9	—	0.36	0.50	0.65
	-007-2	5	39.5	1020.3	9.67	10.22	-5.7	64.5	69.6	136.1	-172.2	150.6	160.2	219.7	0.82	0.52	0.60	0.80
	-008-2	10	40.9	1021.5	9.38	10.36	-10.4	121.9	115.3	240.4	-261.7	282.0	216.0	355.4	0.62	0.85	0.95	1.30
	-009-2	15	41.8	1018.3	9.13	10.15	-11.1	174.3	148.6	323.5	-331.8	397.2	237.2	463.4	1.77	0.92	1.15	1.70
	-010-2	20	41.3	1031.7	8.48	10.24	-20.7	181.9	139.1	321.8	-430.6	449.8	295.3	537.1	3.05	1.26	1.60	2.05
7:00 - 6 Tire, Sand																		
A-73	-011-2	0	44.2	617.5	10.0	10.50	-5.3	-2.3	-1.6	-3.1	-90.9	-4.0	90.6	90.8	—	0.30	0.60	0.65
	-012-2	0	42.1	623.2	9.49	10.00	-5.8	-2.2	-1.0	-2.5	-89.2	-3.0	89.0	89.1	—	0.25	0.45	0.50
	-013-2	0	43.1	551.9	9.90	10.30	-4.2	-2.0	-1.3	-2.6	-67.6	-3.3	67.6	67.6	—	0.13	0.30	0.40
	-014-2	5	41.6	596.0	9.60	10.30	-7.7	30.3	30.8	63.4	-93.7	69.2	88.3	112.3	-0.18	0.35	0.50	0.55
	-015-2	10	43.7	556.6	9.50	10.40	-9.6	63.8	61.6	125.9	-126.2	147.1	102.5	177.0	0.38	0.49	0.70	0.80
	-016-2	15	40.4	533.7	9.10	10.40	-14.1	85.8	77.4	163.3	-169.1	202.2	121.1	235.6	1.15	0.67	1.10	1.20
	-017-2	20	40.0	552.9	8.94	10.50	-22.4	87.2	71.8	159.7	-233.3	229.4	164.6	282.9	2.21	0.90	1.40	1.55
	-018-2	5	40.7	616.6	9.30	10.20	-10.2	30.4	32.9	63.4	-119.9	74.8	115.4	136.0	-0.85	0.41	0.70	0.75
	-019-2	20	40.1	623.3	8.40	10.50	-24.4	93.5	75.9	170.9	-263.9	249.9	190.7	314.6	2.38	1.06	1.50	1.75
	-020-2	10	40.4	628.7	9.30	10.30	-10.5	65.3	65.2	130.5	-153.5	155.5	128.2	201.5	0.02	0.66	0.85	1.10
	-021-2	15	39.8	619.9	8.70	10.20	-17.2	81.3	71.2	152.9	-218.1	204.1	171.3	266.7	1.47	0.87	1.15	1.45

Instantaneous sinkage is determined from axle movement and pin movement.

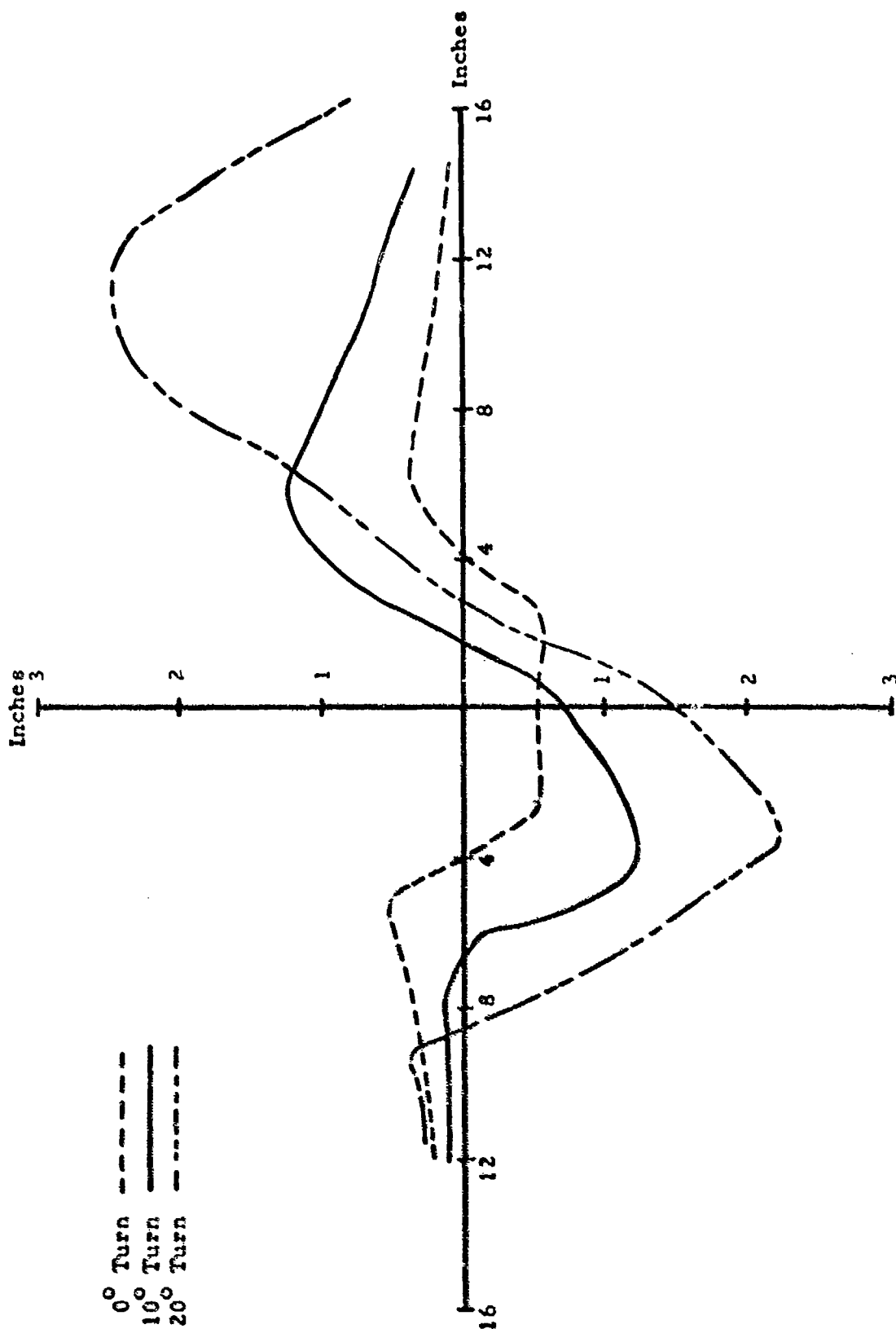


Figure 13. Turned Tire Rut Profile, 8:50-10 Tire, $d = 35\%$, Sand, UD (AEWES)



Ruts left by 8.50-10 tire in sand; turn angle: 15 degrees; deflection: 35 percent; wheel load: 900 lb; CI: 38 psi; carriage velocity: 10 ft/sec.

Figure 14. Rutting from 8:50-10 Tire, 15° Turn Test, Sand, UD (AEWES)

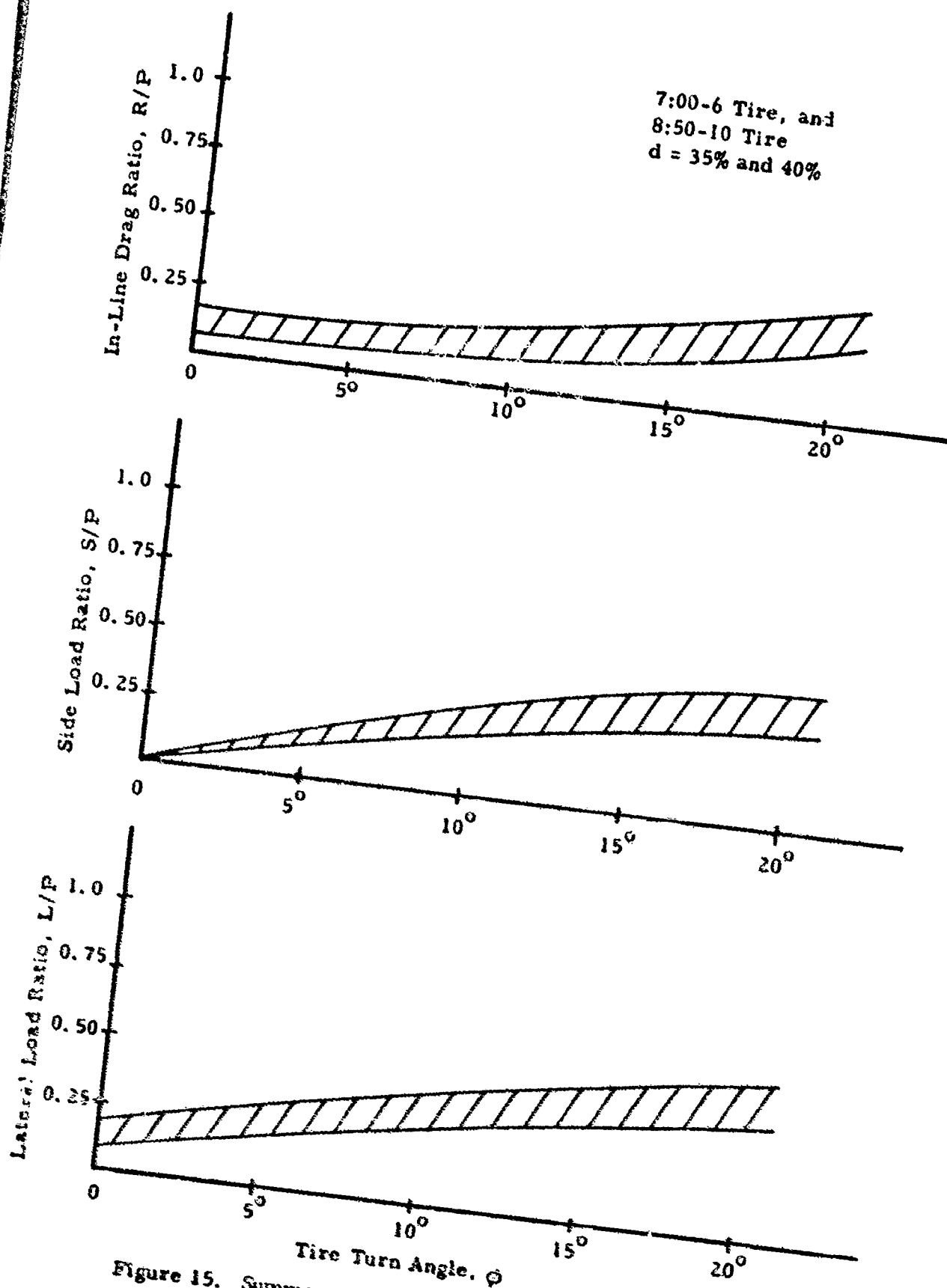


Figure 15. Summary Results - UD (AEWES) Turned Tire Test Program, Sand

The 0° turn angle sinkage ratio (Z/D) was approximately 0.03 for both the 8:50-10 and 7:00-6 tire. The results also indicated that within the 25% to 40% tire deflection range, tire deflection has little if any influence on the resulting tire lateral load ratio (L/P) throughout the 0° to 20° turn angle range. Visual observation of the tests, however, showed that a 40% tire deflection condition at high turn angles (15° to 20°) is an unusually severe condition for the tire and could result in separation or failure of the tire.

Turned Tire Test Results - Buckshot Clay

A total of 23 turned tire tests were conducted in clay with the turn angles again ranging from 0° to 20° . Table IX gives the complete results of this test series. In-line drag (R) and side load (S) listed in Table IX were determined from measured values of longitudinal drag (R') and total lateral (TL). The instantaneous sinkages were determined from the measurement of axle movement, rut depth profile, and previous experience with rebound phenomena for the tests in buckshot clay.

Figure 16 shows a typical resulting rut depth profile for the clay soil tests. A complete set of rut depth profiles is given in Appendix I. Reference to Table IX and Figure 16 shows that increasing turn angles for tires operating in clay has less influence on the resulting sinkage (and rut depth) than is the case for sand. The ratio of the 20° turn angle sinkage to 0° turn angle sinkage in clay ranged from 1-1/2 to 2. As was the case for sands, buildup of soil occurs in the clay away from the direction of the turn. Figure 17 shows a typical rutting result from a turned tire test conducted in clay.

The results of the turned tire tests in clay as given by the variation of in-line drag, side load, and resultant lateral load are presented in summary fashion in Figure 18. The complete results of the clay tests are contained in Appendix I. These results indicate little if any increase in in-line drag with increasing turn angle but significant increases in side load as the turn angle increases. The ratio of the resultant lateral load

TABLE IX - TURNED TIRE TEST RESULTS, CLAY, UD (AEWES)

Test Number	Turn Angle (Deg- cent)	Per Cent Tire Deflection (%)	Car Load P (lbs)	Vertical Load P (lbs)	Wheel Speed F/Sec	Carriage Speed F/Sec	Carriage Slip (%)	Per Cent Slip (%)	Forward Roll Lateral, F.L. (lbs)	Total Lateral, F.L. (lbs)	Drag, R' (lbs)	Slide Load, S (lbs)	In-Line Drag, R (lbs)	Resultant Lateral Load, L (lbs)	Pneumatic Trail F, (in)	Angle Move- ment (in)	Rut Depth (in)	Instantaneous Sinkage, Z (in)
8:50 - 10 Tires, Clay																		
A-73-001-1	0	35	47.6	1323.7	10.04	10.22	-1.8	-2.23	0.5	0.2	-44.7	-1.50	94.9	94.8	—	0.32	0.15	0.45
-002-1	0	25	48.2	1310.3	9.43	9.72	-3.0	1.10	5.2	7.9	-140.5	7.1	139.7	144.3	—	0.47	0.40	0.70
-003-1	0	—	37.0	1531.2	9.22	9.72	-5.3	-51.5	2.1	1.0	-213.2	0.8	215.0	215.0	—	0.64	0.60	0.95
-004-1	9	43	48.7	1520.1	9.52	9.78	-4.8	96.3	120.6	219.7	-198.0	236.8	178.3	295.4	-2.09	0.57	0.45	0.85
-005-1	10	40	33.0	1527	9.02	10.47	-6.5	180.6	202.6	383.6	-278.7	207.8	426.1	474.0	-1.25	0.71	0.70	1.10
-006-1	15	40	41.7	1533.0	9.40	10.30	-7.3	243.8	271.3	525.9	-348.3	585.9	202.2	429.1	-1.69	0.86	0.80	1.30
-007-1	20	40	41.5	1532.3	9.24	10.33	-11.8	278.5	291.3	573.1	-448.0	624.8	224.7	727.4	-0.51	0.89	0.90	1.35
-008-1	5	30	32.9	1510.7	9.13	9.73	-6.5	157.8	122.5	225.7	-163.4	239.0	142.8	278.8	-1.78	0.59	0.45	0.50
-009-1	10	33	39.0	1406.4	9.46	9.93	-5	176.2	188.2	361.3	-210.0	332.9	142.9	418.2	-0.84	0.61	0.55	0.90
-010-1	0	35	38.6	1317.5	9.96	10.25	-1.9	48.4	-10.2	-15.8	-117.1	—	115.6	117.1	—	0.40	0.30	0.60
-011-1	15	35	41.9	1316.6	9.61	10.46	-7.8	256.9	273.5	530.3	-293.1	587.9	145.5	617.3	-0.70	0.71	0.70	1.10
-012-1	20	35	39.6	1507.3	9.09	9.97	10.3	276.1	291.1	576.7	-393.4	667.6	175.7	690.6	-0.61	0.87	0.90	1.35
7:00-6 Tires, Clay																		
A-73-013-1	0	35	70.7	1344.1	9.92	10.12	-2.0	-7.40	-5.5	-12.4	-94.0	-13.7	94.7	95.8	—	0.37	0.15	0.50
-014-1	5	35	70.6	1353.4	9.89	10.20	-2.7	96.1	121.8	218.4	-115.2	226.9	96.2	246.5	-2.55	0.36	0.40	0.50
-015-1	10	35	71.6	1346.0	9.90	10.40	-5.0	184.7	206	392.2	-219.2	423.9	147.6	448.9	-1.19	0.56	0.35	0.80
-016-1	14	35	75.8	1339.7	9.91	10.44	-9.7	251.5	238.0	473.6	-334.6	544.6	200.9	579.9	-0.21	0.65	0.55	1.00
-017-1	20	35	72.7	1338.2	9.39	10.30	-8.5	272.3	292.4	566.9	-355.3	659.7	139.9	669.0	-0.81	0.68	0.55	1.00
-018-1	25	35	72.3	1342.4	9.8	12.52	-7.0	267.1	288.1	565.8	-384.4	663.1	167.7	684.0	-0.87	0.73	0.60	1.10
-019-1	0	40	74.4	1515.6	10.07	10.19	-1.2	-10.0	-7.3	-15.2	-94.0	-16.7	93.6	95.2	—	0.39	0.30	0.55
-020-1	5	40	64.8	1522.3	9.75	10.00	-2.2	42.6	133.0	228.3	-126.6	236.3	107.1	259.5	-1.86	0.40	0.30	0.60
-021-1	10	40	71.3	1508.4	9.89	10.13	-3.1	169.4	211.5	382.6	-208.1	410.3	137.9	432.9	-2.41	0.48	0.35	0.70
-022-1	15	40	73.3	1514.0	9.60	10.50	-9.0	239.6	282.9	528.0	-288.3	584.6	141.8	601.6	-2.84	0.54	0.50	0.80
-023-1	20	40	72.6	1519.2	9.50	10.10	-6.2	290	326.5	622.6	-390.4	718.6	154.3	734.8	-1.35	0.85	0.60	1.30

* Instantaneous sinkage is determined from axle movement and pin movement.

0° Turn ---
 10° Turn ---
 20° Turn ---

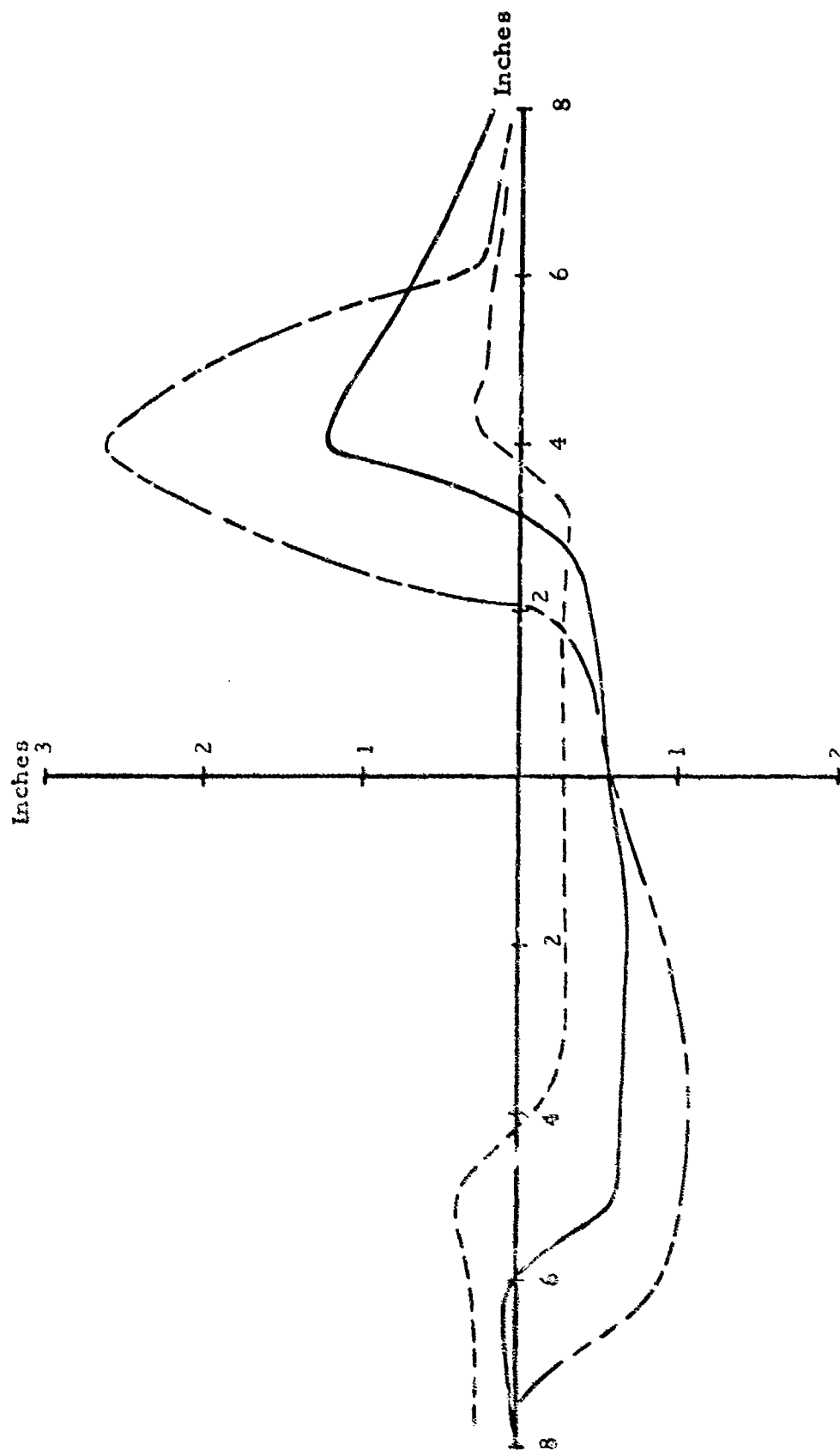


Figure 16. Turned Tire Rut Profile, 8:50-10 Tire, $d = 35\%$, Clay, UD (AEWES)



Figure 17. Rutting from 8:50-10 Tire, 15 Degree Turn Test, Clay, UD (AEWES)

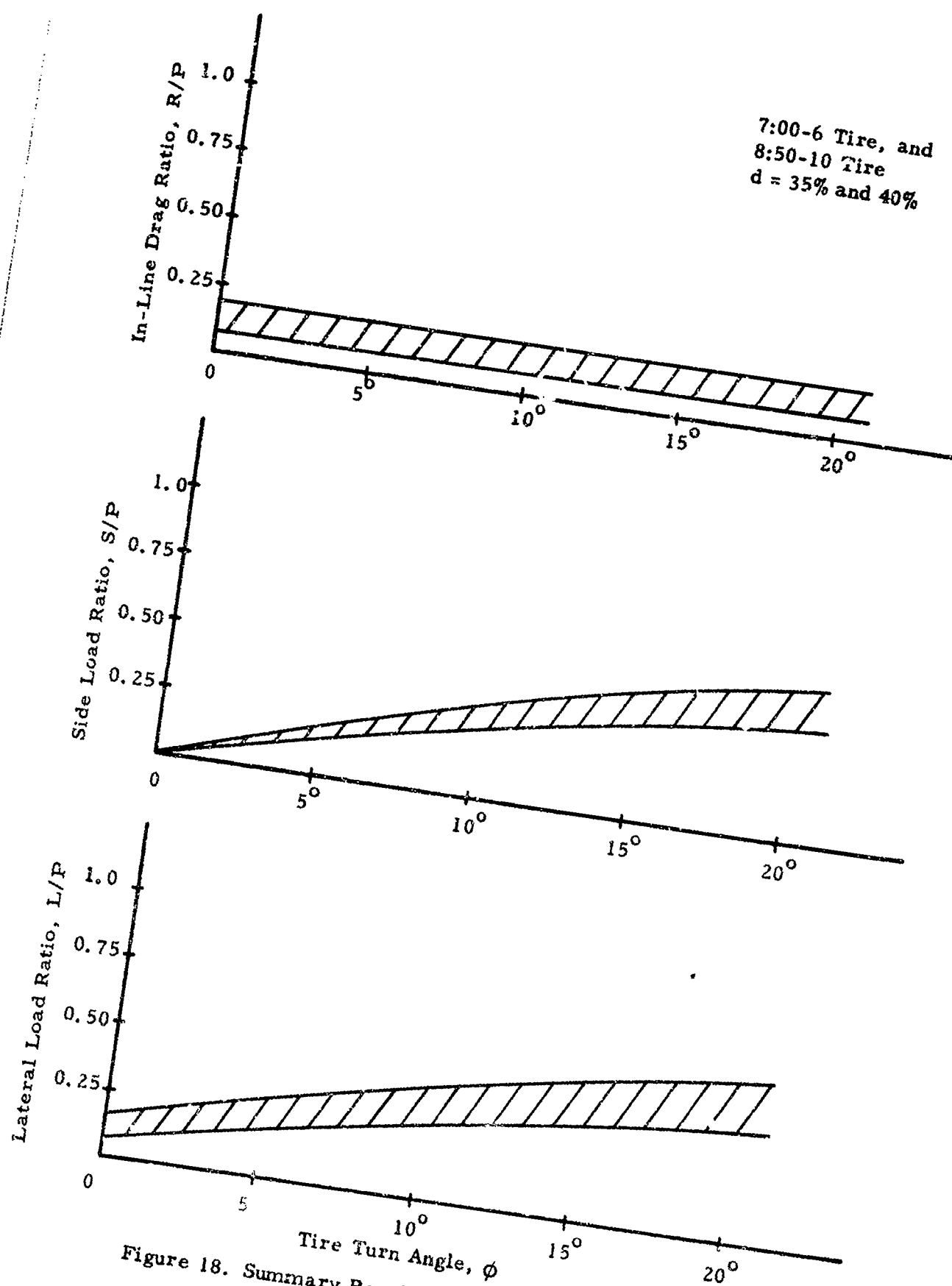


Figure 18. Summary Results - UD (AEWES) Turned Tire Test
Program, Clay

to vertical load approached one-half at the 20° turn condition for both the 7:00-6 tire and 8:50-10 tire. The 0° turn angle sinkage ratio (Z/D) was approximately 0.03 for both tires. For the range of tire deflections tested (35% to 40%), the tire deflection had little if any influence on the resulting lateral load (L/P). The operation of an aircraft tire at an increased tire deflection (40%) and at large turn angles (15° to 20°) was again noted to be an unusually severe condition for an aircraft tire.

C. COMPARATIVE SUMMARY ANALYSIS OF TURNED TIRE TESTS

The results of both turned tire test programs were analyzed and compared. The results of this comparison indicated the following points of similarity:

1. Sinkage and rut depth increase markedly with increasing turn angle for aircraft tires operating on sand (frictional) type soils, but only moderate increases in sinkage occur on clay type soils.
2. The in-line drag ratio remains relatively constant over the 0° to 20° turn angle range for aircraft tires on clay type soils.
3. Significant amounts of soil buildup, opposite to the direction of turn, occur for turning tires in both sand and clay types of soil.

Perhaps the most significant result of the turned tire tests is some preliminary indication of the magnitudes of side load buildup on a turned tire operating on a soil runway. Figure 19 presents this type of result as related to the non-turned tire sinkage ratio (Z/D). Reference to Figure 19 shows that the magnitude of this sinkage has a considerable influence on the resulting lateral loads. Lateral load ratios may very well exceed one-half in situations of tight turn angles and high sinkage conditions. Some of the general conclusions as to turned tire performance on soil runways would include:

1. The lateral load ratio (L/P) very likely will approach and in some cases exceed one-half for aircraft operating on moderate strength soil runways (rolling drag ratios greater than 0.10) where tight turning situations are encountered.
2. The tire negative slip will increase throughout the entire turn angle range of 0° to 20° . Negative slips approached 25% in sand and 15% for clay in the 20° turn situation.

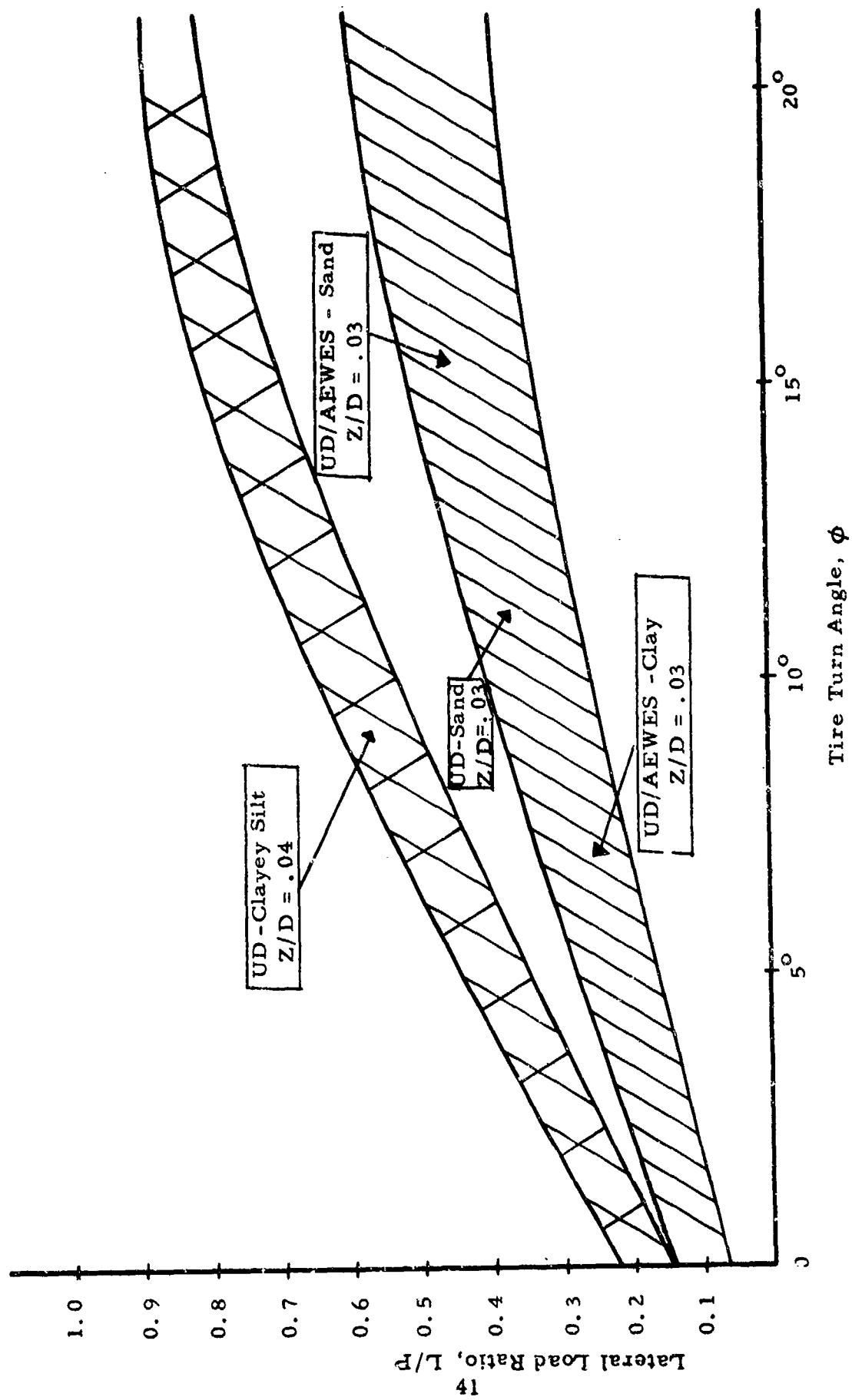


Figure 19. Comparative Turned Tire Test Results - Influence of Sinkage Ratio (Z/D)

3. Unlike the behavior of turned tires on rigid pavement, the percent tire deflection had little influence on the lateral load ratio for either sand or clay operation.
4. More severe rutting will occur for aircraft turning operations on frictional type soils (sand) than on cohesive (clay) type soils.
5. No clear trend existed in the variation of pneumatic trail (r) with turn angle. The pneumatic trail increased with increasing turn angle in sand but decreased with increasing turn angle in clay.

Although sufficient turned tire tests were not conducted to encompass a broad range of sinkage ratios (Z/D), where Z -sinkage, D -tire diameter, the results do indicate that an increase in the sinkage ratio will result in an increased lateral load ratio for a turned tire for all other conditions being constant.

D. AIRCRAFT TURNING OPERATION PREDICTIVE COMPUTER PROGRAM

In order to evaluate the effects of varying turn angles, gear configuration and geometry on the buildup of lateral tire loads, an analytical approach was developed which would permit prediction of side and drag forces for aircraft turning operations on soil runways. Such an analysis and predictive procedure will also lead to a better definition for aircraft turning criteria. The "Aircraft Turning Operation Predictive Computer Program" which is detailed below is restricted to aircraft with a tricycle landing gear system and does not permit differential thrust during turning.

Turning Geometry and Force Analysis

An aircraft with a castered-steerable nose wheel undergoes a turning procedure by the rotation of its nose wheel from the aircraft longitudinal axis, and thus sets up an instantaneous center about which the aircraft turns. Figure 20 shows the instantaneous position of a tricycle landing gear system with a twin nose wheel and four-wheel bogies together with the forces on the nose wheels and main gears. The symbols used in Figure 20 are defined as follows.

ϕ_n = nose wheel turning angle

ϕ_{ml} = left main gear wheel turning angle

ϕ_{mr} = right main gear wheel turning angle

W = weight of aircraft

R = drag loads (braking or driving) in longitudinal wheel direction (R_{n1} , R_{n2} , R_{m1} , R_{m2} , R_{m3} , R_{m4})

S = side load perpendicular to wheel longitudinal direction (S_{n1} , S_{m1} , S_{m2} , S_{m3} , and S_{m4})

V = aircraft forward velocity
 ζ = instantaneous radius of turn
 β = caster angle of nose wheel

The definition of the turning angle and the development of side loads and longitudinal drag loads are given in the next paragraphs.

Side Loads and Pneumatic Trail

When an aircraft tire which is rolling forward in soil is rotated about its vertical axis, the tire will continue to track forward while it rotates in a plane inclined to the line of motion. The angle formed between the forward motion line and the rotated line is referred to as the turning angle. Due to the rotation of the tire, restoring forces develop from the soil. It is convenient to refer to the tire/soil interaction forces in two components: side force (S) acting perpendicular to the plane of the wheel and the in-line drag force (R). This tire side force will vary with tire diameter, vertical tire load, sinkage, soil strength, and the elastic properties of the tire. This side or cornering force is generally offset from the center of the tire/soil contact area by a distance which is termed pneumatic trail, r . The pneumatic trail distance will vary with the turning angle, ϕ . It is also possible that for a castered wheel, that the caster axis is displaced from the wheel vertical axis by a mechanical trail distance, h . The sum of the mechanical trail plus the pneumatic trail is then used to compute the restoring torque caused by the side forces.

In-Line Drag Forces

The in-line drag forces will vary with slip, tire diameter, vertical tire load, sinkage, and soil strength. The results of the recently completed turned tire test programs will permit the establishment on a preliminary basis of the relationships between in-line drag and turn angle.

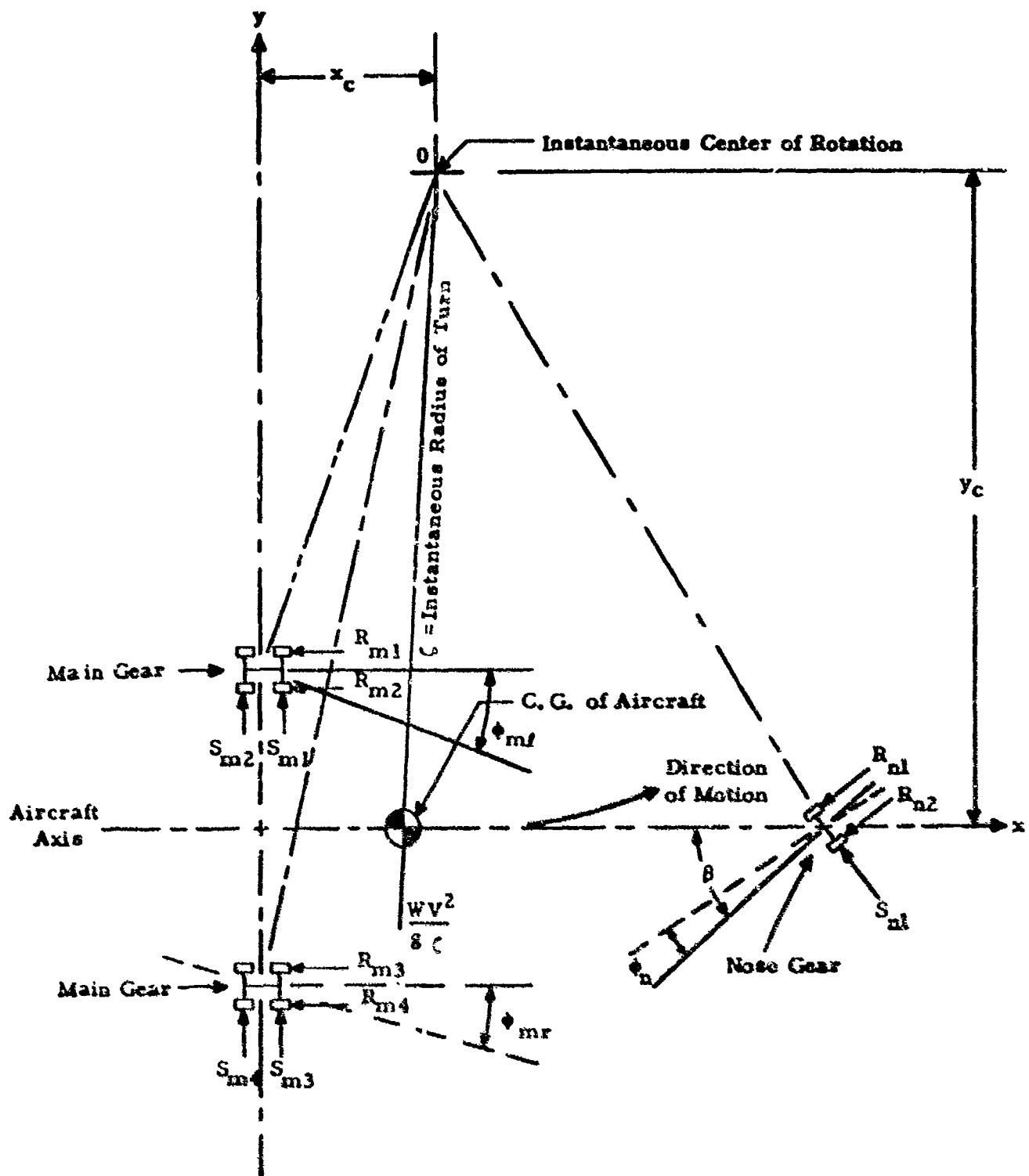


Figure 20. Aircraft Turning Geometry and Force System

Computer Program for Turning Force Interaction Analysis

In order to determine the maximum side and drag forces on the landing gears of an aircraft during turning operations, it is necessary to follow through the force interaction analysis of the complete turn. The reason being that the side force depends on the turning angle of the tire which is the angle between the longitudinal plane of the tire and the direction of motion of the center of the tire, and the magnitude of the turning angle depends on the location of the instantaneous center of rotation, which, in turn, depends on the complete force interaction analysis.

The computer program requires two input curves, besides the aircraft and tire parameters, to analyze the force interaction during the complete turn. One is the nose gear steering angle vs. time curve, and the other is the left main gear brake-slip vs. time curve (the computer program considers the aircraft making a left turn). A third curve of differential thrust vs. time curve may be added, but was not done because this preliminary analysis does not consider differential thrust but does consider differential braking. At present, an assumed curve is used for the nose-gear steering angle vs. time relationship. Experimental measurements of some typical turning operations by aircraft pilots could eventually supply better data for this curve. Both input curves are broken into 20 time increments and supplied as part of the input data. For each time increment, the instantaneous center of rotation is determined and the aircraft is assumed to move through a circular arc in each time increment. Thus, the path of turn is assumed to be formed by segments of circular arcs. A general flow chart of the computer program is shown in Figure 21. A complete description of the computer subroutines and a program listing is given in Appendix II.

The computer program is currently being used to evaluate the proposed medium STOL transport aircraft during turning operations on soil runways.

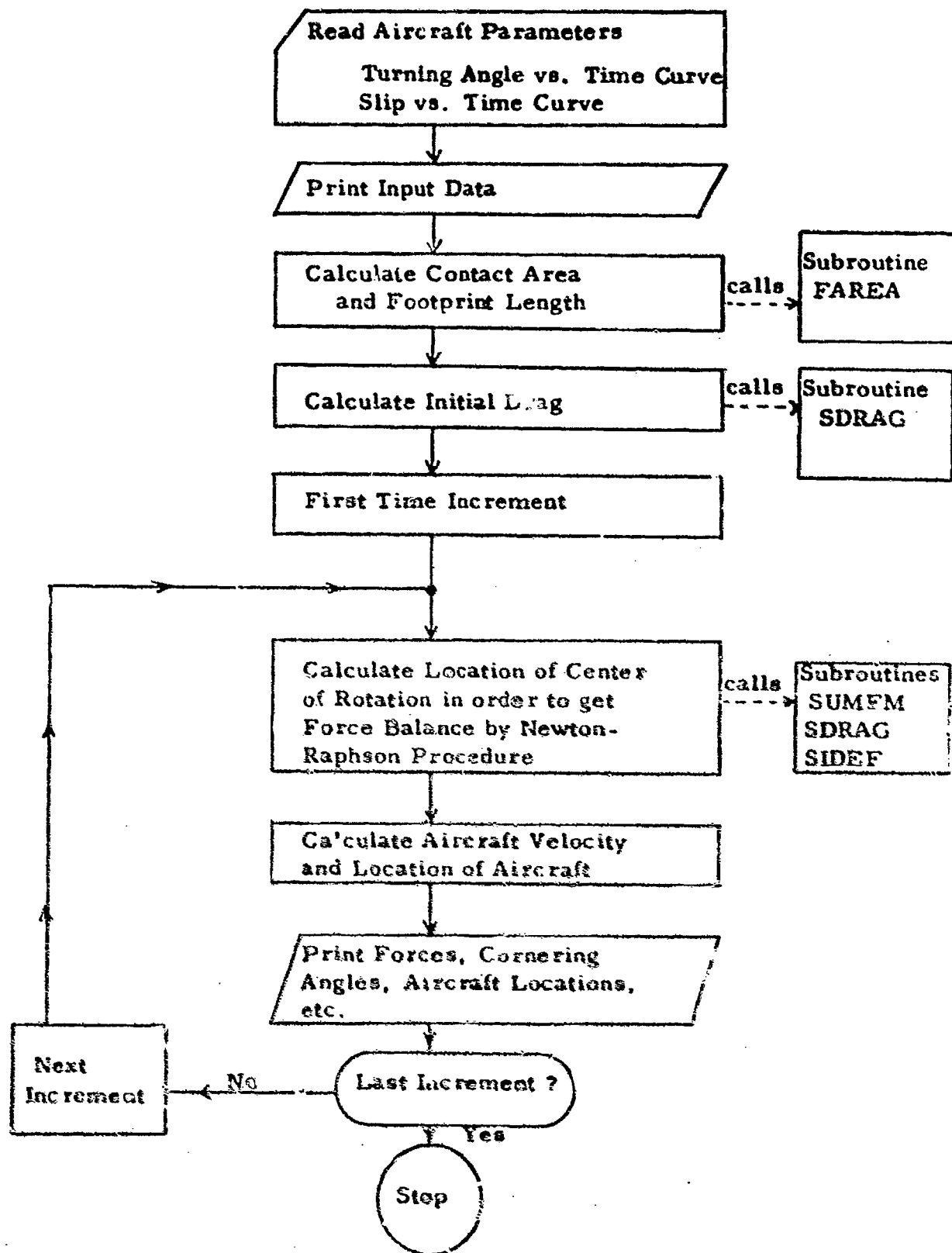


Figure 21. General Flow Chart of Computer Program for Turning Operation

The aircraft parameters are given in Table X. The results of the turned tire test programs will be used to define the in-line drag and side force vs. turn angle relationship. Subsequent to the medium STOL turning evaluation, additional existing aircraft (i. e. , C-130) will be evaluated in order to develop a turning operation criteria.

A review of existing literature still indicates very little design or experimental information is available concerning turning operations of aircraft on either paved or soil runways. The turned tire on soil tests described previously represent the first experimental data for turned aircraft tires. While these test results will prove very helpful in turning analysis studies, additional research and development requirements are needed as follows:

- a) A better definition of the characteristic turning pattern for those aircraft which operate on soil runways.
- b) Additional turned tire tests to extend the range of the sinkage ratio and to evaluate the effects of speed on drag and side loads.
- c) Extension of the computer program capability to include differential thrust and to conduct parametric studies of turning operations.
- d) Verification of turning relationships developed through a full scale field operation test program.

TABLE X
AIRCRAFT PARAMETERS FOR TURNING ANALYSIS

General Data

Gross Weight = 100,000 lbs.
Ground Velocity Going into Turn = 15 knots
Mass Moment of Inertia About a Vertical Axis at C. G. = 3.5×10^{-3} slug - ft²

Tire Data

	<u>Nose</u>	<u>Main</u>
Tire Deflection (%)	35	35
Tire Diameter (in.)	33.4	38.5
Flange Diameter (in.)	18.0	18.5
Tire Type	Type III	Type III
Total No. of Tires	2	8
No. of Tires per Bogie	-	4
No. of Tires in Twin	2	4
No. of Tires in Tandem	0	4

Tire and Aircraft C. G. Distances (in inches)

Nose Gear C. G. to Forward C. G.	235.0
Nose Gear C. G. to Aft C. G.	250.0
Nose Gear C. G. to Main Gear C. G.	275.0
Main Gear C. G. to Forward C. G.	25.0
Ground Level to Forward C. G.	80.0
Ground Level to Engine Centerline	110.0
Between C. G. 's of Left and Right Main Gears	140.0
Twin Spacing of Nose Tires	20.0
Twin Spacing of Main Tires	25.5
Tandem Spacing of Main Tires	70.0

SECTION III

ROLLING HIGH SPEED DRAG RATIO PREDICTION TECHNIQUE AND COMPUTER PROGRAM

A. GENERAL

The definition of the performance of an aircraft on a soil runway includes the determination of rolling tire sinkage and drag over the full aircraft takeoff velocity range. Aircraft in their takeoff runs go through a velocity range of approximately 0 to 120 knots. Early vehicle mobility studies and flotation studies conducted for aircraft tires were accomplished at low velocities (generally less than 5 knots) and resulting flotation criteria generally presumed that tire sinkage and drag (as determined from low speed tests) remained constant over the entire velocity range. With the growing importance of aircraft mission assignments on unprepared runways, it was recognized that if the rolling drag did, indeed, vary with velocity, provisions would have to be made for sufficient aircraft power (thrust) to overcome potentially higher rolling drags in takeoff operations.

With this background of general unavailability of high speed tire/soil interaction experimental data, Boeing ⁽⁸⁾ in 1964 conducted a number of high speed full-scale tests using a modified KC-137 prototype aircraft. One of the primary purposes of these tests, which were conducted at Harpers Lake, California, on a lean clay, was to observe the influence of speed on the aircraft rolling drag ratio, R/P (R = rolling drag; P = vertical load). The results of these tests which are summarized in Figure 22, demonstrated very clearly that speed was an important parameter in defining rolling drag and that higher drags can be anticipated at high speed for aircraft operating on soil runways. The results, however, generally could not be extended to other aircraft, loads, tire sizes, etc., since the tests encompassed one aircraft under one loading condition on one type of soil. More recently, the Air Force again sponsored a series of full scale

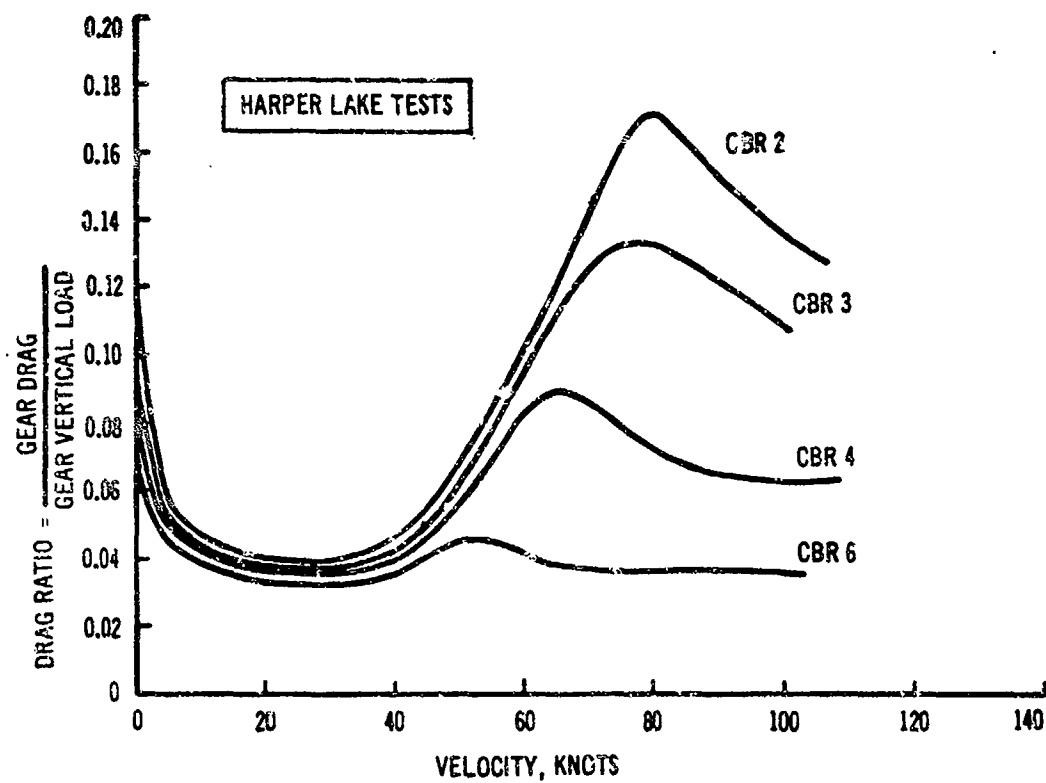


Figure 22. Boeing-High Speed Rolling Drag Tests (8)

speed tests conducted by Lockheed ⁽⁶⁾ at the NASA-Langley test track. These tests were conducted with a 29 x 11 -10, 8 PR tire loaded to 5,000 lbs. on a buckshot clay at CBR's of 1.5, 2.3, and 4.4 and on a sand at a CBR of 1.5. The test results, summarized in Table XI represented the first high speed tire/soil interaction experimental data taken under controlled conditions. Previous experience by UD ^(3,4) with aircraft tire sinkages in buckshot clay indicated that measuring rut depth, as was done in these tests, was not the same as sinkage since the clay type soil partially rebounds after passage of the tire. Consequently, Table XI includes a listing of sinkages (as determined from rut depths) for the tests on buckshot clay. Rut depths and sinkages in sand are approximately the same.

In analyzing the experimental data and attempting to extend the results to other operating conditions (tire size, soil strength, vertical load, etc.) leading to the development of a high speed drag prediction model, both Boeing ⁽⁸⁾ and Lockheed ⁽⁶⁾ noted the similarity in the shape of the drag ratio vs. velocity relationship (See Figure 22) to that observed in tire hydrodynamics studies on water, and proposed the use of the same basic type equation:

$$R = P(\mu_o + \tan \theta) + \frac{C_{DI}}{2} \rho b Z V^2 \quad (1)$$

where

R = total rolling drag

P = total vertical load

μ_o = coefficient of rolling friction on a rigid surface

$\tan \theta = Z/l$

C_{DI} = soil inertia drag coefficient (a function of the planing velocity)

b = tire width

TABLE XI
LOCKHEED/LANGLEY HIGH SPEED TEST
PROGRAM SUMMARY RESULTS

Soil Type	Soil Strength (CBR)	Tire Pressure (psi)	Velocity (knots)	Nominal Vertical Load (lbs)	Average Values for Rolling Condition			
					Sinkage* (in)	Vertical Load (lbs)	Drag Load (lbs)	Drag Ratio R/P
Clay	1.5	30	Tow	5000	1.0	5918	1186	0.20
Clay	1.5	30	22	5000	1.0	5819	700	0.12
Clay	1.5	30	35	5000	1.0	5879	883	0.15
Clay	1.5	30	50	5000	1.2	5779	1211	0.21
Clay	1.5	30	64	5000	1.0	5846	990	0.17
Clay	1.5	30	72	5000	0.7	6243	865	0.14
Clay	1.5	30	83	5000	0.6	5919	801	0.14
Clay	1.5	30	90	5000	0.5	5640	819	0.15
Clay	1.5	45	Tow	5000	1.6	6151	1520	0.25
Clay	1.5	45	21	5000	1.6	5969	1318	0.22
Clay	1.5	45	32	5000	1.8	5761	1489	0.26
Clay	1.5	45	44	5000	2.0	6700	1200	0.18
Clay	1.5	45	61	5000	1.6	6181	1370	0.22
Clay	1.5	45	83	5000	1.0	5856	907	0.15
Clay	1.5	45	93	5000	0.8	6115	822	0.13
Clay	1.5	70	Tow	5000	2.4	5150	2011	0.39
Clay	1.5	70	20	5000	2.5	5996	1875	0.31
Clay	1.5	70	32	5000	2.7	6308	2649	0.42
Clay	1.5	70	41	5000	2.4	6500	2900	0.45
Clay	1.5	70	62	5000	2.2	8100	2075	0.26
Clay	1.5	70	82	5000	1.5	5350	1680	0.31
Clay	1.5	70	91	5000	1.3	5937	1147	0.19
Clay	2.3	30	Tow	5000	0.3	5380	354	0.07
Clay	2.3	30	20	5000	0.3	5625	467	0.08
Clay	2.3	30	34	5000	0.4	5695	506	0.09
Clay	2.3	30	47	5000	0.6	5613	482	0.09
Clay	2.3	30	61	5000	0.5	5350	400	0.07
Clay	2.3	30	80	5000	0.3	5540	250	0.05
Clay	2.3	30	88	5000	0.2	5125	425	0.08

* determined from rut depth.

TABLE XI (continued)

Soil Type	Soil Strength (CBR)	Tire Pressure (psi)	Velocity (knots)	Nominal Vertical Load (lbs)	Average Values for Rolling Condition			
					Sinkage* (in)	Vertical Load (lbs)	Drag Load (lbs)	Drag Ratio (R/P)
Clay	2.3	45	Tow	5000	0.7	5480	400	0.07
Clay	2.3	45	19	5000	0.9	5446	388	0.07
Clay	2.3	45	24	5000	1.0	5449	779	0.14
Clay	2.3	45	28	5000	1.1	5449	600	0.11
Clay	2.3	45	30	5000	1.2	5468	729	0.13
Clay	2.3	45	41	5000	1.2	4821	497	0.10
Clay	2.3	45	44	5000	1.1	5477	903	0.17
Clay	2.3	45	61	5000	1.0	2512	435	0.17
Clay	2.3	45	65	5000	0.9	4760	240	0.05
Clay	2.3	45	78	5000	0.7	5492	691	0.13
Clay	2.3	45	91	5000	0.4	4497	512	0.11
Clay	2.3	70	Tow	5000	1.4	5565	855	0.15
Clay	2.3	70	22	5000	1.6	5607	1246	0.22
Clay	2.3	70	29	5000	1.7	5381	1361	0.25
Clay	2.3	70	42	5000	1.7	5266	1512	0.29
Clay	2.3	70	59	5000	1.6	5237	1169	0.22
Clay	2.3	70	73	5000	1.4	5117	996	0.19
Clay	2.3	70	89	5000	1.3	5199	727	0.14

* determined from rut depth.

and

V = forward velocity of the tire

l = tire footprint length

ρ = soil density

Reference to the above equation indicates that the total drag is made up of a term which is independent of velocity and a term which is a function of the velocity squared (inertia) but is independent of the vertical load. The second term (inertia effects) does not become significant until the forward velocity exceeds approximately 30 knots. Reference to Figure 22 also suggests that for rolling tires which undergo low sinkage (low vertical load or high soil strength) in the low speed range, very little increase in drag will occur through the higher velocity region. Knowledge of the dynamic behavior of soils also suggests that the drag ratio response can be split into three regions as shown in Figure 23 and as indicated below:

- Region 1 - Low speed range, less than approximately 5 knots, where soil viscous effects control the response (sinkage and drag).
- Region 2 - Intermediate speed range, from approximately 5 knots to 30 knots, where both viscous effects (rate of loading is too high) and inertia effects (rate of loading is too low) are not significant in influencing sinkage and drag.
- Region 3 - High speed range, greater than approximately 30 knots, where soil inertia effects predominate in defining sinkage and drag.

Comparisons between measured drag and predicted drag by use of Equation 1 or its modified form ⁽⁶⁾ have not been completely satisfactory due to the necessity of introducing several empirical coefficients (or constants) in order to better curve fit the experimental data. The primary reason for these poor comparative results is that in a high speed rolling

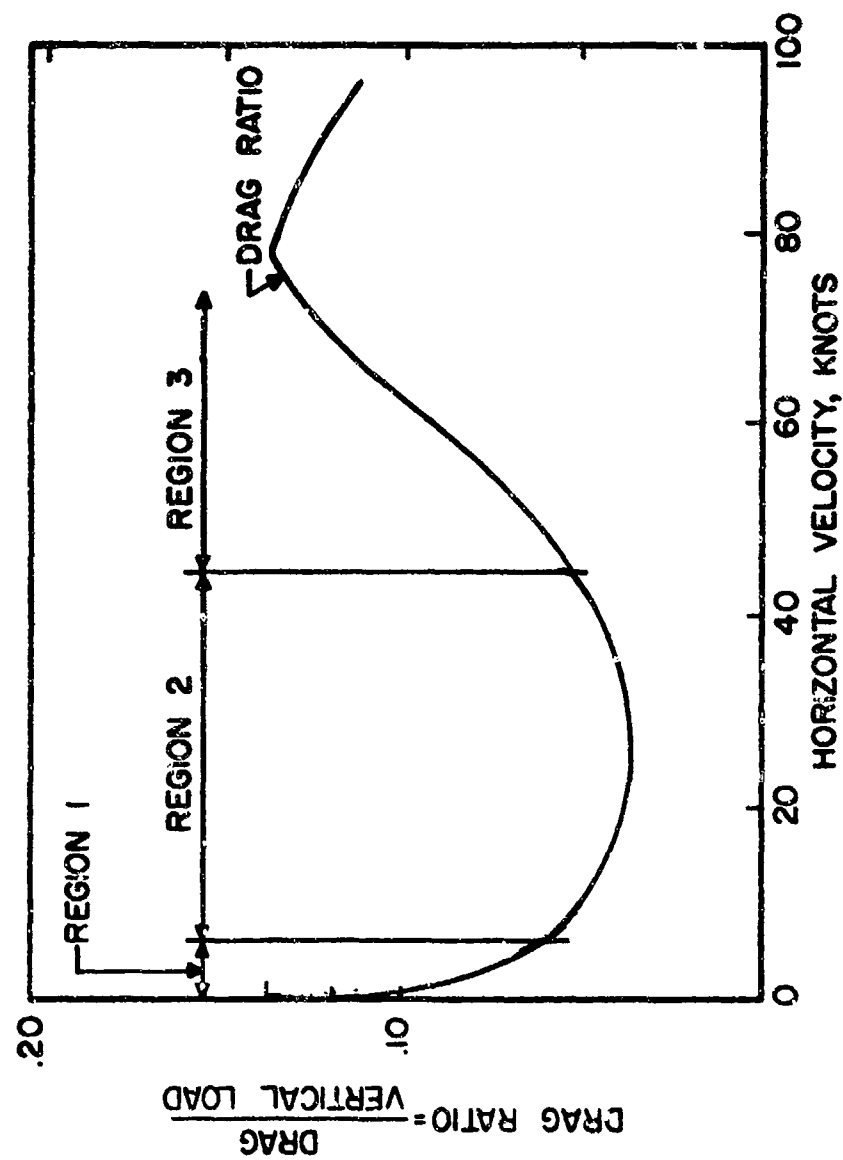


Figure 23. Typical Drag Ratio vs. Horizontal Velocity Relationship in Soil.

drag situation as defined by Equation 1, four unknowns are present (rolling drag, sinkage, soil inertia drag coefficient, and planing velocity). Since only one equation exists, the other three unknowns must be determined empirically. Until additional high speed tire/soil rolling drag experimental tests are conducted, it is unlikely that a drag prediction model based solely on theoretical concepts (verified by experimental tests) will be developed which will have a sufficient degree of reliability and accuracy. It is possible, however, to combine dimensionless analysis techniques with the limited amount of existing experimental data in a semi-analytical approach in order to develop a high speed drag prediction model. Such a technique and the resulting model is described below.

B. HIGH SPEED DRAG RATIO ANALYSIS

As an aircraft tire moves through the soil at increasingly higher speeds, a system of forces acts on the tire as shown in Figure 24. These forces include the resistance to forward motion brought about by soil inertia and a dynamic uplift pressure exerted on the tire (referred to as hydrodynamic lift). The soil inertia (tending to increase the drag acting on the tire) causes an increase in sinkage, while the hydrodynamic lift (which reduces the net effective downward force on soil) tends to decrease the sinkage. The instantaneous soil sinkage and drag can then be represented by an interactive equation as follows:

$$Z_{\text{instantaneous}} = Z_{\text{Region II}} + \Delta Z_{\text{inertia drag}} - \Delta Z_{\text{lift}} \quad (2)$$

(at any speed) (where viscous and
inertial effects are
minimal)

Reference to Figure 24 and Equation 2 suggests that as the forward speed increases the incremental sinkage from inertia effects is greater than that due to lift, resulting in an overall increase in instantaneous sinkage and rolling drag.

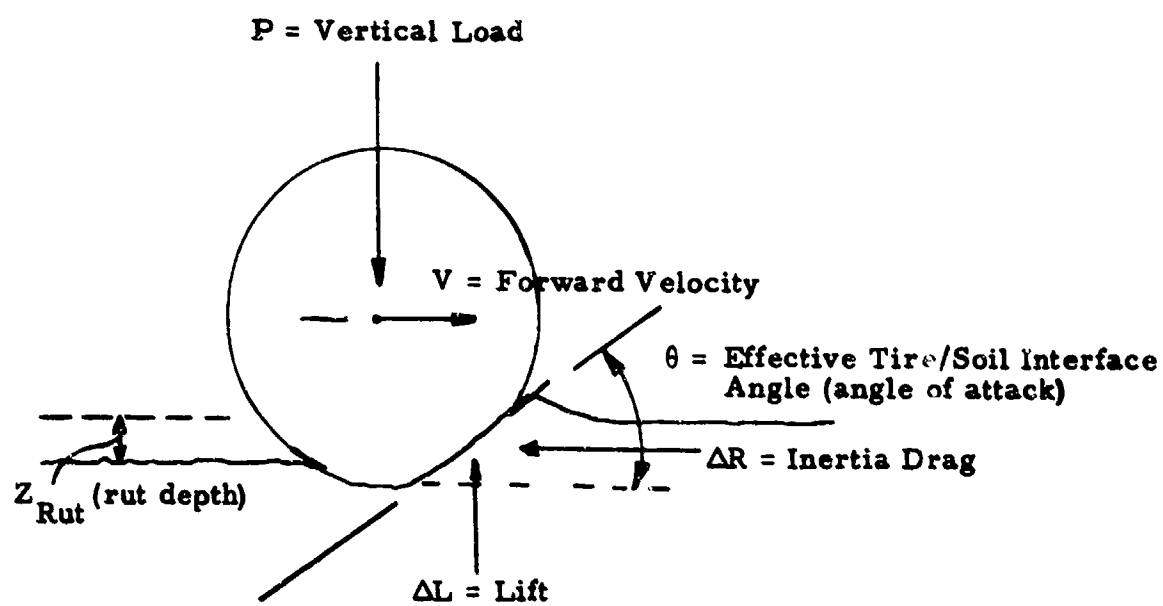


Figure 24. Tire/Soil Interaction at High Speed

In order to further define these two incremental sinkage terms, application of the hydrodynamic equations at the tire/soil interface (see Figure 24) gives a lift as defined by

$$\Delta L = \rho b Z V^2 \sin \theta \cos \theta, \quad (3)$$

and an inertia drag term given by

$$\Delta R = \rho b Z V^2 \sin^2 \theta \quad (4)$$

where

θ = angle defining the effective plane of contact at the tire/soil interface (see Figure 24) and is determined empirically.

Using the expressions for lift and drag as defined above, it is then necessary to define the associated incremental sinkages using known relationships between vertical load, drag load, and sinkage. The results of previous Air Force sponsored research efforts (1, 2, 3, 4) have resulted in a definition of these relationships for both sands and clays as shown in Figures 25, 26, and 27. The test data shown in these figures represent a wide range of tire diameters, loads, and soil strengths. Using linear (straight line) approximations to the trends of the data in Figures 25 through 27, the incremental sinkages associated with inertia drag and lift are given by

$$\Delta Z_{\text{inertia drag}} = \frac{\Delta R \cdot D}{K_1 P'} \quad (5)$$

where

P' = total vertical load minus the lift

$$\Delta Z_{\text{lift}} = \frac{K_2 \Delta L l}{A \cdot C_{I_{\text{avg}}}} \quad (6)$$

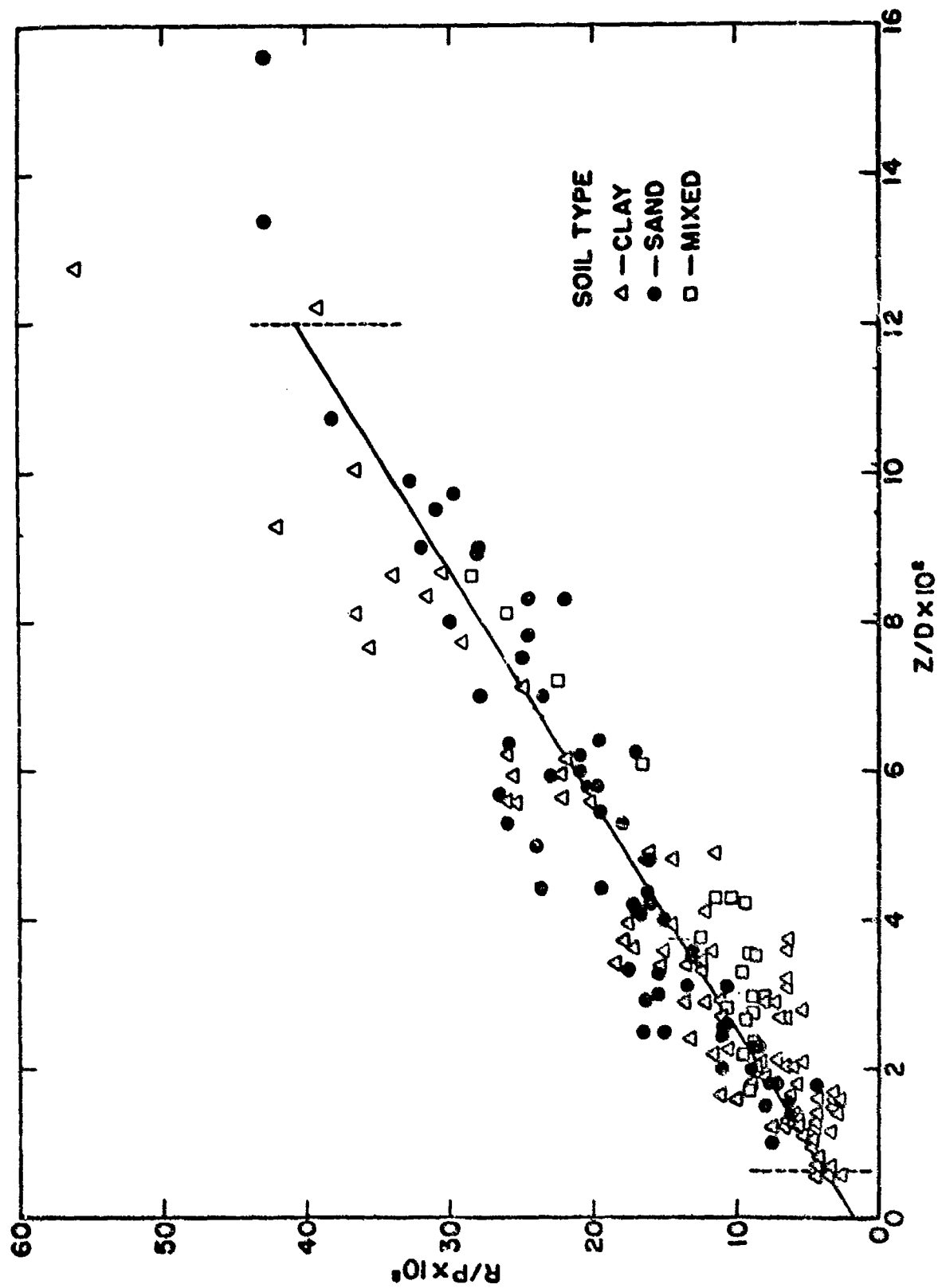


Figure 25. Drag Ratio-Sinkage Ratio, Single Wheels on Soil

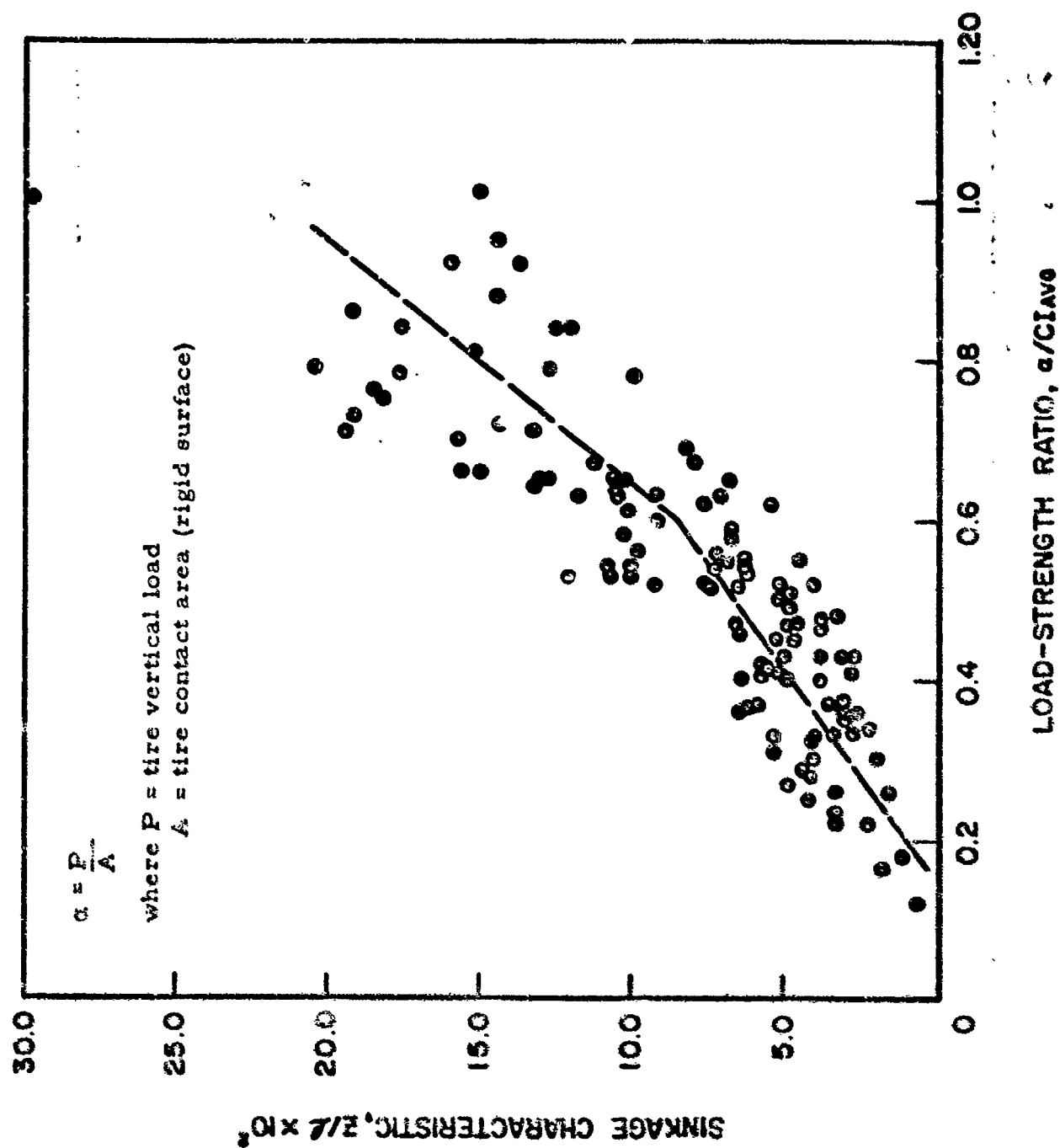


Figure 26. Sinkage Characteristics vs. Load-Strength Ratio, Cohesive Soil

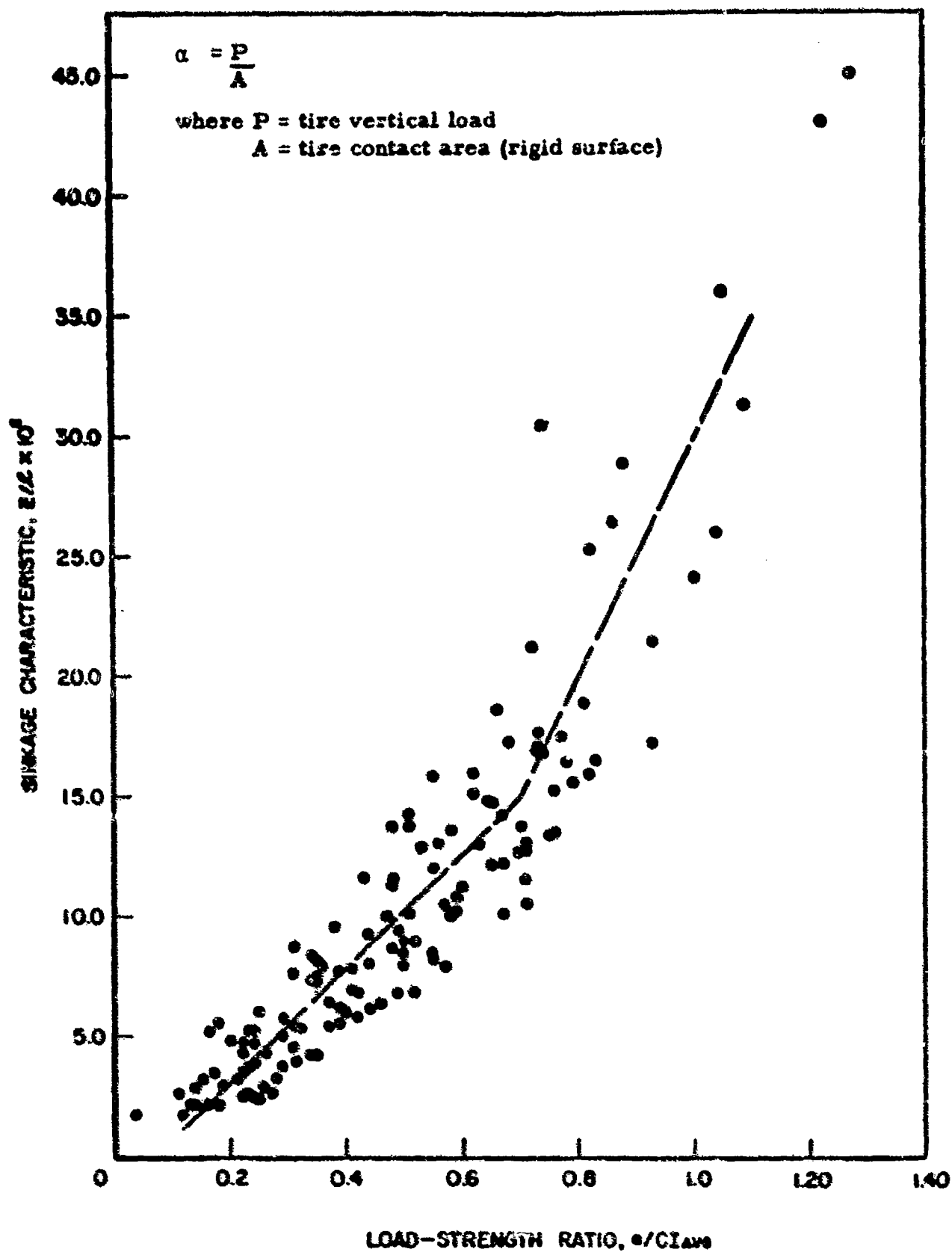


Figure 27. Sinkage Characteristics vs. Load-Strength Ratio, Cohesionless Soils

and K_1 and K_2 are constants.

Based on known conditions of tire size and operating conditions, soil type and strength, aircraft loading conditions, and the velocity range of interest, the incremental sinkages can be calculated for each velocity from which the instantaneous sinkage (for that velocity) can be determined by use of Equation 2. The corresponding high speed rolling drag ratio is then given by

$$\frac{R}{P} = \left(\frac{Z_{\text{instantaneous}}}{D} \right) + \frac{\Delta R_{\text{inertia}}}{P} \quad (7)$$

In using the approach outlined above, it is necessary to define the angle of attack, θ , at the tire/soil interface for a range of operating conditions and speeds. The existing state of the art of high speed tire/soil interaction phenomena does not permit an accurate definition of θ on a strictly theoretical basis. Dimensionless analysis techniques suggest that an expression for the angle of attack based on the variables involved in the problem would take the form

$$\theta_v = f_1 \left(\frac{Z_0}{D}, \frac{l}{D} \right) \cdot f_2 \quad (8)$$

where θ_v = aircraft tire/soil angle of attack

Z_0 = low speed (Region II) rolling sinkage

l = rigid surface tire footprint length

D = tire diameter

for aircraft type tires operating near standard tire deflections. Both f_1 and f_2 were empirically determined and are given in the Source Program Listing in Appendix III. Existing high speed test data from the Lockheed-Langley program were used in conjunction with Equation 8 to determine an

expression for the angle of attack in the development of the computer program predictive technique described in the next section. Since the main effort in the Lockheed test program was on clay, the angle of attack expression was only developed for tire/clay soil conditions. Resulting comparison between predicted and measured results were also limited to the clay soil condition.

C. HIGH SPEED DRAG RATIO PREDICTION COMPUTER PROGRAM AND COMPARATIVE STUDY

Equations 2 through 8, together with an empirical definition of the angle of attack, θ , at the tire/soil interface (clay soil) were used to develop a FORTRAN IV computer program predictive technique on the CDC 6600 Computer at Wright-Patterson Air Force Base. Use of the computer program is currently restricted to clay type soils and the program is detailed in Appendix III. The program was initially developed for use in a predictive/comparative study with the NASA-Langley High Speed Test Data given in Table XII. The program was subsequently generalized for use with a broader range of tire and soil parameters. A general flow chart of the Predictive Computer Program is given in Figure 28.

The experimental test conditions and variables from the previously described Lockheed-NASA Langley test program were used as input data to the "Rolling High Speed Drag Ratio Prediction Computer Program". The tire/soil input data is given in Table XII. The results of this comparative study (for the clay type soil only) are given in Figures 29 through 31 for the CBR 1.5 soil, and Figures 32 through 34 for the CBR 2.3 soil. Reference to these figures indicate that the experimental data exhibits a great deal of scatter (reference Figure 31 at speeds approximately 80 to 90 knots). This type of experimental data scatter for tests on soil is expected. In general, however, the predicted variation of the drag ratio with speed for

TABLE XII

TEST CASE INPUT DATA
 LOCKHEED/LANGLEY TEST PROGRAM (see Table XI)

Input Parameter	Case Number					
	I	II	III	IV	V	VI
Tire Deflection	3.4	2.85	2.2	3.4	2.85	2.2
Initial Sinkage	1.05	1.40	2.30	0.40	0.80	1.25
Cone Index	69.0	69.0	69.0	97.0	97.0	97.0
California Pearing Ratio	1.5	1.5	1.5	2.3	2.3	2.3
Tire Inflation Pressure	30.0	45.0	70.0	30.0	45.0	70.0

Tire Diameter D = 29.0 inches

Tire Section
Width B = 10.7 inches

Vertical Load P = 5000.0 lbs.

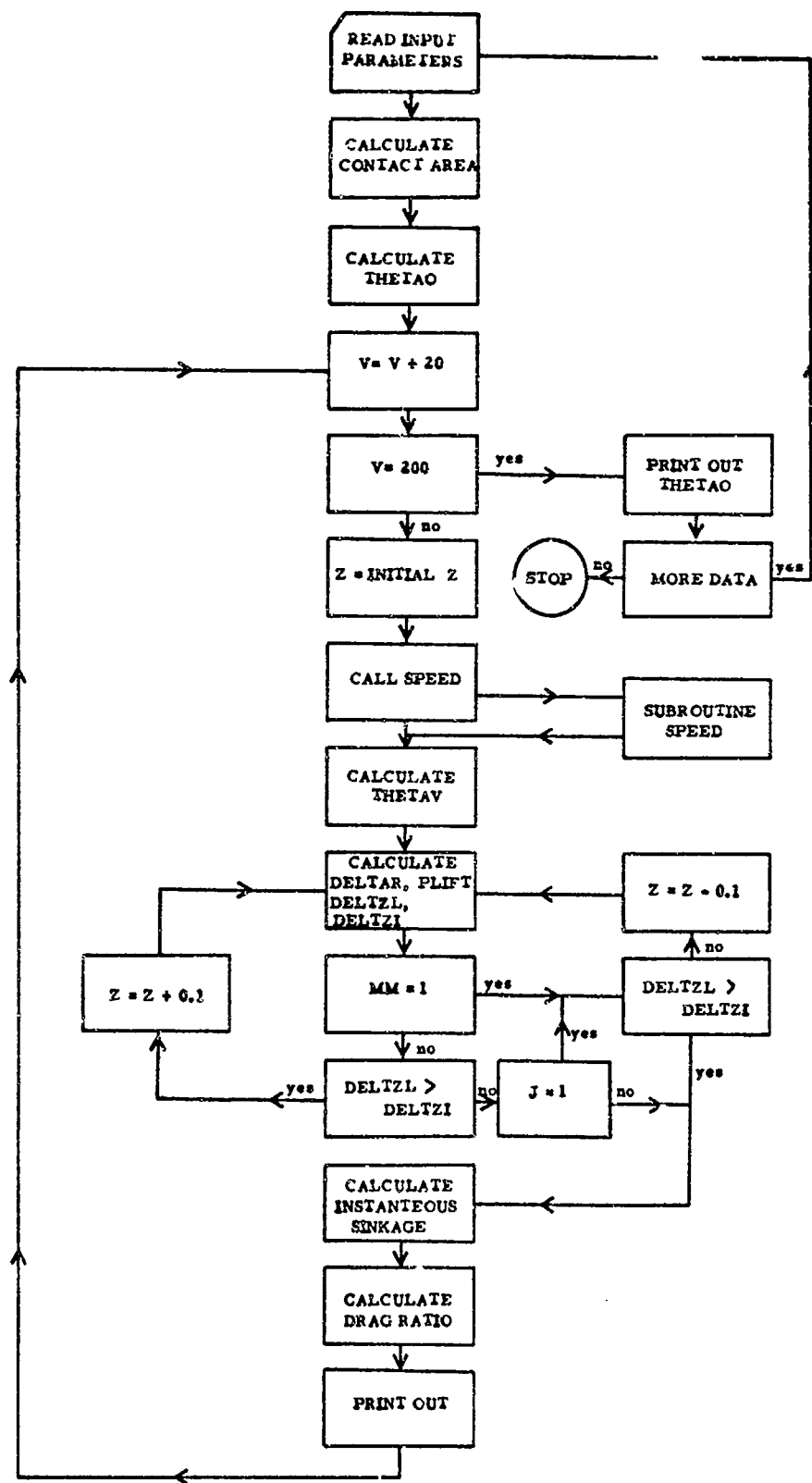


Figure 28. Rolling-High Speed Drag Ratio Prediction Computer Program Flow Chart

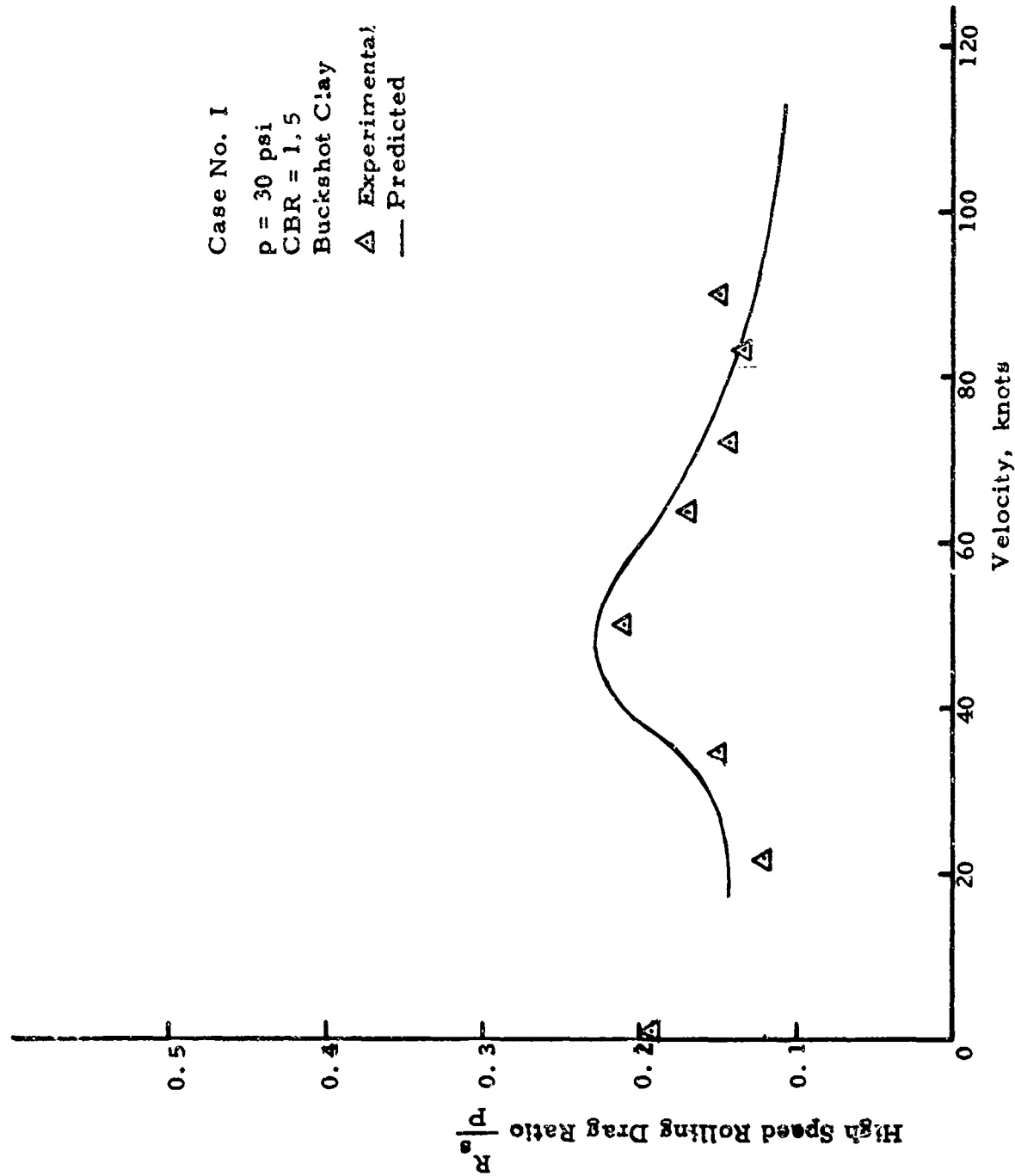


Figure 29. Experimental-Predicted, High-Speed Sinkage - Lockheed/Langley Tests, Case No. 1

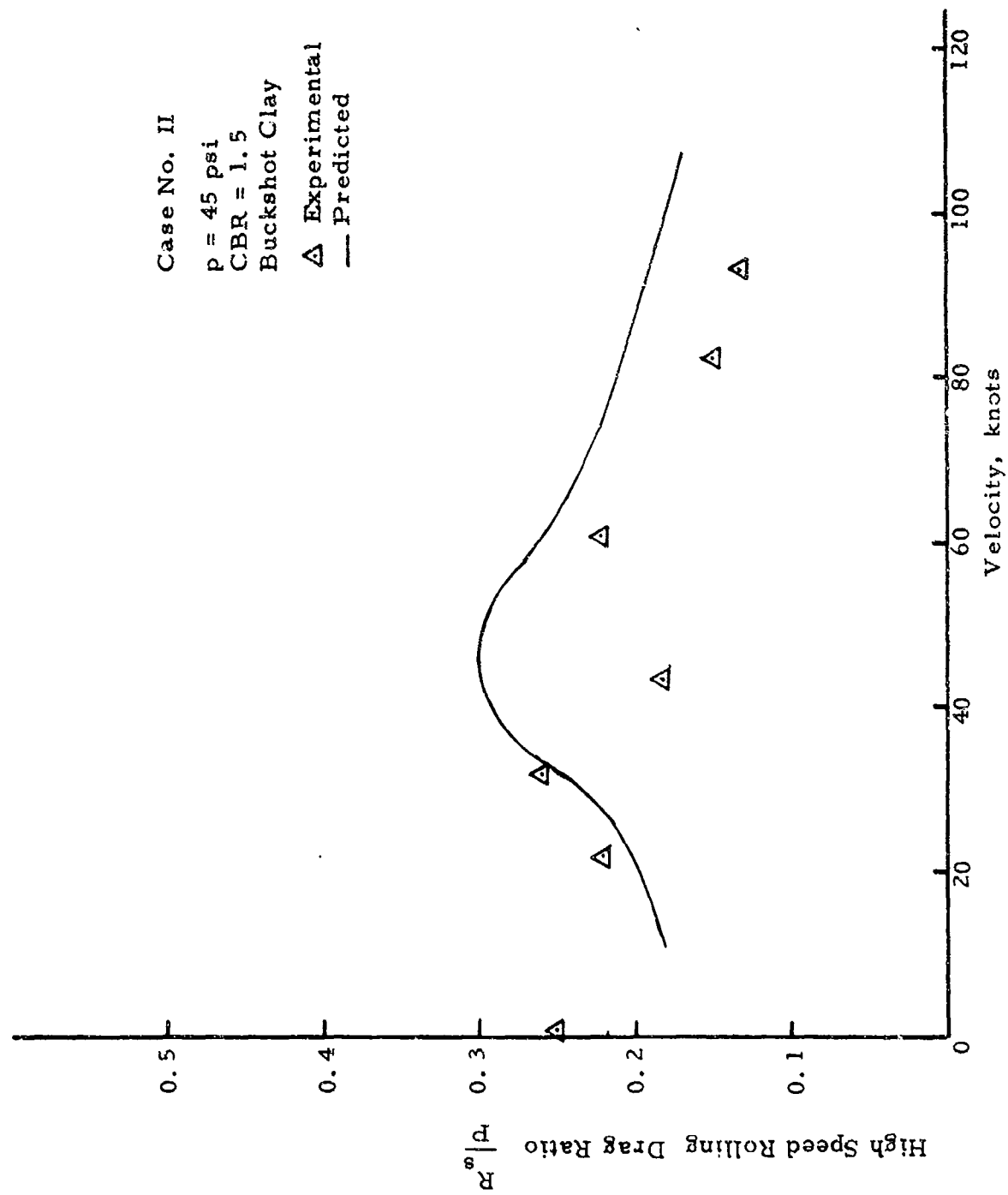


Figure 30. Experimental-Predicted, High-Speed Sinkage - Lockheed/Langley Tests, Case No. 2

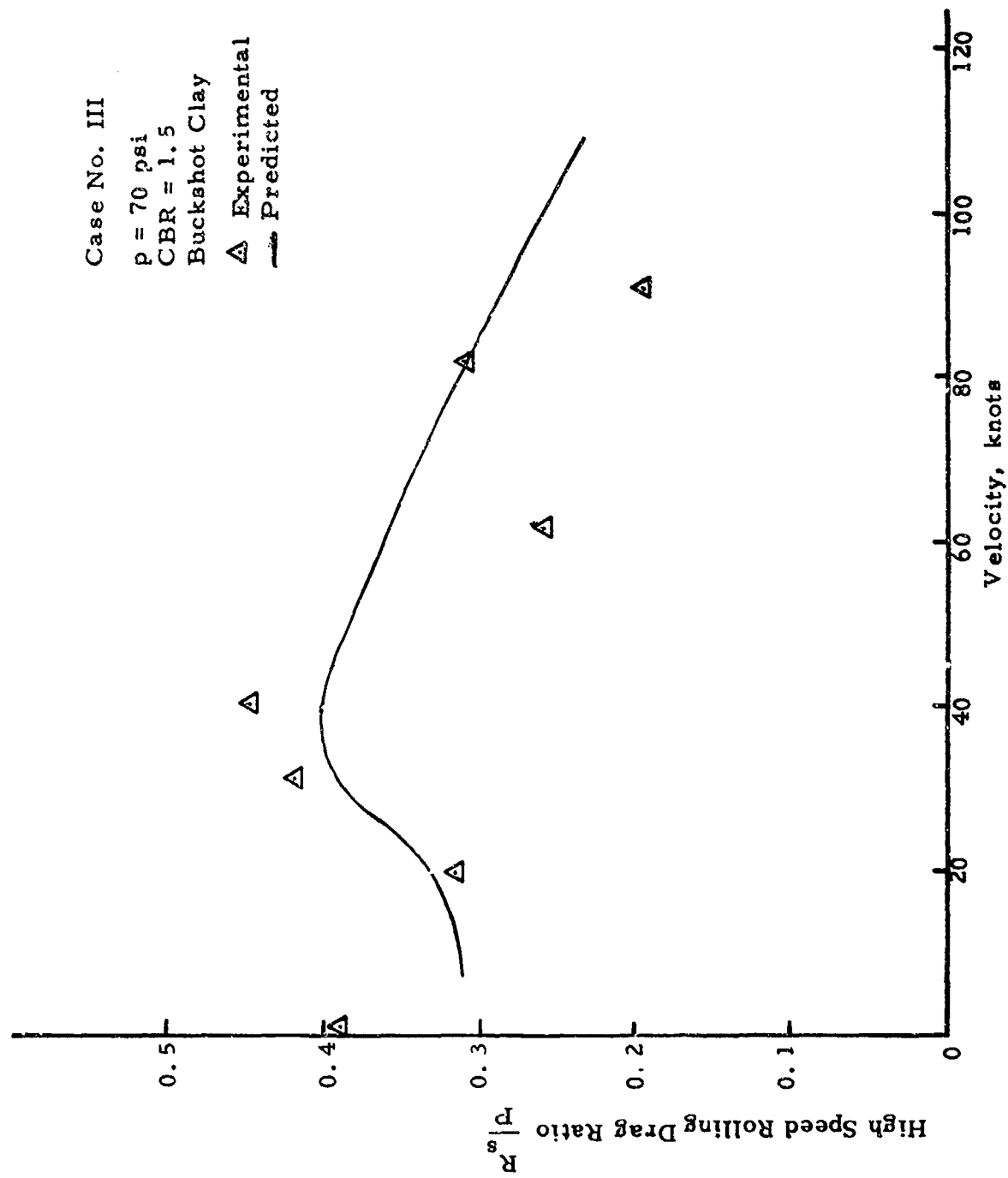


Figure 31. Experimental-Predicted, High-Speed Sinkage - Lockheed/Langley Tests, Case No. 3

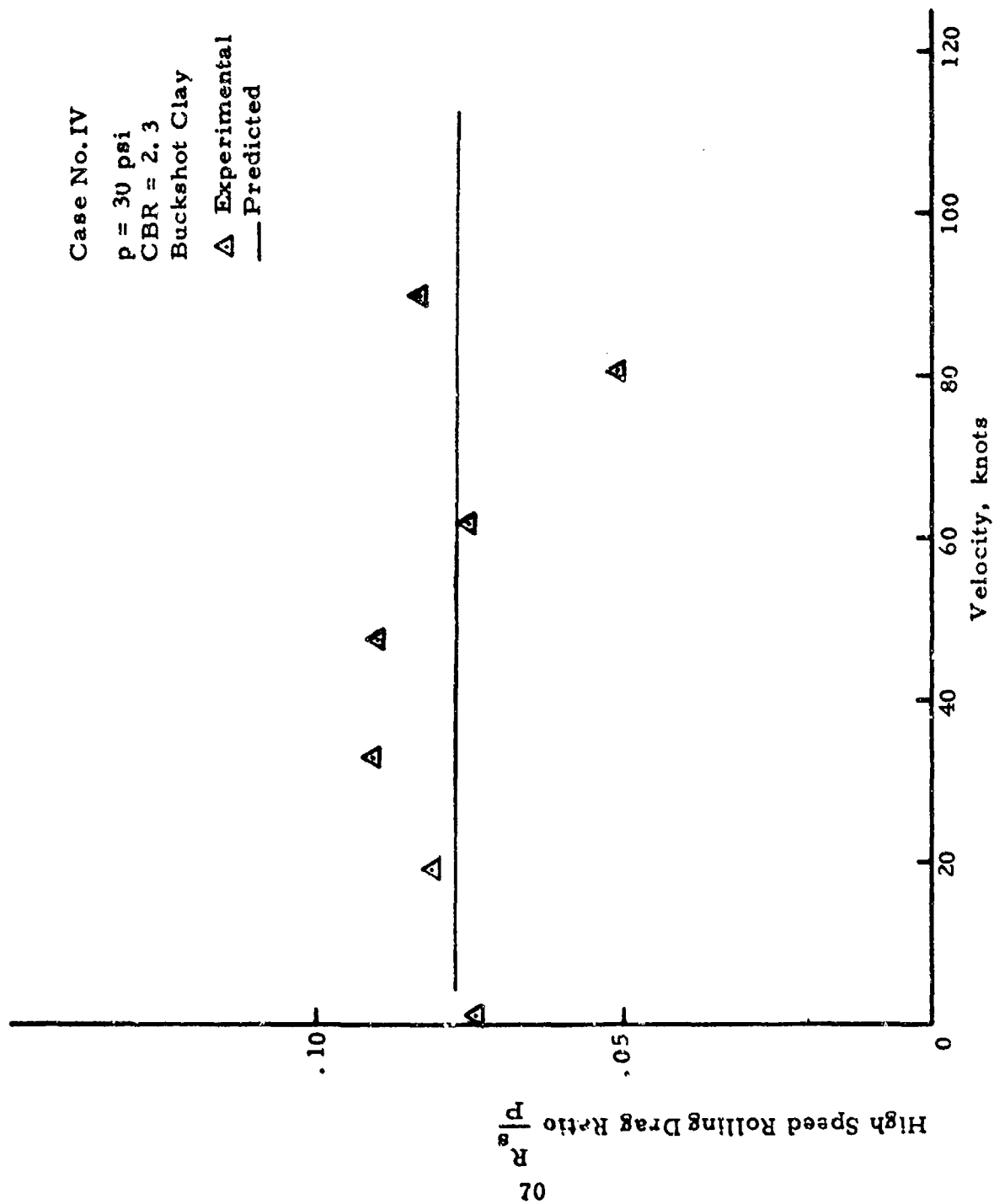


Figure 32. Experimental-Predicted, High-Speed Sinkage - Lockheed/Langley Tests, Case No. 4

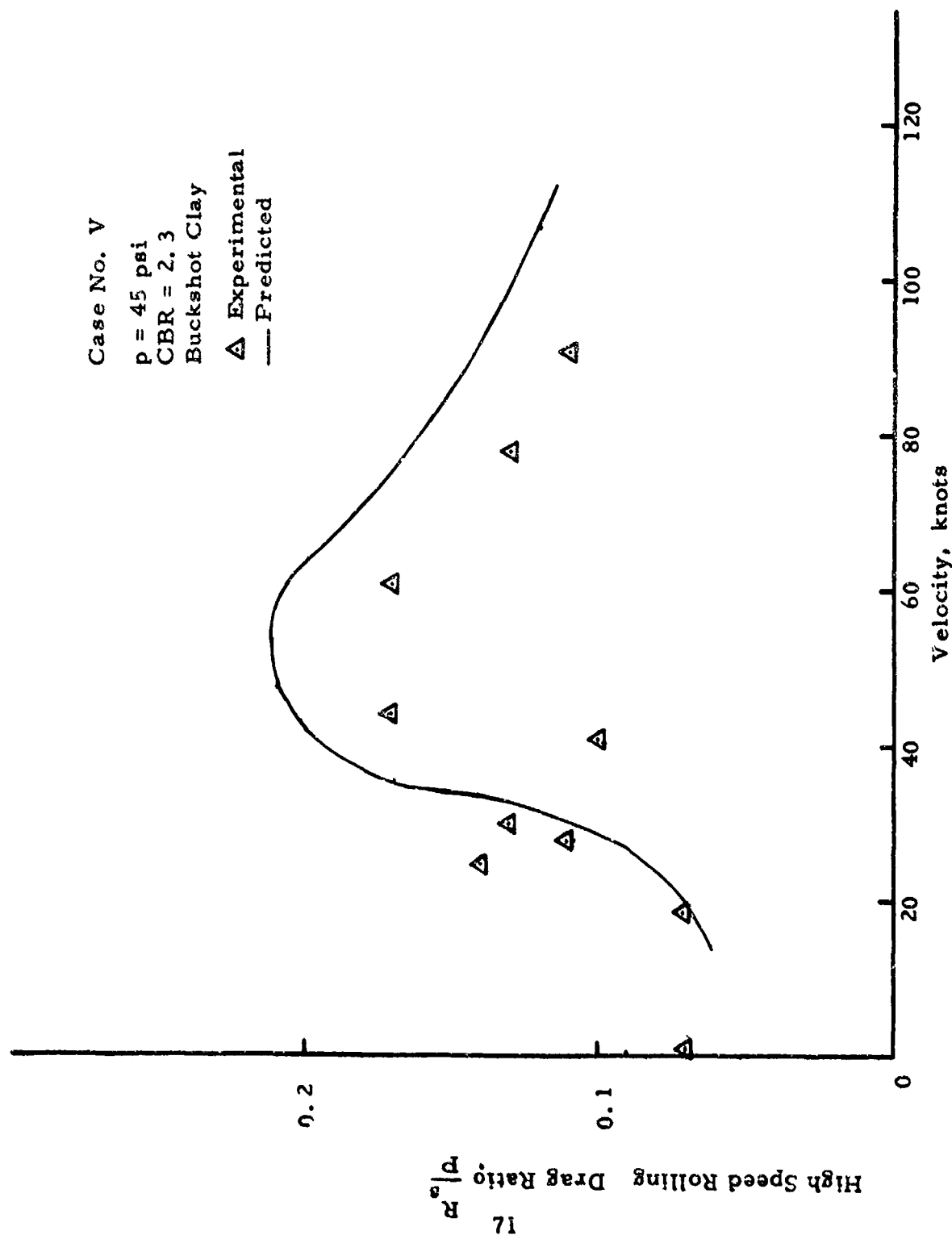


Figure 33. Experimental-Predicted, High-Speed Sinkage - Lockheed/Langley Tests , Case No. 5

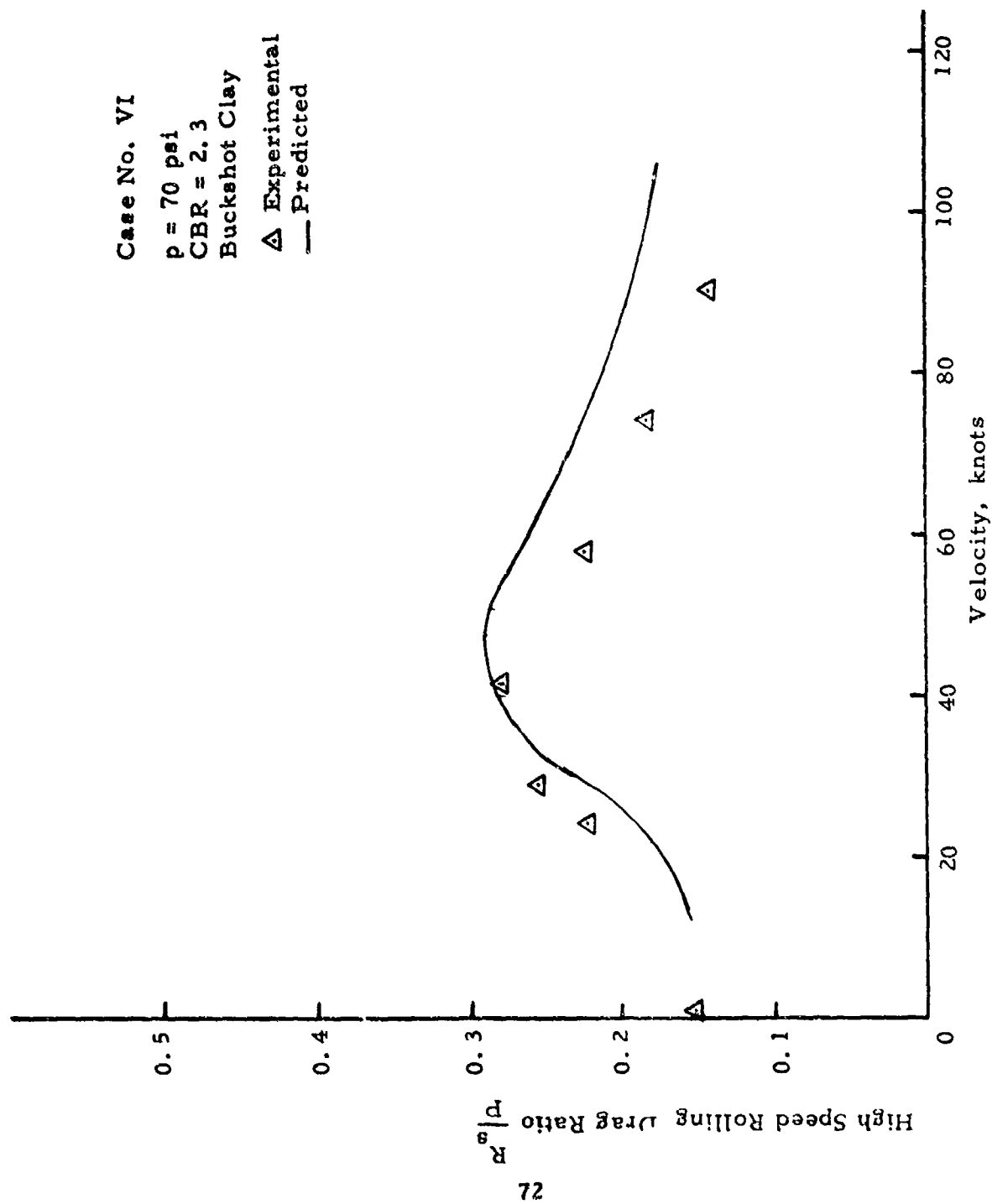


Figure 34. Experimental-Predicted, High-Speed Sinkage - Lockheed/Langley Tests, Case No.6

each of the cases does follow the trend of the experimental data. Reference to Figure 32 again points out that for low sinkage conditions in the 5 to 30 knot range (brought about by either low vertical tire loads or high soil strength), very little increase in the rolling drag ratio will occur at high speeds. For sinkage ratios (Z/D) less than about 0.02, very little increase in the drag ratio will occur at high speed.

In order to generalize the high speed rolling drag ratio predictive technique and extend its capability to a broader range of tire sizes and soil strengths, the empirically generated formula for determining the angle of attack, θ , was modified slightly and the computer program was used to evaluate about twelve different cases for a cohesive type soil. In general, the tire sizes ranged from 26" to 56". The results of two of the evaluations are given in Figure 35.

The results of the prediction technique development and comparative study are felt to be sufficiently promising to warrant the use of the technique, on a preliminary basis, to predict high speed rolling drag for aircraft operating on clay type soils. The use of dimensionless analysis techniques permits a limited extension to other aircraft, aircraft parameters, and operating conditions on cohesive type soils with the recognition that additional high speed experimental test data is necessary to fully document either this approach or a modified approach.

The results of the high speed tire/soil interaction studies conducted to date (December 1973) indicate the need for additional research and development as follows:

- additional high speed experimental test data in both the rolling and braking mode (either controlled or full scale field operation)
- instrumented tire-high speed soil interaction tests to better define the tire/soil contact geometry (angle of attack, etc.)

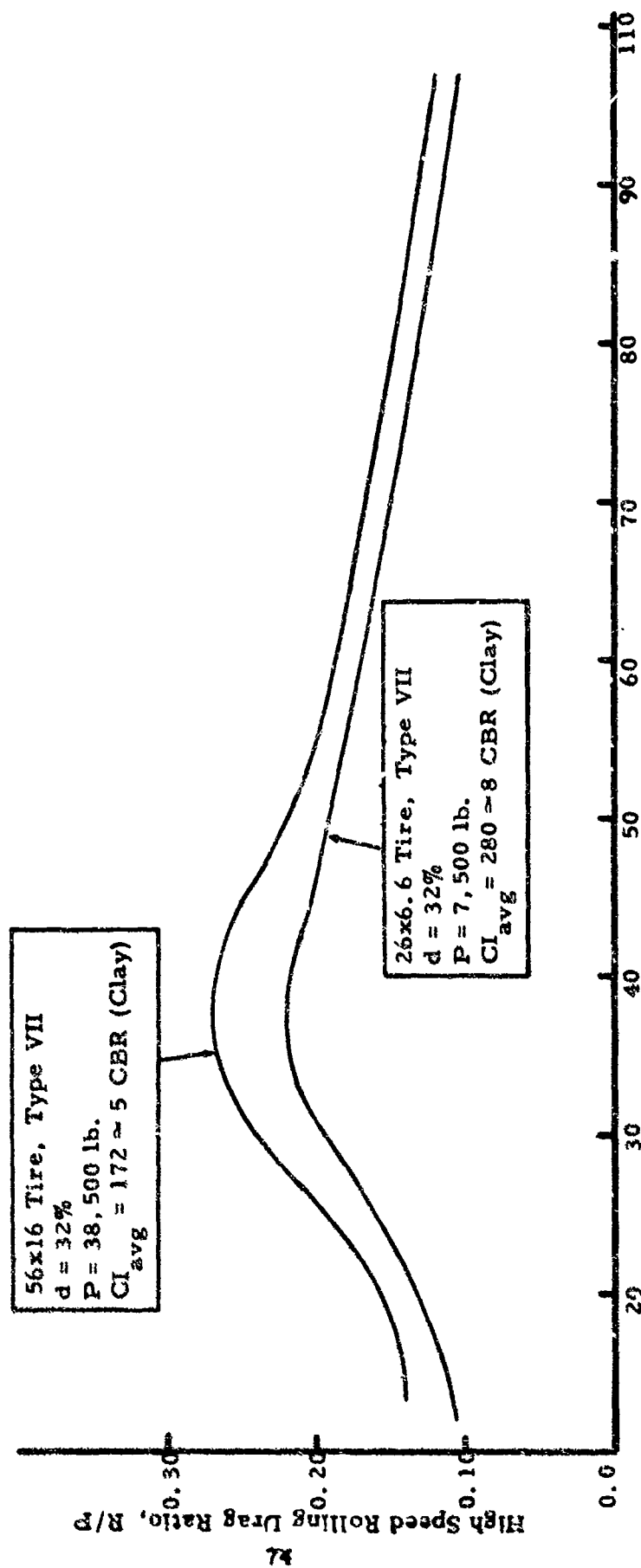


Figure 35. Examples of High Speed Rolling Drag Ratio Determinations Using Predictive Computer Program.

- incorporation of high speed drag prediction techniques in takeoff length prediction computer program (currently in progress in this research program)

SECTION IV

ADDITIONAL STUDIES IN TIRE/SOIL INTERACTION

A. AIRCRAFT TAKEOFF LENGTH PREDICTION COMPUTER PROGRAM

Incorporating the latest results of U. S. Air Force sponsored research on tire/soil interaction, a computer program is currently under development which will provide a predictive capability for aircraft soil drag, sinkage, and takeoff performance operating on soil runways. This FORTRAN IV computer program, with its various subroutines, has been written and is currently (December, 1973) being debugged. The takeoff length predictive capability accounts for:

1. Any loading gear configuration
2. Multiple wheel effects
3. Variable tire types and sizes
4. Variable soil strength
5. Variable aircraft gross weight and related parameters
6. High speed effects (restricted to clay type soils at present)
7. Runway slope.

The current program does not include the effects of runway roughness and variable dynamics loads and consequently is not a predictor of dynamic landing gear loads.

B. TRAINING SESSION - SHORT COURSE ON LANDING GEAR/SOIL INTERACTION AND FLOTATION SYSTEM DESIGN

Under sponsorship of AFFDL, a training session - short course on landing gear/soil interaction and flotation system design was held at the University of Dayton on September 18 and 19, 1973. The purpose of the short course was to disseminate the results of recent research activities in the study of tire/soil interaction effects to those individuals who are directly involved in aircraft planning, design, and use. A total of 18 individuals attended representing aircraft manufacturers, aircraft tire suppliers, and

government organizations involved in aircraft operation on soil runways. In covering the training material summarized below, videotapes and workshop problem sessions were used.

- Aircraft Tire Drag and Sinkage Analysis and Prediction
- Multiwheel Sinkage and Drag Effects and Prediction
- High Speed Rolling Drag Ratio Analysis and Prediction
- Braking Sinkage and Drag Analysis and Prediction
- Integrated Flotation Design System and Prediction Computer Programs

A complete set of instructional materials including videotapes, is available from the University of Dayton for the cost of reproduction. This information can be obtained from:

Dr. David C. Kraft
Professor of Civil Engineering
University of Dayton
Dayton, Ohio 45469

C. INTEGRATED FLOTATION DESIGN SYSTEM

Because of the significant research activities in aircraft tire/soil interaction conducted over the past five years, it is now possible to begin to put together the individual performance parameters (rolling performance, braking performance, multi-wheel effects, etc.) into a single comprehensive design system (procedure). Such a design system would utilize the aircraft performance requirements (gross load, performance in air, turning performance, etc.), the landing gear design limitations (number and location of bogies, number of tires per bogie, weight, etc.) and the soil parameters (soil strength, initial surface conditions, maximum allowable roughness of the soil surface) to select an optimum landing gear configuration, geometry, aircraft tires and to develop the operational criteria for the aircraft. The resulting aircraft performance factors such as rolling drag ratio, braking drag ratio, takeoff and landing lengths, turning effects, etc. could then

be used in conjunction with weighting factors to make a final selection of the appropriate landing gear system. A preliminary effort in this direction was made by the University of Dayton and used in the prototype studies for the medium STOL aircraft.

This design procedure⁽²⁾ was a first attempt and included the latest results of U.S. Air Force sponsored research and the previously developed WES coverage techniques. The design procedure, subject to certain limitations, includes techniques for:

- 1) Predicting rolling and braking drags and drag ratios.
- 2) Incorporating multiwheel influences on sinkage and drag.
- 3) Determining aircraft passes.

Takeoff length technique and computer program, briefly described in A above, will be added to the design procedure in the near future so that the design procedure capability will be expanded to include:

- 4) High speed rolling drag and drag ratios.
- 5) Aircraft takeoff length.

This design procedure computer program⁽²⁾ is also available on the CDC 6600 Computer located at Wright-Patterson Air Force Base.

Current restrictions in the design procedure are:

- 1) Tricycle landing gear type aircraft.
- 2) Aircraft takeoff/landing weights in the 150,000 to 250,000 pound range.
- 3) Lower speed performance (< 40 knots, the incorporation of the takeoff length portion will extend predictive capability throughout the entire takeoff speed range).
- 4) Low speed (< 15 knots) braking.
- 5) Cohesive type soil and soil strength of CBP or equivalent (this was done specifically for the MSTOL design and the program is being generalized to a variable soil strength).

Restrictions (2), (3), and (5) will not be present upon completion of the current modifications in the design computer program.

The general procedure for optimizing the flotation capability of landing gears consists of a series of calculations which must be performed for each of the selected tires and landing gear systems (groups of tires). The result will be a number of tire/landing gear systems to which appropriate weighting factors can be assigned for:

- minimization of rolling drag
- maximization of passes

Additional weighting factors must be assigned to such parameters as gear weight, surface area of gear, storage volume requirements, etc., leading to the final selection of the tire/landing gear system which is most appropriate for the aircraft.

SECTION V

APPLICATIONS TO CURRENT MILITARY SPECIFICATIONS

The results of the turned tire tests can be related to existing specifications for the design of aircraft. Military Specification MIL-A-008862A, Airplane Strength and Rigidity, Landing and Ground Handling Loads, contains specified values for limiting side force ratios of tires. Paragraph 3.3.2, Turning, limits the ratio of side force to vertical load to 0.5 on any wheel. The results of the test data presented indicate that this is a reasonable limit.

Side force ratios for tire tests in sand and clay type soil approach and in some cases may exceed 0.5. The curves indicate that for the configurations tested the side force ratio at angles greater than 20 degrees may be decreasing. Apparently, there is some limiting side force which can be developed for a particular tire. Increasing the turn angle beyond that point may not increase the force developed. Testing at very large turn angles could verify or refute this.

Paragraph 4.6 of the specification provides additional means of specifying tire/soil loads in turns. The equations and figures presented indicate that side forces on tires will not exceed 0.5 times the vertical load. As mentioned above, this is consistent with the data collected.

Air Force Systems Command Design Handbook Chapter 4, Ground Flotation, indicates that the current criteria for multipass operation on unprepared soils is based upon permanent rutting to a depth of three inches on a heavy clay soil. The rutting measured indicates that the ratio of turning sinkage to non-turning rolling sinkage may approach a factor of three. Therefore, it appears that additional multipass criteria should be formulated either to express failure in terms of rut depth for a vehicle configuration, or to indicate that runway areas used for turning should be avoided. Turn around areas may require special analysis to determine their operational limits.

Rolling drag ratio is mentioned in MIL-A-008862A only in paragraph 3.3.1, Braking. In this section, the unbraked wheel drag for bare soil fields is specified at 0.2 times the vertical reaction. Previous research as well as current high speed rolling drag prediction effort indicates that sinkage (and hence drag) are dependent upon many variables. While low speed-small sinkage conditions will not significantly influence takeoff length, high speed-high sinkage conditions should be mentioned. Rolling drag ratios twice as great as specified are possible.

The specifications mentioned do not reflect the state-of-the-art in calculating tire/soil interaction. The turned tire data do indicate the side force ratios for the tire are realistic. However, the loads equations do not reflect the fact that there are different soils, soil strength, tire configurations and variable forward velocity. The turning criteria indicate how centrifugal force influences vertical forces but ignores the pitching moment due to soil drag which could be significant.

In any calculation of drag, velocity effects are not mentioned, the drag to be calculated is only a function of a coefficient of friction. Tire configuration, landing gear configuration, soil strength and type are not required. The effects of these parameters could be included by a presentation of a tabulated procedures in the same manner as shown in the Design Handbook to determine allowable number of passes.

The difficulty in generating specifications for soil forces is due to the fact that the mechanism that generates side and drag force is a function of many variables. There is no "coefficient of friction" that can be easily used and accurately represent the phenomena.

SECTION VI

CONCLUSIONS AND RECOMMENDATIONS

The results of the first year efforts (Part I) of the two-year landing gear/soil interaction research program have provided considerable insight into the response mechanism and the buildup of side loads on aircraft tires as they undergo a turning operation. More specifically, the turning studies have shown that:

- (1) The lateral load ratio, L/P (where L = resultant lateral load and P = vertical load on tire) will exceed one-half for aircraft operating in a turning mode at moderate sinkage levels.
- (2) Severe rutting will occur for aircraft turning on soil runways. The most severe rutting will occur in frictional type soils (the ratio of turning sinkage to non-turning rolling sinkage may approach 3.0 in granular soils).
- (3) Within the normal operating range of aircraft tire deflections (32% to 40%), tire deflection has very little influence on side load buildup for turning aircraft tires.
- (4) The aircraft turning operation predictive technique and computer program provides a means both for design evaluation and the establishment of turning criteria for aircraft operating on soil runways.

The high speed rolling drag ratio (R/P , where R = rolling drag and P = vertical load on tire) analysis generally indicates that:

- (1) For low speed (5 knots to 25 knots) -small sinkage conditions ($Z/D < 0.02$), the high speed drag ratio will not increase significantly and will have little influence on the takeoff length.

- (2) In those situations where low speed (5 knots to 25 knots) sinkages are moderate to high ($Z/D > 0.03$), the increase in the high speed drag ratio will be substantial and will significantly influence the takeoff length.
- (3) The high speed rolling drag ratio predictive technique and computer program, although subject to certain limitations, does permit preliminary estimates on the influence of aircraft forward speed on rolling drag ratios and takeoff lengths.

The state of the art developments in tire/soil interaction research now permits substantial efforts and progress to be made in establishing an integrated approach to design procedures and criteria for aircraft whose mission includes the requirement for operating from unimproved runways. The design procedure developed for the medium STOL aircraft ⁽²⁾ represents a first step in that direction.

Future research efforts for landing gear/soil interaction should be directed in the following areas:

- (1) Continuing effort to gather operational data for aircraft on soil runways (i.e., steer angles in turning, side loads in turning, etc.) in order to continually verify and update predictive techniques.
- (2) Evaluation of advanced tire types and designs (i.e., expandable tire, replaceable tread tire, etc.) to establish their flotation characteristics and performance on soil.
- (3) Instrumentation of aircraft tires to provide a better insight into the boundary conditions and forces at the tire/soil interface leading to an improved interaction mathematic model.
- (4) High speed effects on braking and turning tire/soil loads and interaction response.

REFERENCES

1. Kraft, David C., et. al, "Multiwheel Landing Gear-Soils Interaction and Flotation Criteria - Phase III, Part II, " AFFDL-TR-71-12, Part II, Air Force Flight Dynamics Laboratory, Wright-Patterson Air Force Base, Ohio, January 1972.
2. Kraft, David C. and Hoppenjans, J. Richard, "Design Procedure for Establishing Aircraft Capability to Operate on Soil Surfaces," AFFDL-TM-71-09-FEM, Air Force Flight Dynamics Laboratory, Wright-Patterson Air Force Base, Ohio, September 1971.
3. Kraft, David C., Luming, Henry, and Hoppenjans, J. Richard, "Multiwheel Landing Gear-Soils Interaction and Flotation Criteria - Phase III, Part I, " AFFDL-TR-71-12, Part I, Air Force Flight Dynamics Laboratory, Wright-Patterson Air Force Base, Ohio, May 1971.
4. Kraft, David C., Luming, Henry, and Hoppenjans, J. Richard, "Aircraft Landing Gear-Soils Interaction and Flotation Criteria, Phase II," AFFDL-TR-69-76, Air Force Flight Dynamics Laboratory, Wright-Patterson Air Force Base, Ohio, November 1969.
5. Kraft, David C., "Analytical Landing Gear-Soils Interaction, Phase I," AFFDL-TR-68-88, Air Force Flight Dynamics Laboratory, Wright-Patterson Air Force Base, Ohio, May 1968.
6. Crenshaw, B. M., and Butterworth, C. K., "Aircraft Landing Gear Dynamic Loads from Operation on Clay and Sandy Soil," AFFDL-TR-69-51, Air Force Flight Dynamics Laboratory, Wright-Patterson Air Force Base, Ohio, September 1968.
7. Turnage, G. W., and Brown, D. N., "Prediction of Aircraft Ground Performance by Evaluation of Ground Vehicle Rut Depths," Technical Report - Working Draft Only, U. S. Army Engineers Waterways Experiment Station, Vicksburg, Mississippi, 1973.
8. Richmond, L. D., et. al., "Aircraft Dynamic Loads from Substandard Landing Sites, " AFFDL-TR-67-145, Air Force Flight Dynamics Laboratory, Wright-Patterson Air Force Base, Ohio, September 1968.
9. Ladd, D., et. al., "Aircraft Ground Flotation Investigation," AFFDL-TR-66-43, Air Force Flight Dynamics Laboratory, Wright-Patterson Air Force Base, Ohio, August 1967.

10. Islinger, J. S., Investigation to Determine Criteria for Designing Aircraft Nose Gear Steering Systems, Technical Report WADC-TR-55-34, Wright-Patterson Air Force Base, Ohio, November 1955.
11. Hancock, K. G., and Pearson, P., "Steering Aircraft on the Ground," Aeroplane, London, 82:239-241 (February 29, 1952).
12. Schwanghart, H., "Lateral Forces on Steered Tires in Loose Soil," Journal of Terramechanics, 5/1: 9-29 (1968).
13. Taylor, P.A. and Bertwistle, R., "Experimental Studies of Force Systems on Steered Agricultural Tires," Institution of Mechanical Engineers, (London) Automobile Division Proceedings, 181/4:133-148 (1966-1967).

APPENDIX I

1. UNIVERSITY OF DAYTON LINEAR TIRE/SOIL TEST TRACK AND TURNED TIRE TEST PROGRAM

A. Test Setup and Instrumentation

The test facility consists of a linear tire/soil interaction test track with a powered carriage for moving the tire over the soil bed, the required force and velocity sensing devices, and a data recorder.

Test Track

The test track is 24 feet long, 2.5 feet wide, and 3 feet deep. For this series of tests, a false bottom was used to provide an 8-foot long "test section" in the center of the track with a soil depth of about 12 inches. The false bottom at either end of the "test section" tapered to zero soil depth at the ends of the track. An overall view of the test track is shown in Figure 3.

Rails at the top, on both outer edges of the track, provide guidance for a carriage assembly which may be towed the entire length of the track by means of an endless cable and capstan arrangement. The carriage is supported by hard rubber guide wheels which provide complete vertical and lateral control of the carriage position. The test tire is supported by a fixture which is, in turn, attached to the carriage assembly by means of a pivoted bracket as shown in Figure 4. This permits the tire and test fixture to move in a vertical plane parallel with the direction of motion of the carriage. The pivot bearings which provide this vertical motion are the same distance above the soil bed as the nominal position of the test wheel axle. This prevents the introduction of vertical loads into the test wheel by the towing force. The proper vertical loading on the test tire is obtained by attaching weights to the free (rear) end of the pivoted bracket as shown in Figure 4. The test tire is "turned" at various angles to the direction of travel by bolting the test fixture to the pivoted bracket at the appropriate angle. A series of holes is provided in the bracket to accommodate turn angles of 0, 5, 10, 15, and 20 degrees. Figure 4 shows the tire turned 20 degrees.

Carriage Drive System

The carriage is towed along the test track by means of an "endless" cable which wraps around a driving capstan. The ends of the cable are attached to the forward and rear ends of the carriage. This scheme is shown in Figure 3. The cable runs over sheaves at both ends of the track so the "return" side of the cable is about two feet above the test bed. The "return" side of the cable is also equipped with a turnbuckle so that cable tension may easily be adjusted to the proper value. This system allows the carriage to be towed in either direction and also permits braking action at the end of the run.

The cable capstan is driven, through a belt and gear-box arrangement, by a 7-1/2 H.P., 3-phase induction motor. The load on the motor is so small compared to its rating that it is essentially a constant speed drive. A motor control system consisting of a portable control station, carriage actuated limit switches, a relay/timer unit, and a reversing motor starter is used to control the carriage motion. Limit switches provide for positive motor power shut-off when the carriage reaches either end of the track and initiates the braking sequence during a test run as the test wheel leaves the "test section" of the track. Braking action consists of a momentary reversal or "plugging" of the drive motor. By controlling the time that the motor is reversed, a relatively smooth deceleration is achieved that does not overstress the load measuring fixtures. A "jog" feature is also provided to allow positioning of the carriage at any point along the track. A typical operation sequence for the turned tire tests involves positioning the carriage at the "start" end of the track and actuating a RUN switch. The carriage is towed through the "test section" of the track and then braked before it reaches the end of the track. The motor drive and capstan system used for this series of tests results in a carriage velocity of about 6 feet per second.

Instrumentation

The turned tire tests require the measurement of the vertical, in-line drag, and side loads on the test tire. A special test wheel support fixture was designed to separate and measure these three load components. The fixture is shown in Figure 36, and consists of an instrumented axle, supported by two instrumented vertical support members which, in turn, are attached to a mounting plate. As indicated in the figure, the axle is connected to the left-hand support member by means of a spherical bearing and to the right-hand support member by a spherical bearing and a linear ball bearing. Assuming that these bearings are frictionless (for the light loadings involved, the friction is very low), the axle and the vertical support members will be subjected only to bending forces as a result of forces on the tire; and the vertical, in-line drag, and side forces will be effectively isolated from each other. The axle has bending sections provided on either side of the wheel, and these are instrumented with a four-active-arm strain gage bridge connected to respond to bending. The output of these two bridges, therefore, is a function of the vertical load on the tire. The vertical support members also have bending sections that are instrumented with four-active-arm strain gage bridges. The member on the left side of the wheel (see Figure 36) has gages to measure both the in-line drag and side loads, while the right-hand support member is instrumented only for in-line drag load. No side load is fed into the right-hand member because of the linear ball bearing connection to the wheel axle. The strain gages are not visible in Figure 36 because the gages and associated wiring have been covered with a protective rubber compound.

All the force measuring members on the test fixture were made of 7075-T6510 aluminum in order to achieve a high strain to yield stress ratio. Maximum design load limits for the test fixture are as follows: vertical load 250 lbs each side of axle, 500 lbs total; in-line drag load 250 lbs each side, 500 lbs total; side load 400 lbs total. The strain gages (Micro-Measurements Type E A 13250 MQ-350) were bonded to the aluminum with epoxy adhesive to

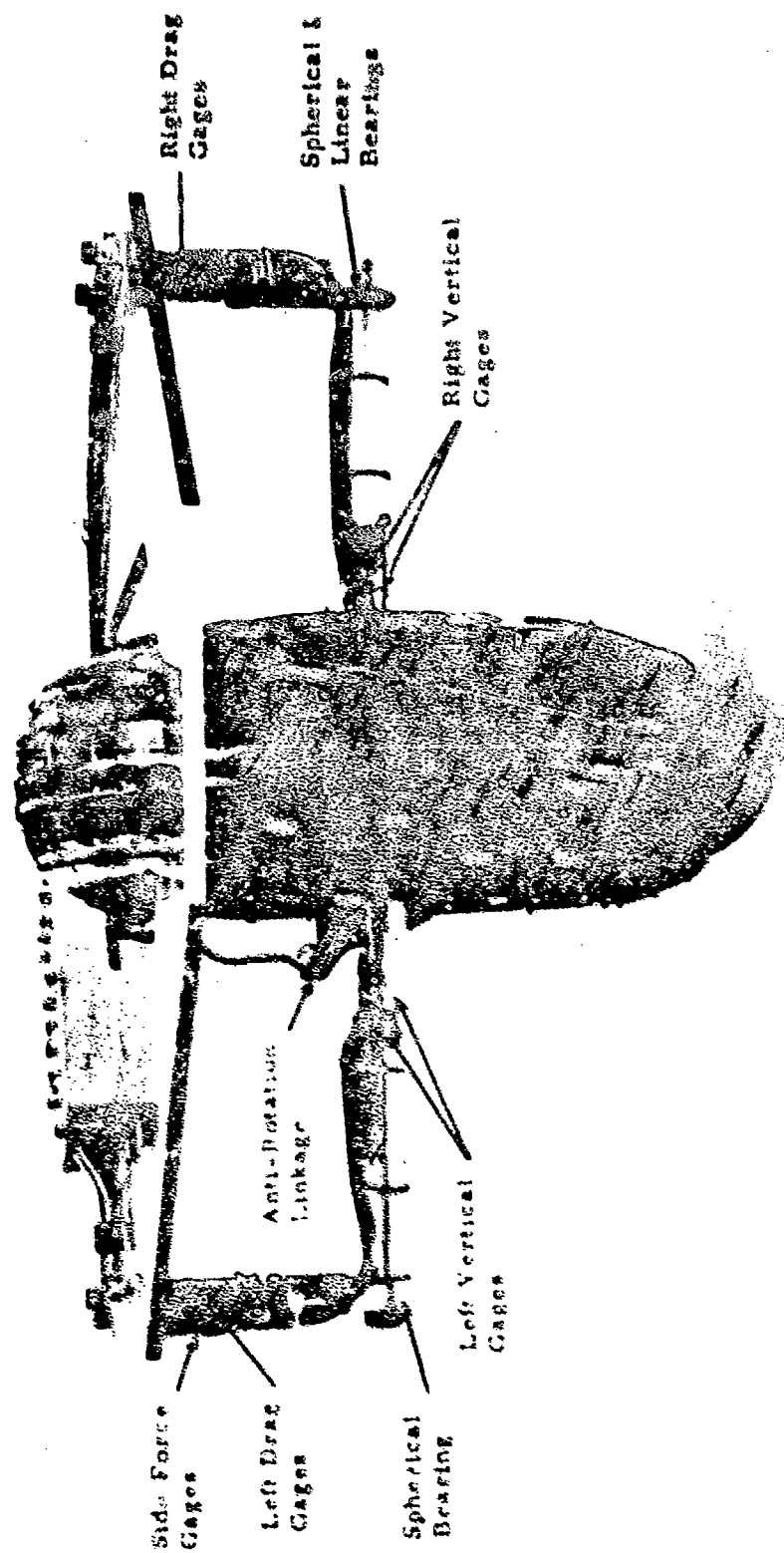


Figure 16. Load Measuring Test Fixture, UD Linear Test Track

provide a strong, long term bond. The gage installations were covered with rubber compound to exclude moisture and to provide physical protection.

Recording of the strain bridge outputs was accomplished with D.C. bridge excitation; a CEC (Consolidated Electrodynamics Corp.) model 8-108 bridge balance unit and a CEC model 5-114 recording oscillograph. The model 8-108 bridge balance provides all the balancing, sensitivity, and shunt resistance calibrations functions required for the bridge circuits. Electrical connections between the instruments and the test track carriage were made with a bundle of 4-conductor, shielded cables running from the bridge balance to the ceiling of the laboratory and down to the carriage. Bungee cord was used to keep the cables taut as the carriage moved along the track.

In addition to the measurement of loads on the test tire, it is necessary to know the position and velocity of the test carriage. This measurement utilized an assembly consisting of a phototransistor viewing a light source, mounted on the test carriage, and a series of light beam interrupting brackets mounted on the test track braces. These items may be seen in Figure 3. Interruption of the light beam to the phototransistor caused an event mark on the oscillogram. The devices were located to provide event marks as the tire entered the test section of the track, as it left the test section, and three intermediate points.

Calibration of the various load measuring members of the test fixture was accomplished using the dead-weight method. Before assembly of the fixture, the individual members were clamped to supports and dead weight loads were applied to the same locations as the actual test loads would be introduced. Because the test fixture utilized the spherical and linear bearings in the connections between members, there is no interaction between members and this type of calibration technique is valid.

As the loads were applied in a series of steps, the strain bridge output was recorded on the oscillograph using the same cables and equipment as

used on the test track. Shunt resistance calibration steps were also recorded on the oscillograph. By using this technique and recording shunt resistance calibration steps prior to each series of test track runs, data reduction is performed in terms of "percent of calibration" and all changes in galvanometer sensitivity, bridge excitation voltage, etc., are automatically compensated for. Figure 37 shows the results of a typical force member calibration.

Test Procedure

Prior to the start of a series of test runs and after all equipment has become temperature stabilized, a shunt resistance calibration is performed on each force measuring data channel. This is accomplished by operating the controls on the CEC bridge balance unit and making a short oscillogram for each calibration. Also, the zero position of all traces is recorded by supporting the carriage test fixture so the tire just clears the test track. Under these conditions there is no force on the tire.

When all test conditions have been properly set (soil bed prepared, soil tests completed, tire inflated, turn angle set, vertical load set, drive cable tensioned) and the instrumentation is prepared (calibrations and zeros recorded, velocity sensor light on), the carriage is jogged to the starting position with the tire supported above the test bed. The test run sequence consists of lowering the wheel onto the test bed, starting the oscillograph, initiating the carriage "run" function, and, after the carriage has stopped, turning off the oscillograph. The necessary measurements and documentation of the tire rut completes the test.

Typical Test Data

A typical oscillogram for a test run is shown in Figure 38. This is a record of a test with a zero turn angle and shows only the initial part of the test run. The zero positions of the traces are not shown on this segment of the oscillogram, however, the force and time scales give some indication of the sensitivity of the recording.

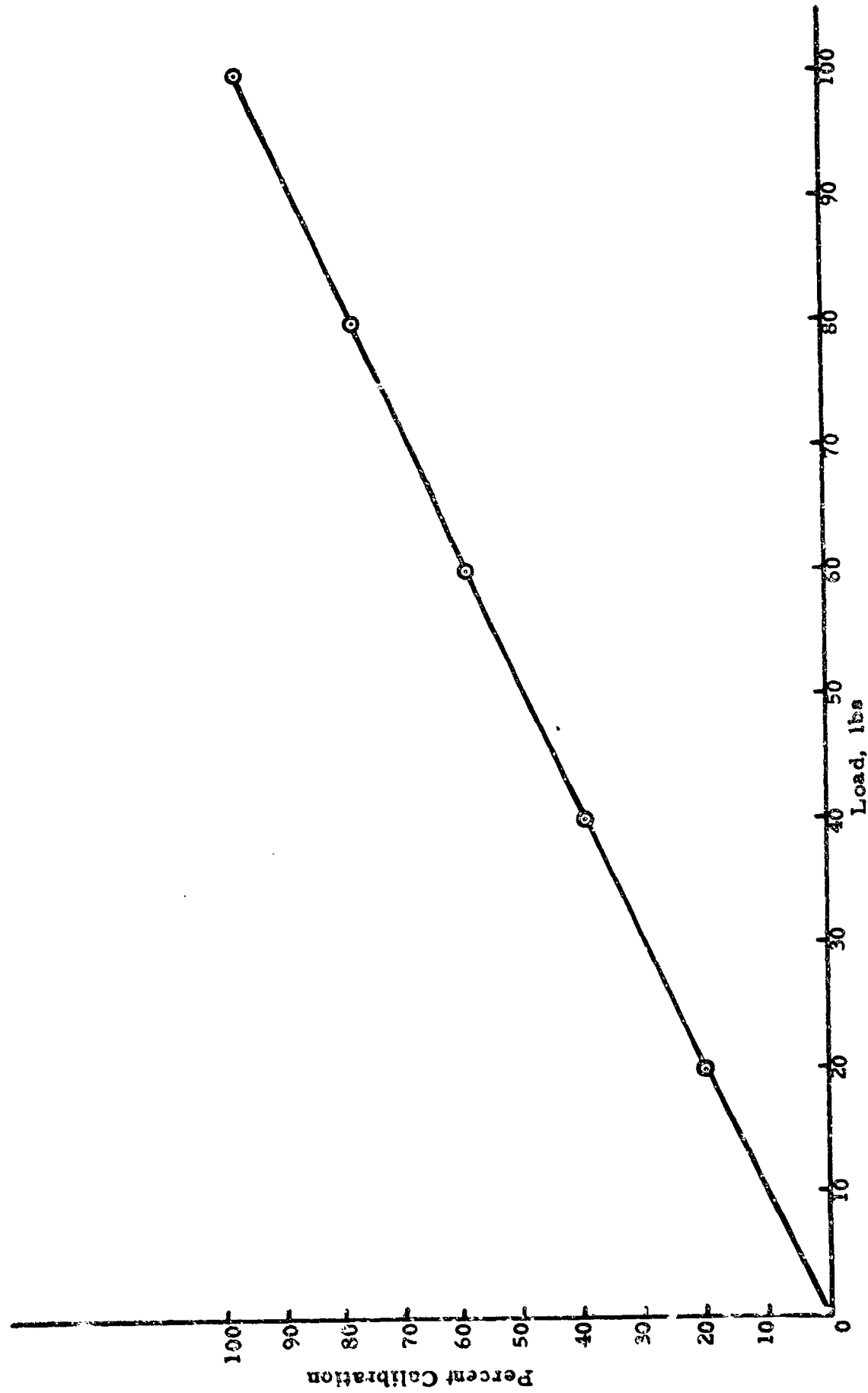


Figure 37. Typical Force Member Calibration, UD Test Carriage

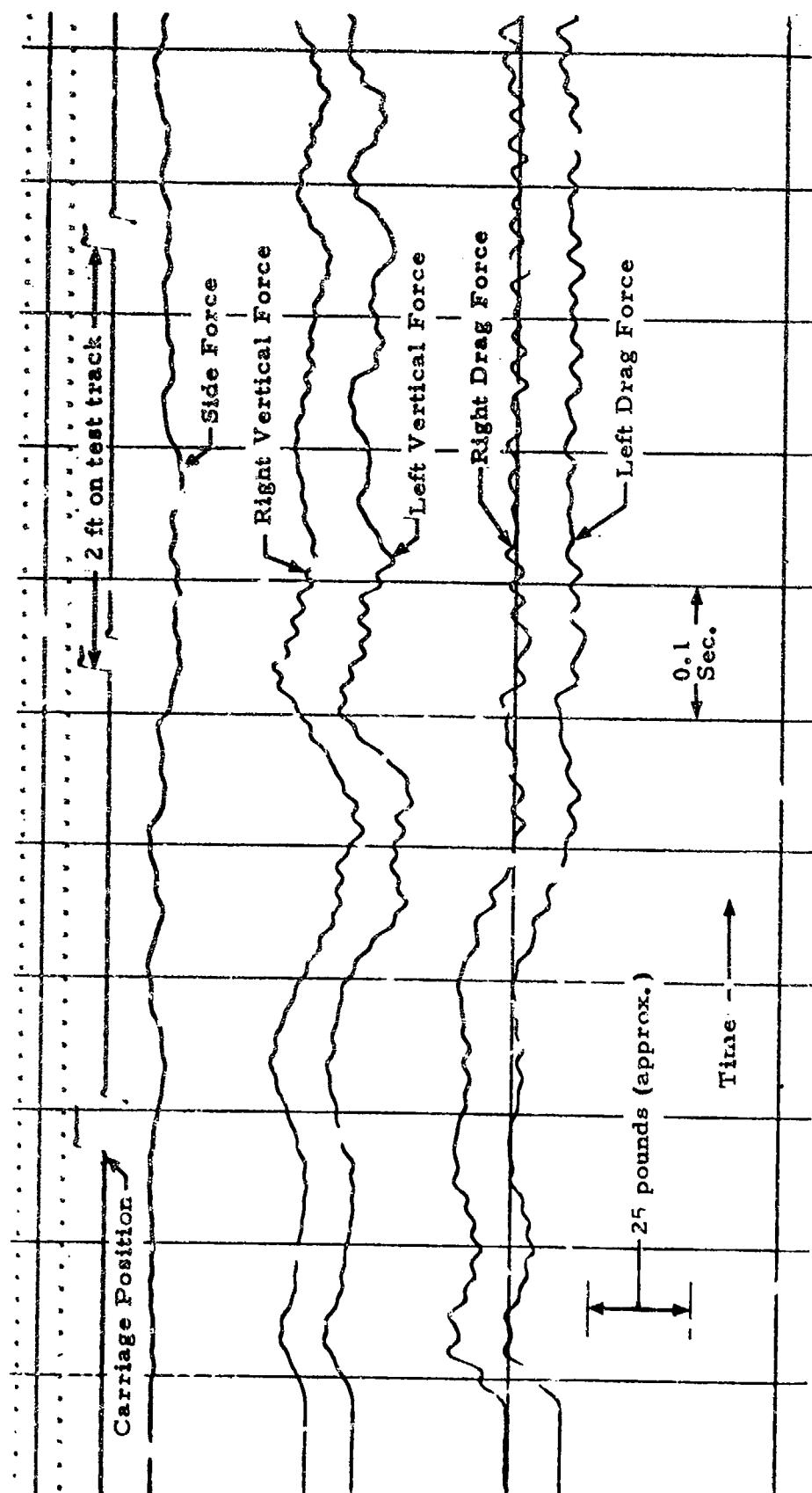


Figure 38. Typical Oscillographic Data Recording, 0° Turn Angle

B. Soil and Test Tire Property Data

Soil Preparation and Test Procedure

The following procedure was used in preparing the soil test bed and conducting each test:

1. Prepare the soil test section to a uniform strength and surface elevation. Both the sand and clayey silt soil were prepared to a predetermined moisture content by thorough mixing in a Porto-Muller mixer. The soil was then placed in the test bed section in approximate 6" to 8" thick loose lifts and compacted using a Master T-2000 vibratory compactor. In subsequent tests on a given soil, only the upper 8" was loosened and recompact before the next test run.
2. Cone index penetration tests were conducted along the soil bed to determine a soil strength profile. The soil surface elevation profile was also determined. The average penetration resistance for each test-bed is given in Table XIII and a moisture-density summary is given in Table XIV.
3. Calibration checks were made on the test instrumentation and sensing devices.
4. The tire load was set and tire deflection was checked.
5. The test was conducted and all test parameters were recorded.
6. Post test soil strength (cone index) tests and rut depth measurements were made.

Soil Properties of Test Beds

TABLE XIII
SOIL TEST BED - AVERAGE SOIL STRENGTH RESULTS (UD TESTS)

Turn Angle	Soil Type	Average Cone Index CI_{avg} *
0°	Riverwash Sand	74.7
5°	Riverwash Sand	72.5
10°	Riverwash Sand	73.1
15°	Riverwash Sand	74.7
20°	Riverwash Sand	76.8
0°	Clayey Silt	43.0
5°	Clayey Silt	31.7
10°	Clayey Silt	35.1
15°	Clayey Silt	33.8
20°	Clayey Silt	34.9

* CI_{avg} is average penetration resistance over 0" to 6" depth
(number shown in Table is average of several tests)

TABLE XIV
MOISTURE-DENSITY SUMMARY (UD TESTS)

Soil Type	Dry Unit Weight (lbs/ft ³)	Moisture Content (%)
Riverwash Sand	-	6.3
Clayey Silt	129.0	29.6

TABLE XV
CLAYEY SILT SOILS DATA (UD TURNED TIRE TEST PROGRAM)

Dry Unit Weight	=	129.0 PCF
Moisture Content	=	29.6%
Liquid Limit	=	31.0
Plastic Limit	=	24.0
Plastic Index PI	=	7.0

TABLE XVI
5.00-5 TIRE TEST DATA

Tire Type	Carcass Diameter (in)	Section Width (Unloaded) (in)	Wheel Load (lbs)	Rigid Surface Tire Print Area (in ²)	Rigid Surface Tire Print Length (in)	Tire Per Cent Deflection (%)
5.00-5, 4 PR	14.2	4.8	145	5.7 in ²	3.6	17
5.00-5, 4 PR	14.2	4.8	115	6.1 in ²	3.7	17

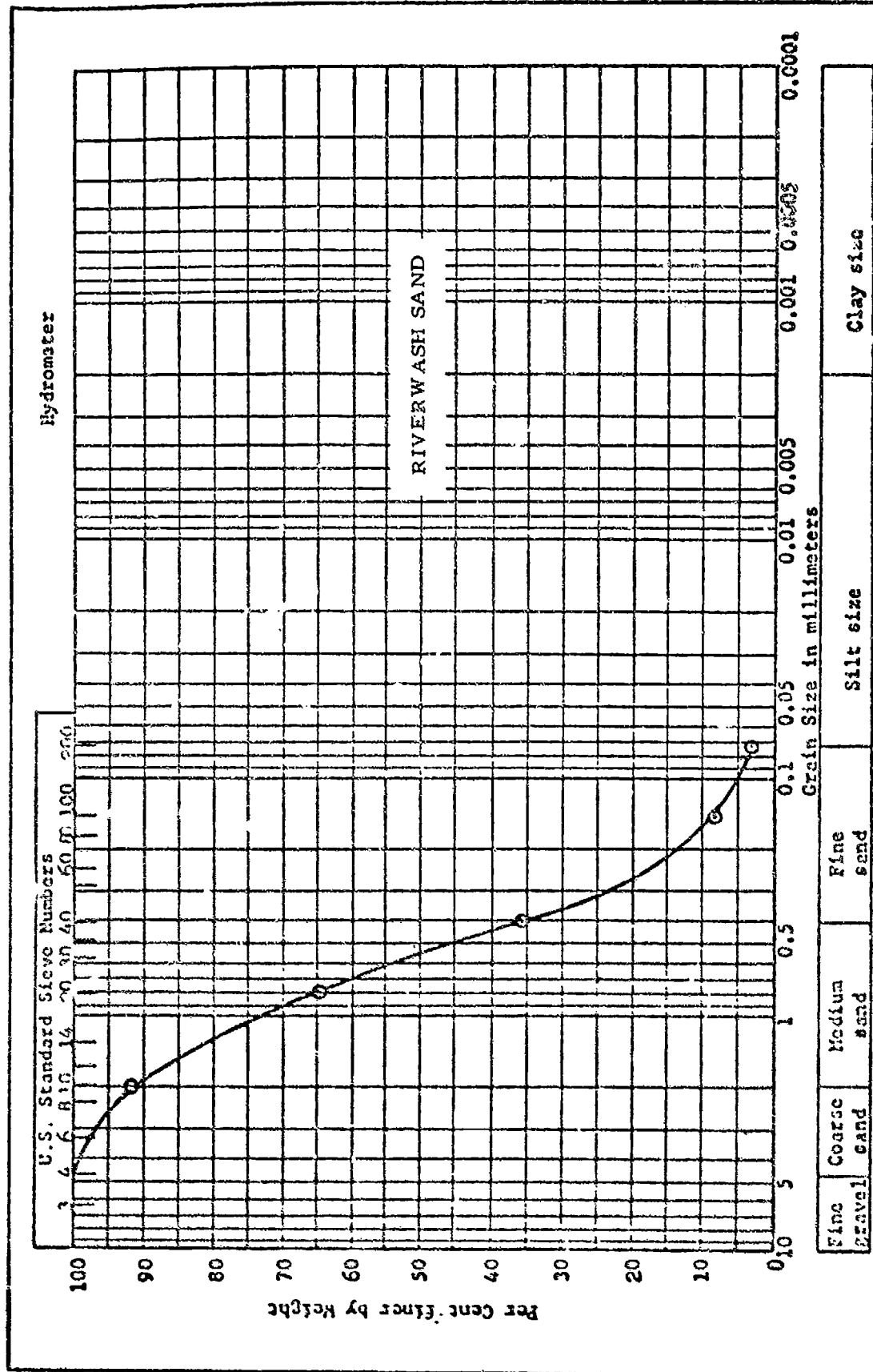


Figure 39. Grain Size Distribution - Riverwash Sand

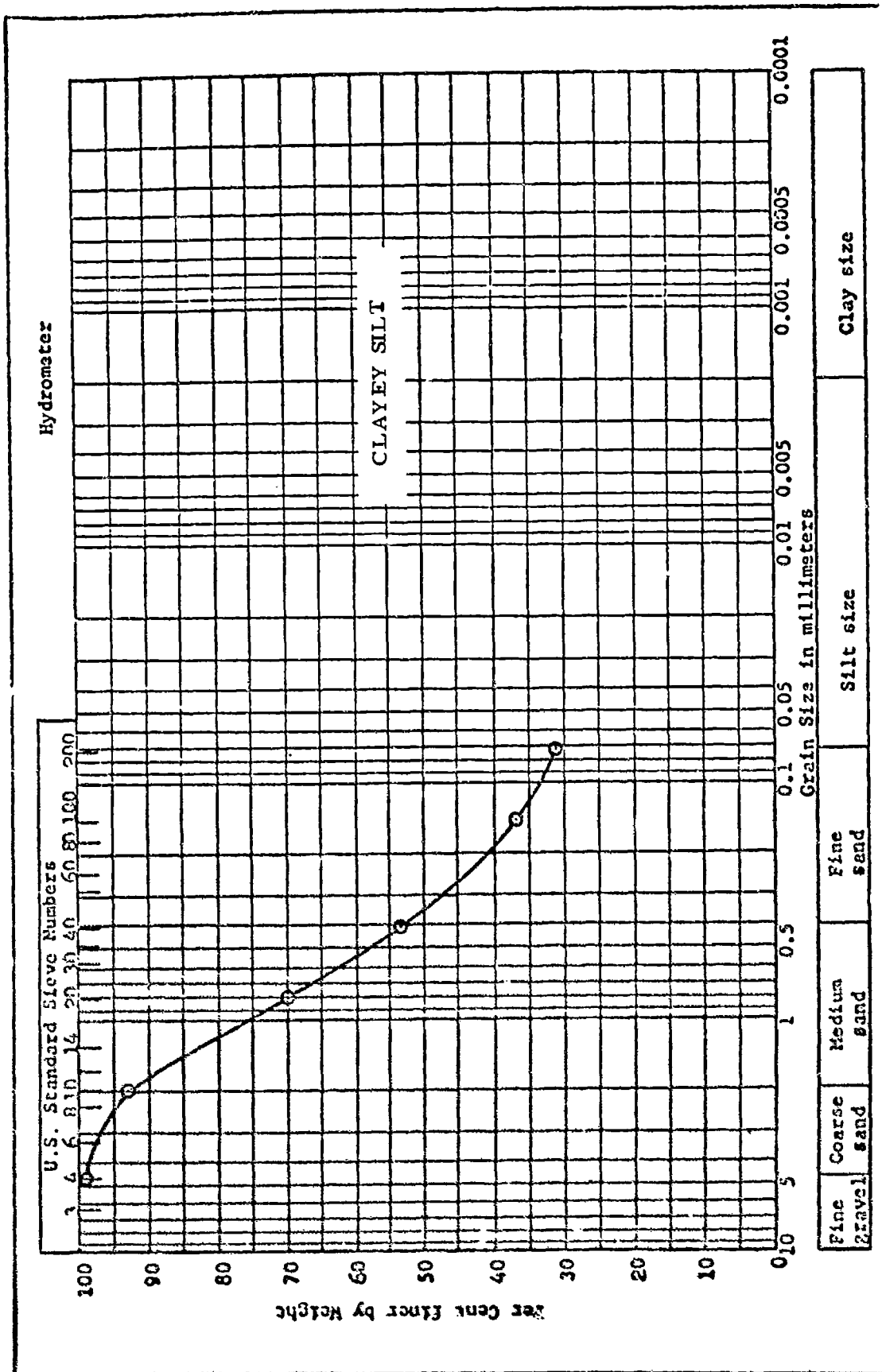


Figure 40. Grain Size Distribution - Clayey Silt

C. Test Results

The complete results of the turned tire tests conducted using the UD Test Track are given in Figures 41 through 46. The results include both tire loads for the tests in sand and clayey slit.

Numerous tests have been conducted in the past for rolling aircraft tires (non-turned) on soil. Since the 0° turn was included in this Tests Program, Figure 47 was developed showing results of a comparison between the rolling tire (0° turn) tests in this program with the least square fit trend to all previous data. The results are in relatively close agreement, which indicates a good baseline from which to compare turned tire trends.

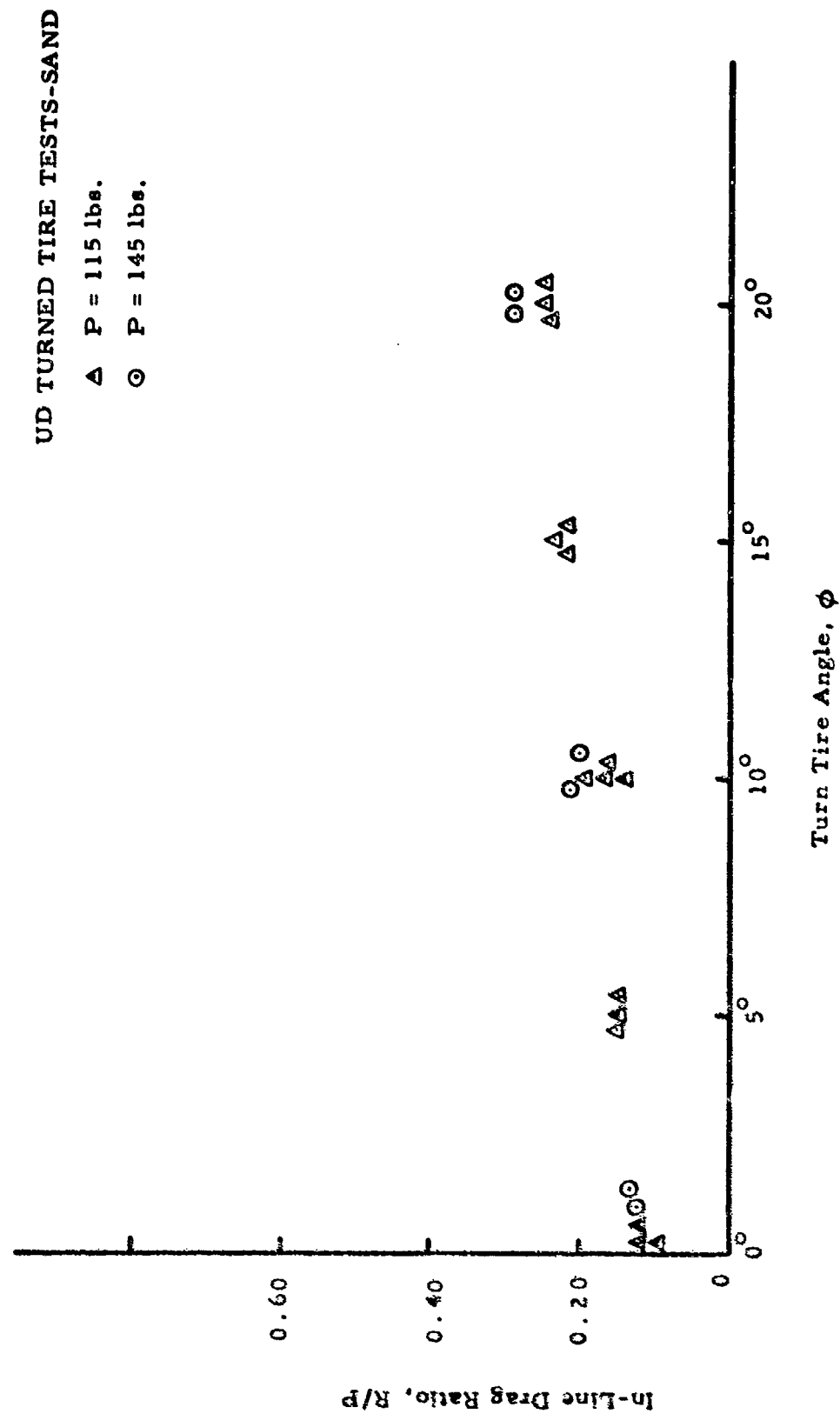


Figure 41. In-Line Drag Ratio (R/P) vs. Tire Turn Angle, Sand (UD Tests)

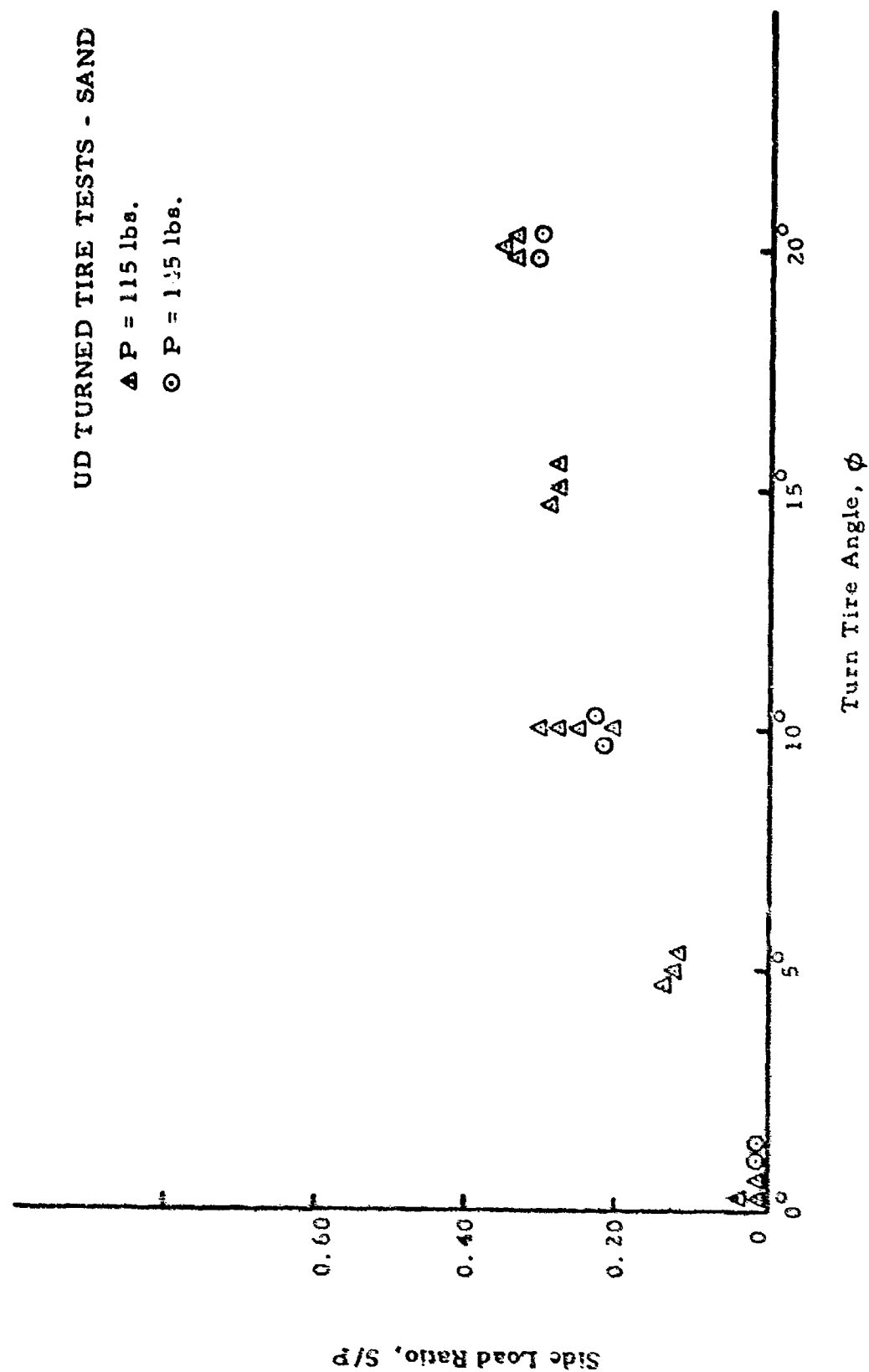
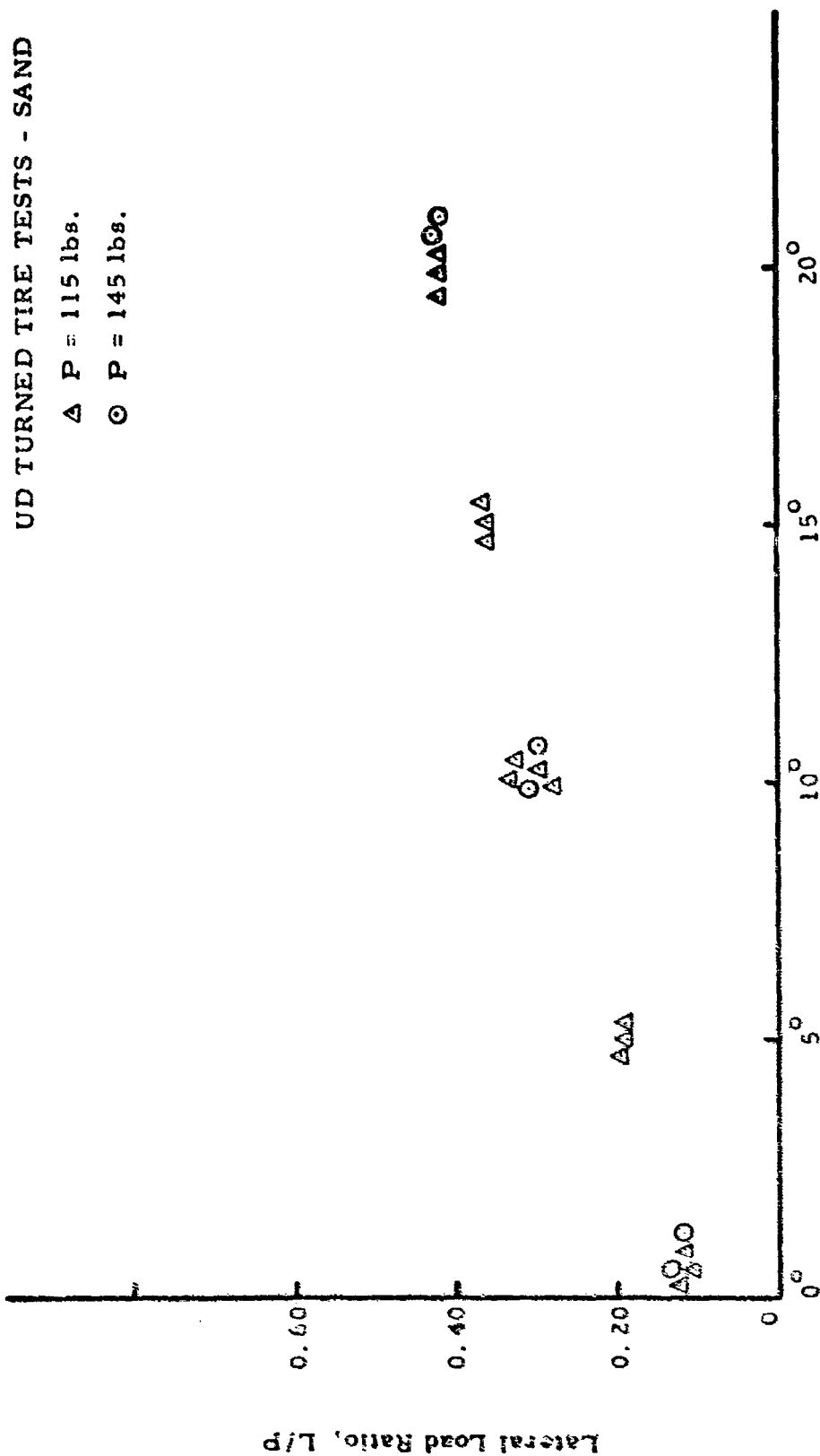


Figure 42. Side Load/Ratio (S/P) vs. Tire Turn Angle, Sand (UD Tests)



Turn Tire Angle, ϕ

Figure 43. Lateral Load Ratio (L/P) vs. Tire Turn Angle, Sand (UD Tests)

UD TURNED TIRE TESTS-CLAYEY SILT

Δ $P = 115$ lbs.

\odot $P = 145$ lbs.

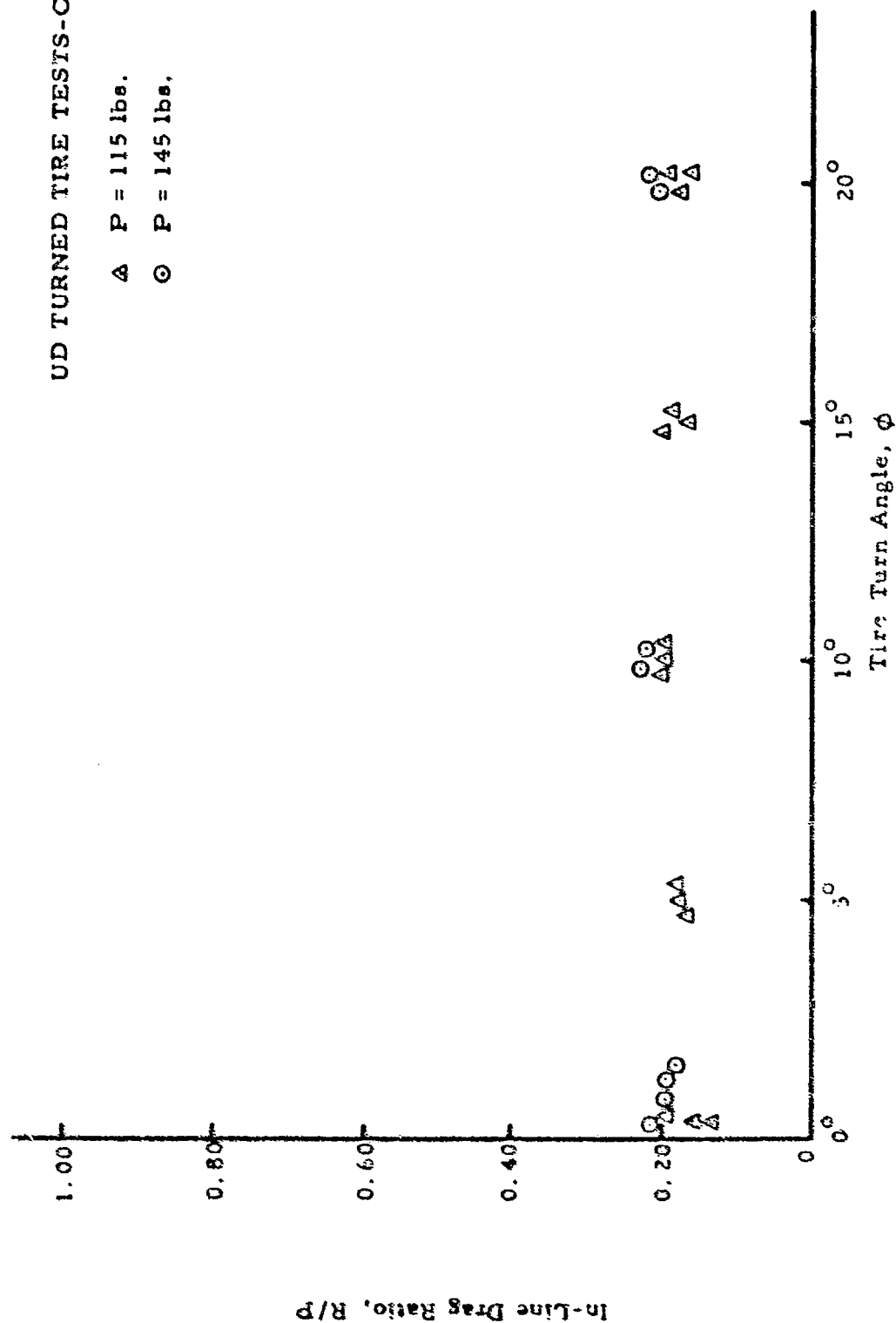


Figure 44. In-Line Drag Ratio (R/P) vs. Tire Turn Angle, Clayey Silt (UD Tests)

UD TURNED TIRE TESTS - CLAYEY SILT

△ P = 115 lbs.

○ P = 145 lbs.

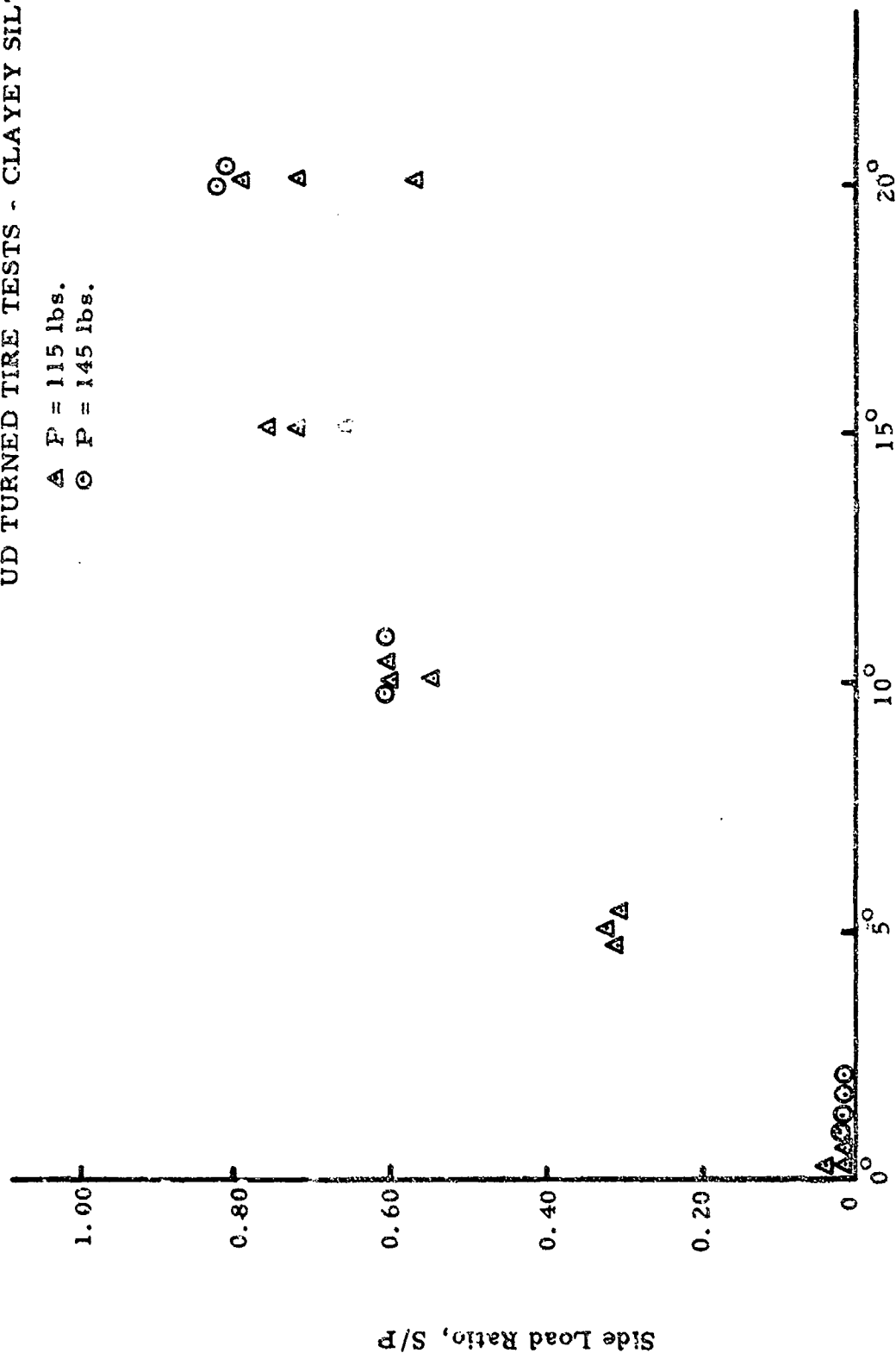


Figure 45. Side Load Ratio (S/P) vs. Tire Turn Angle, Clayey Silt (UD Tests)

UD TURNED TIRE TESTS-CLAYEY SILT

Δ P = 115 lbs.

\odot P = 145 lbs.

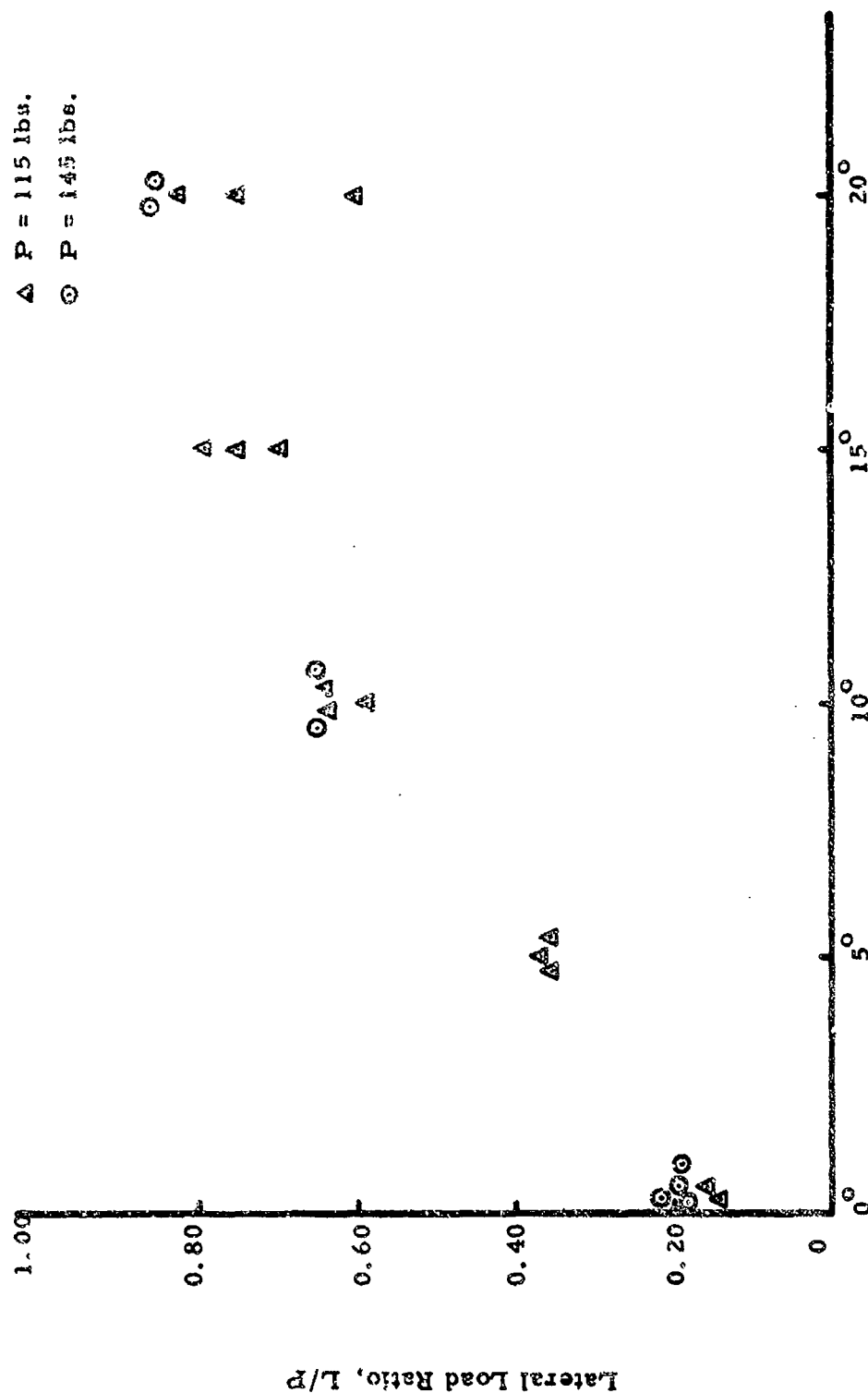


Figure 46. Lateral Load Ratio (L/P) vs. Tire Turn Angle, Clayey Silt (UD Tests)

UD TURNED TIRE TEST PROGRAM

○ = Sand

△ = Clay

Reference Phase II Report (4)

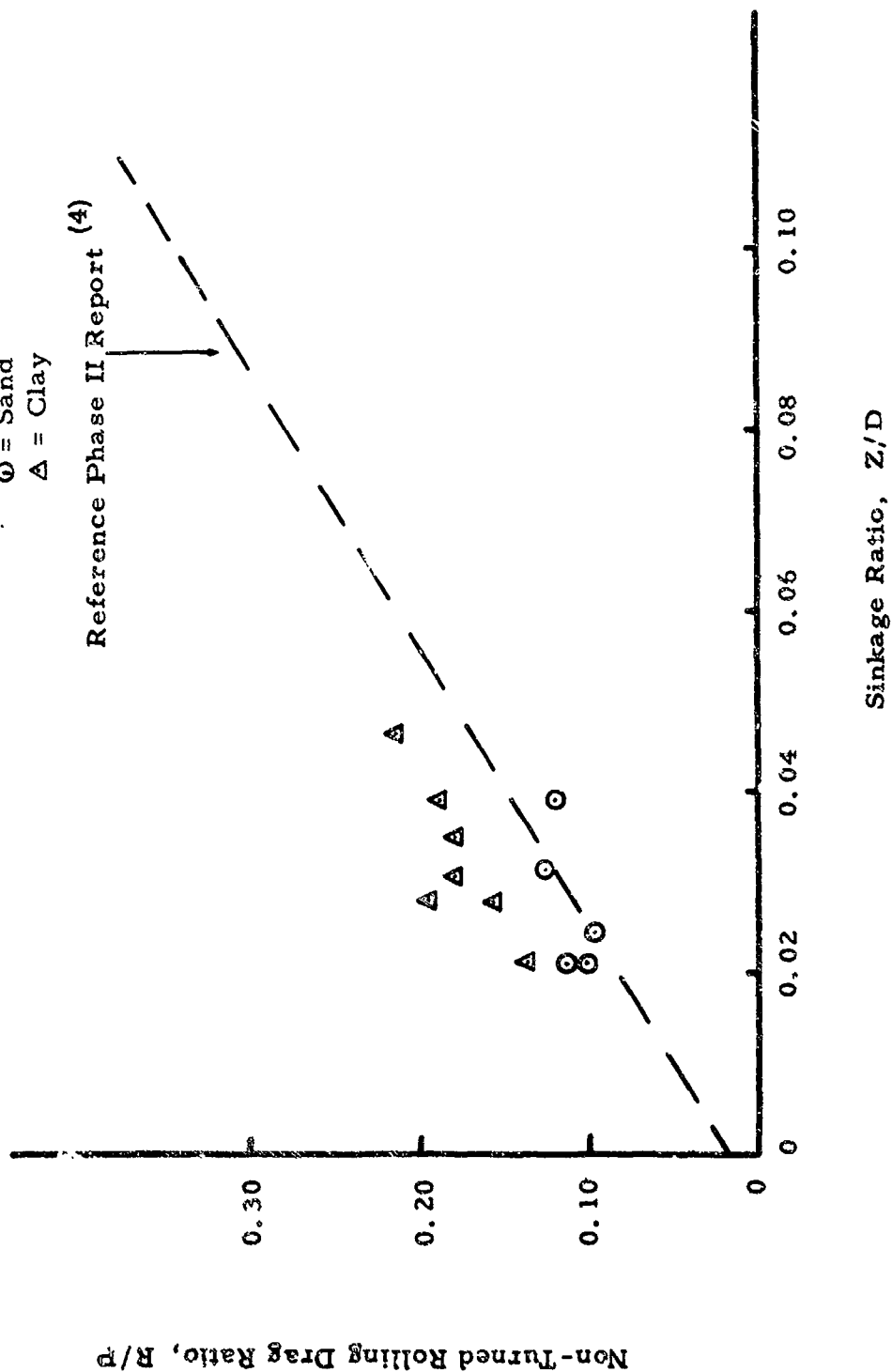


Figure 47. Drag Ratio vs. Sinkage Ratio, 0° Turned Tire, (UD Tests)

APPENDIX I

2. UD (AEWES) TURNED TIRE TEST PROGRAM

A. Soil Preparation, Test Procedure, and Tire/Loads Geometry

As in previous testing programs conducted at AEWES under UD supervision, a set procedure was followed in conducting each test. A summary of this procedure is as follows:

1. Prepare the soil test section to a uniform strength and surface elevation. The buckshot clay was prepared at a predetermined moisture content by thorough mixing in a pug mill, placed in the test track carts in lifts and compacted using a pneumatic tired roller. The mortar sand was placed in the test track carts in an air dry condition in lifts and compacted using a vibratory plate compactor. In subsequent tests, only the upper 6" to 8" was loosened and recompactd before the next run.
2. Cone index penetration tests were conducted along the length of the soil bed to determine a soil strength profile. Additional soil property tests included moisture content, density, and CBR. Surface elevation profiles were also taken.
3. Check all calibrations, put on FM tape, make trial run to establish inertia drag.
4. Load tire; set tire deflection and inflation pressure.
5. Run test; record all parameters on FM tape and oscillographic tape. Figure 48 shows a test in progress.
6. Take post test soil strength profile and rut depth profile and cross section.

This procedure was followed very carefully with great attention to detail to insure the uniformity of test results.

The relationship between in-line drag and side loads and longitudinal and transverse loads on a turned tire is presented in Figure 49.

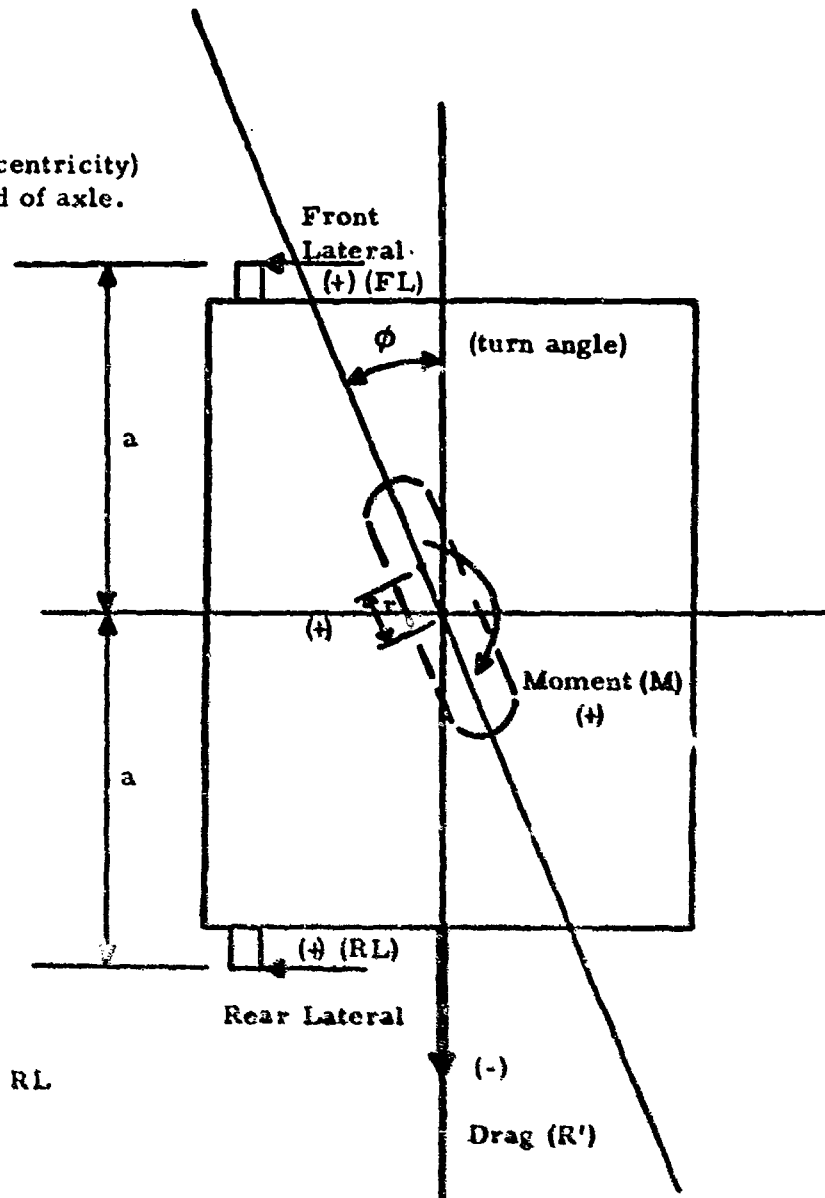


Test with 8.50-10 tire in sand; wheel load: 900 lb; deflection: 35 percent; turn angle: 0 degree; C_1 - 34 psi; carriage velocity: 10 ft/sec.

Figure 48. Turned Tire/Soil Test UD (AEWES).

Sign Convention

1. As shown.
2. Pneumatic trail, r , (eccentricity) is positive when forward of axle.



$$\text{Total Lateral (TL)} = \text{FL} + \text{RL}$$

$$\text{Total Drag} = R'$$

$$\text{Moment (M)} = (\text{FL} - \text{RL})a$$

$$\text{Pneumatic Trail (r)} = \frac{(\text{FL} - \text{RL})a}{\text{FL} + \text{RL}} \cdot \frac{L}{\cos \phi} = \frac{M}{R' \cos \phi}$$

$$\text{Resultant Lateral Load (L)} = \sqrt{(R')^2 + (\text{TL})^2}$$

$$\text{Direction of Resultant } \gamma = \tan^{-1} \frac{\text{TL}}{R'}$$

$$\text{In-Line Drag (R)} = R' \cos \phi - \text{TL} \sin \phi$$

$$\text{Side Load (S)} = R' \sin \phi + \text{TL} \cos \phi$$

Figure 49. Turned Tire-Load Geometry Relationships UD (AEWES) Tests

B. Soil and Test Tires Property Data

The results of the moisture-density tests are given in Table XVII while the results of the cone penetration tests (CI_{avg}) are given in the Test Result Summary Tables (Tables VIII and IX).

TABLE XVII
MOISTURE-DENSITY SUMMARY UD (AEWES)

Soil Type	Dry Unit Weight (lbs/ft ³)	Moisture Content (%)	CBR
Mortar Sand	100.6	Air Dry	-
Buckshot Clay CI ~ 39	82.6	37.6	1.4
Buckshot Clay CI ~ 71	89.0	32.2	2.2

C. Test Results

The variation in rut depth and rut depth profile for the (AEWES) UD turned tire tests are shown in Figures 50 through 53 for sand and Figures 54 through 57 for clay. Reference to these Figures indicates significant buildup of soil away from the direction of turn. Also noted is the greater increase in sinkage with turn angle which occurs in sand type soil in comparison to clay type soil.

Figures 58 through 69 give the complete results of the variation in in-line drag and sideload for the turned tire in sand and clay type soil for tire deflections of 35% and 40%.

Again, for comparative purposes to previous tire/soil test results, Figure 70 was prepared using the test data from the 0° (non-turned) test conditions. The results can then be compared to the least square fit line of previous test data and in general show a relatively close agreement.

TABLE XVIII
TURNED TIRE TEST PROGRAM - TIRE DATA UD (AEWES)

Tire Type	Per Cent Deflection %	Wheel Load (lbs)	Inflation Pressure (psi)		Carcass Diameter (in)	Section Height (in)		Section Width (in)		Rigid Surface Tire Print		
			Loaded	Unloaded		Loaded	Unloaded	Loaded	Unloaded	Length (in)	Width (in)	Area (in ²)
8.50-10, 8 PR	35	900	6.4	5.4	24.4	4.02	6.22	9.31	8.01	11.42	6.90	67.5
8.50-10, 8 PR	35	1300	12.2	11.2	24.7	4.12	6.34	9.32	8.03	11.70	6.91	69.0
8.50-10, 8 PR	40	1000	6.0	5.0	24.5	3.74	6.23	9.62	8.01	12.35	7.02	77.1
8.50-10, 8 PR	40	1500	12.2	11.0	24.7	3.80	6.34	9.57	8.03	12.40	7.14	76.9
8.50-10, 8 PR	40	1550	12.4	11.1	24.7	3.80	6.34	9.61	8.03	12.50	7.10	77.7
7.00-6, 6 PR	35	540	7.6	6.4	17.7	3.26	5.08	7.45	6.73	8.92	5.53	44.0
7.00-6, 6 PR	35	600	9.7	8.6	17.7	3.34	5.09	7.93	6.75	8.59	5.50	40.4
7.00-6, 6 PR	35	1100	25.5	24.1	18.0	3.44	5.25	7.94	6.78	8.92	5.52	43.9
7.00-6, 6 PR	35	1500	30.0	28.0	18.1	3.46	5.29	7.93	6.80	8.90	5.52	41.9
7.00-6, 6 PR	40	600	7.2	6.1	17.7	3.04	5.07	8.10	6.74	9.33	5.60	45.7
7.00-6, 6 PR	40	1500	26.0	24.2	18.0	3.15	5.25	8.08	6.79	9.58	5.62	46.5

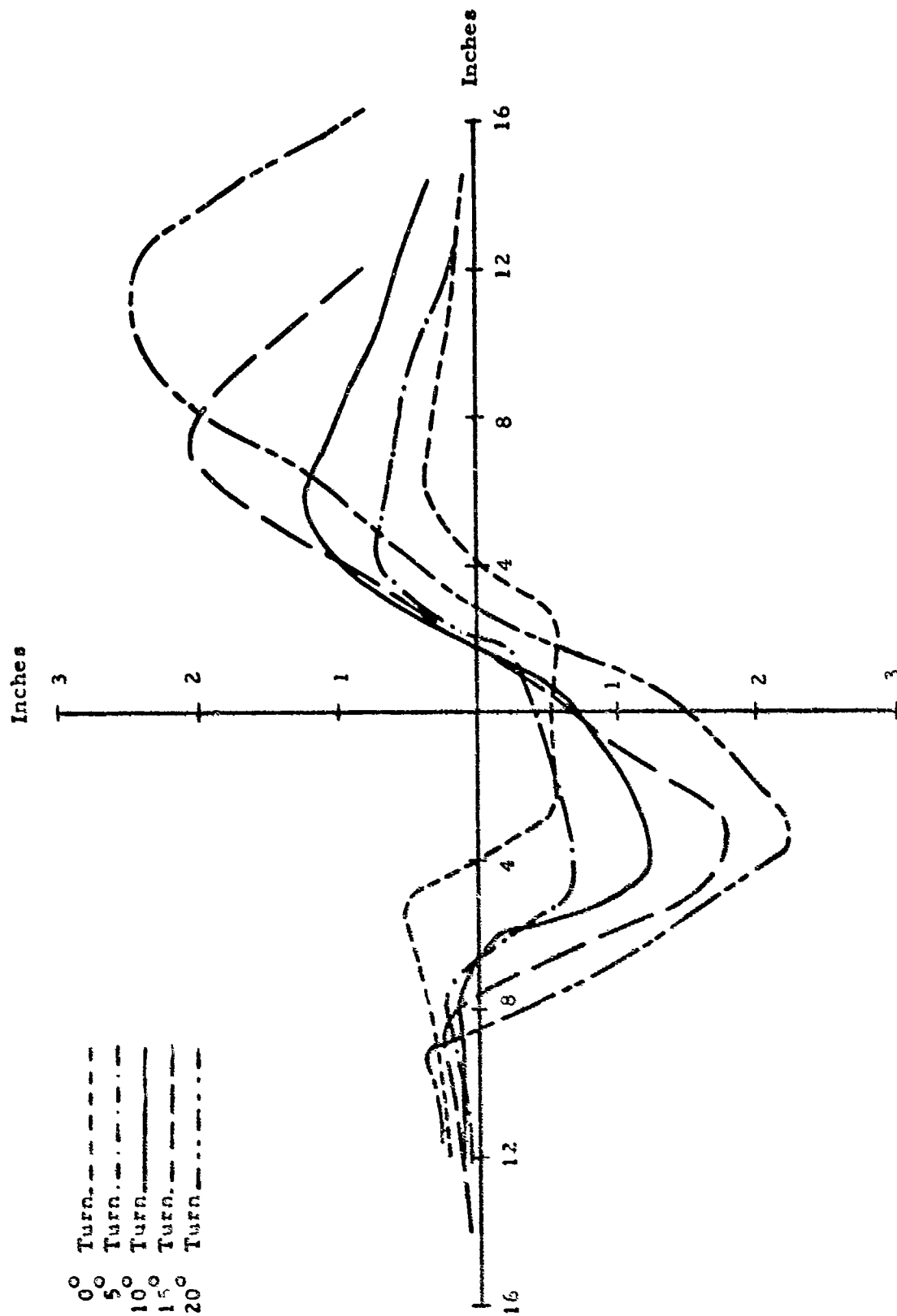


Figure 50. Turned Tire Rut Profile, 8:50 - 10 Tires, $d = 35\%$ Sand UD (AEWES).

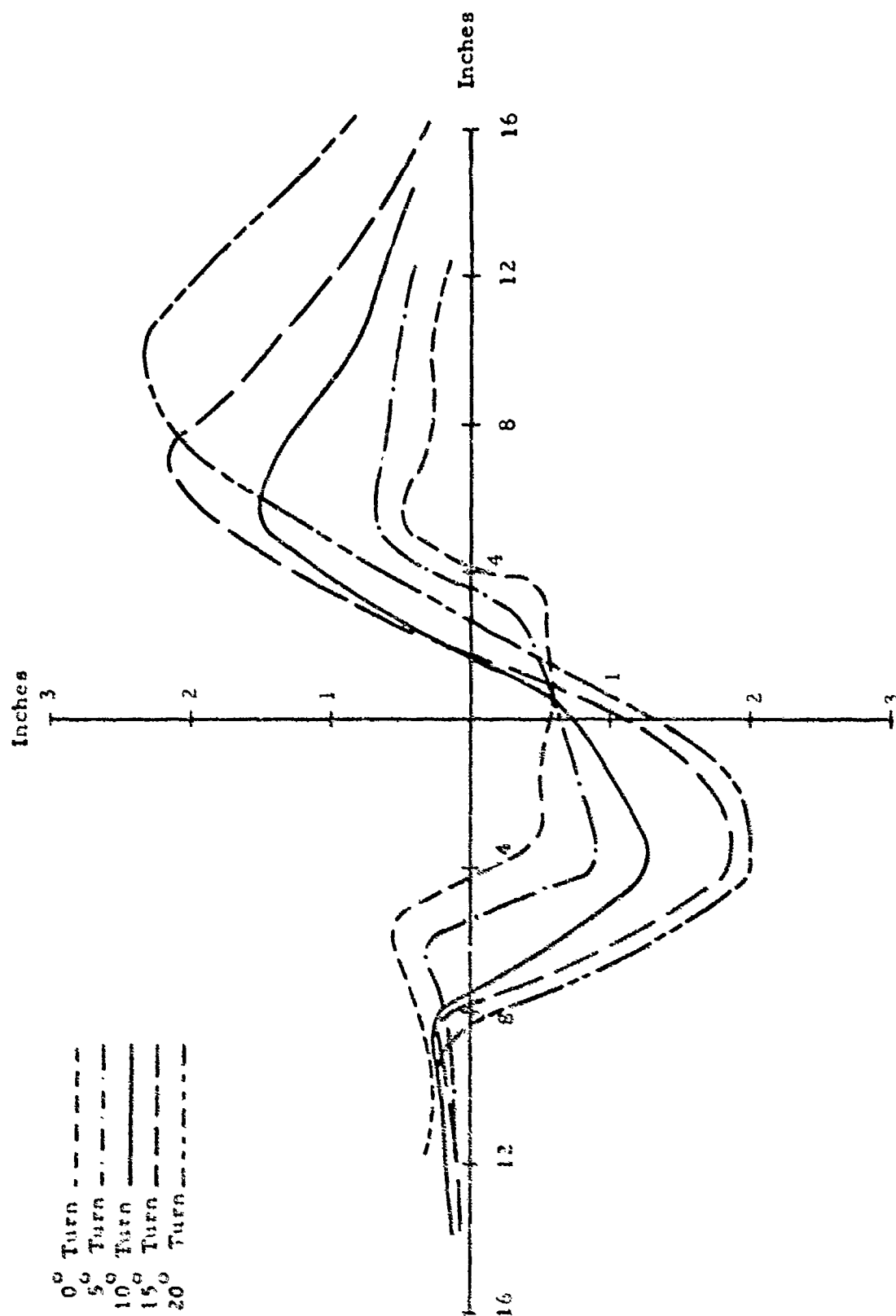


Figure 51. Turned Tire Rut Profile, 8:50 - 10 Tires, $d = 40\%$ Sand UD (AEWES).

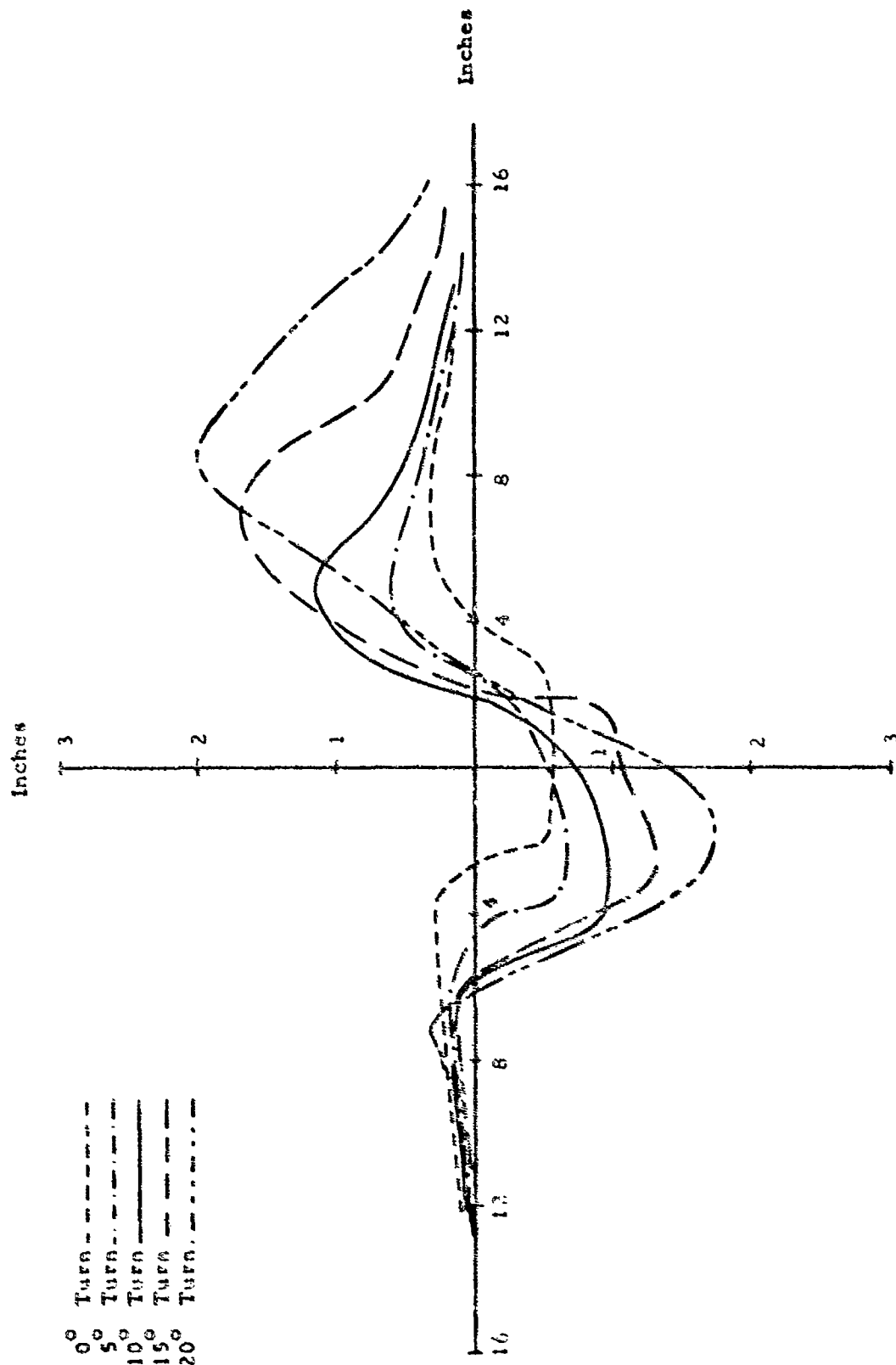


Figure 52. Turned Tire Rut Profile, 7:00 - 6 Tires, $d = 35\%$ Sand UD (AEWES).

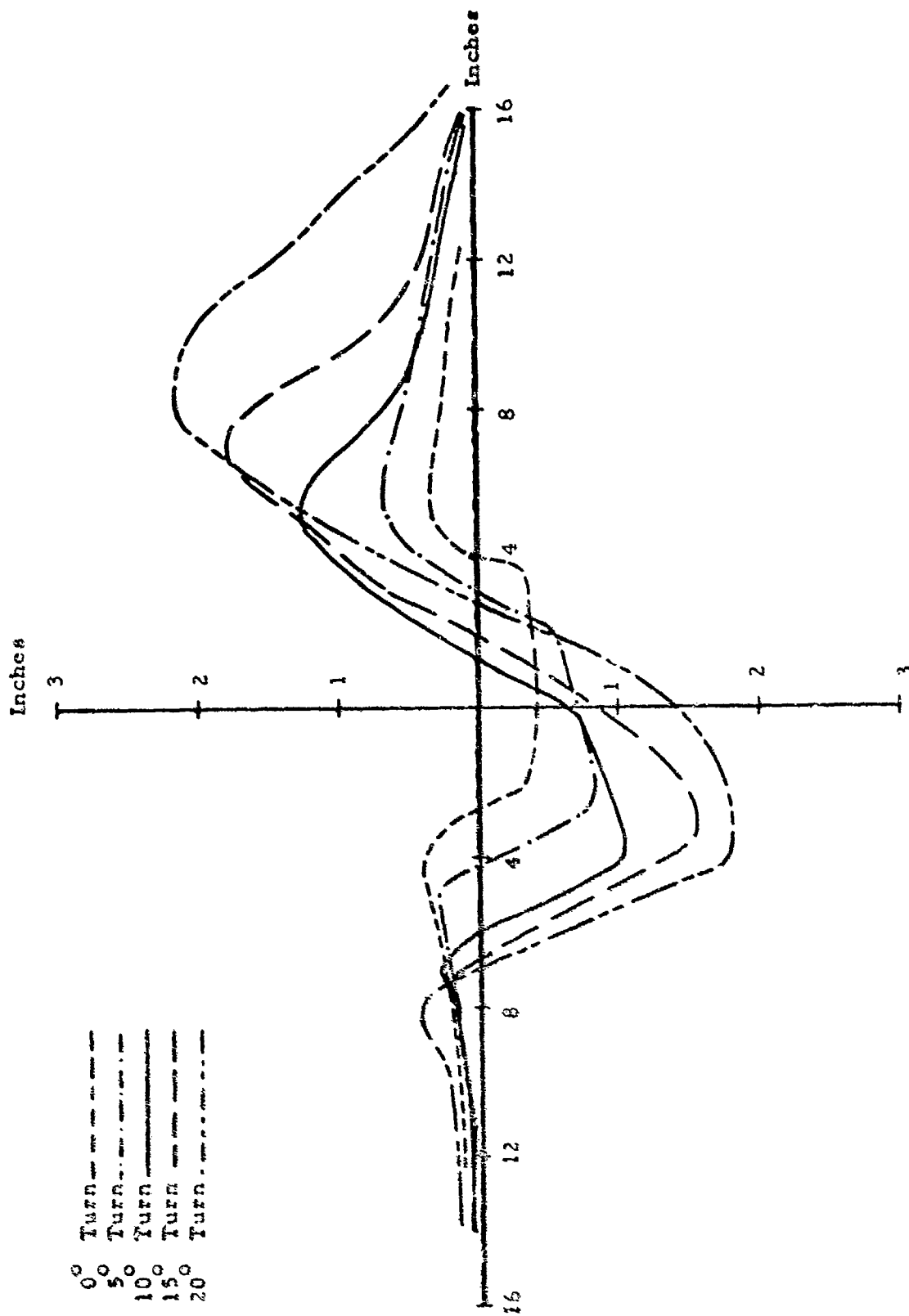


Figure 53. Turned Tire Rut Profile, 7:00 - 6 Tires, $\beta = 40\%$ Sand UD (AEWES).

0° Turn ———
 5° Turn ———
 10° Turn ———
 15° Turn ———
 20° Turn ———

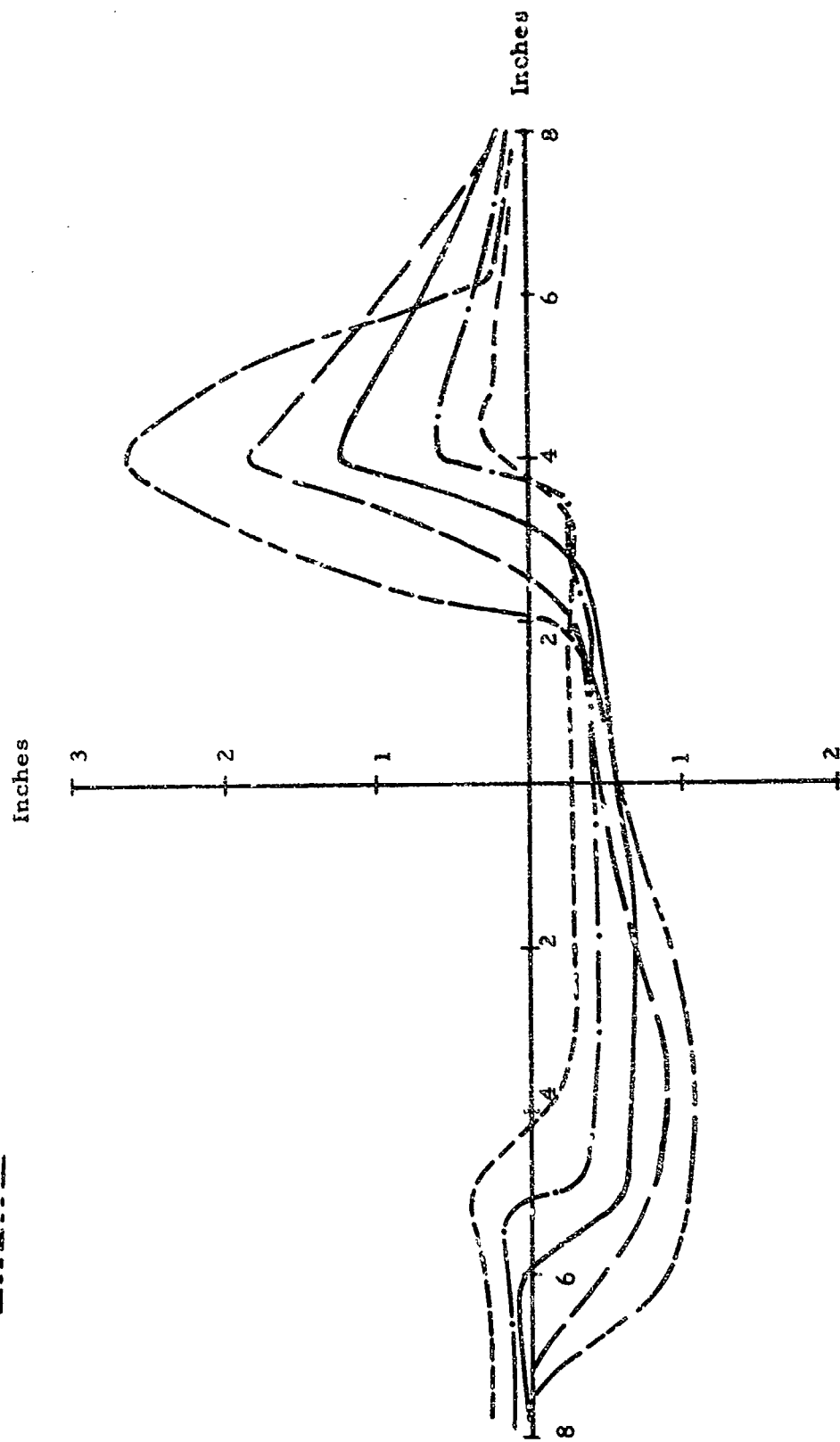


Figure 54. Turned Tire Rut Profile, 8:50 - 10 Tires, $d = 35\%$ Clay UD (AEWES).

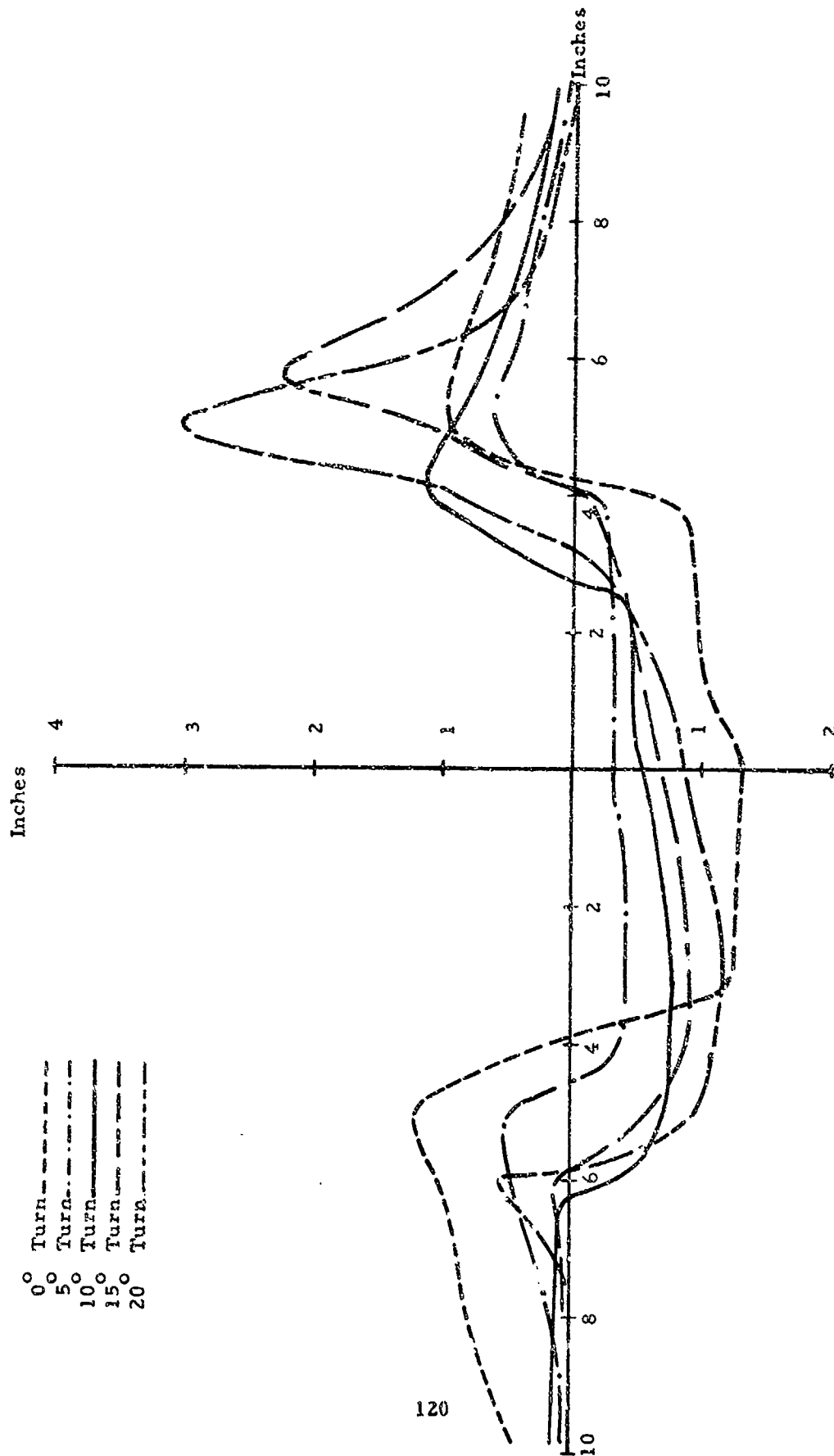


Figure 55. Turned Tire Rut Profile, 8:50 - 10 Tires, d = 40% Clay UD (AEWES).

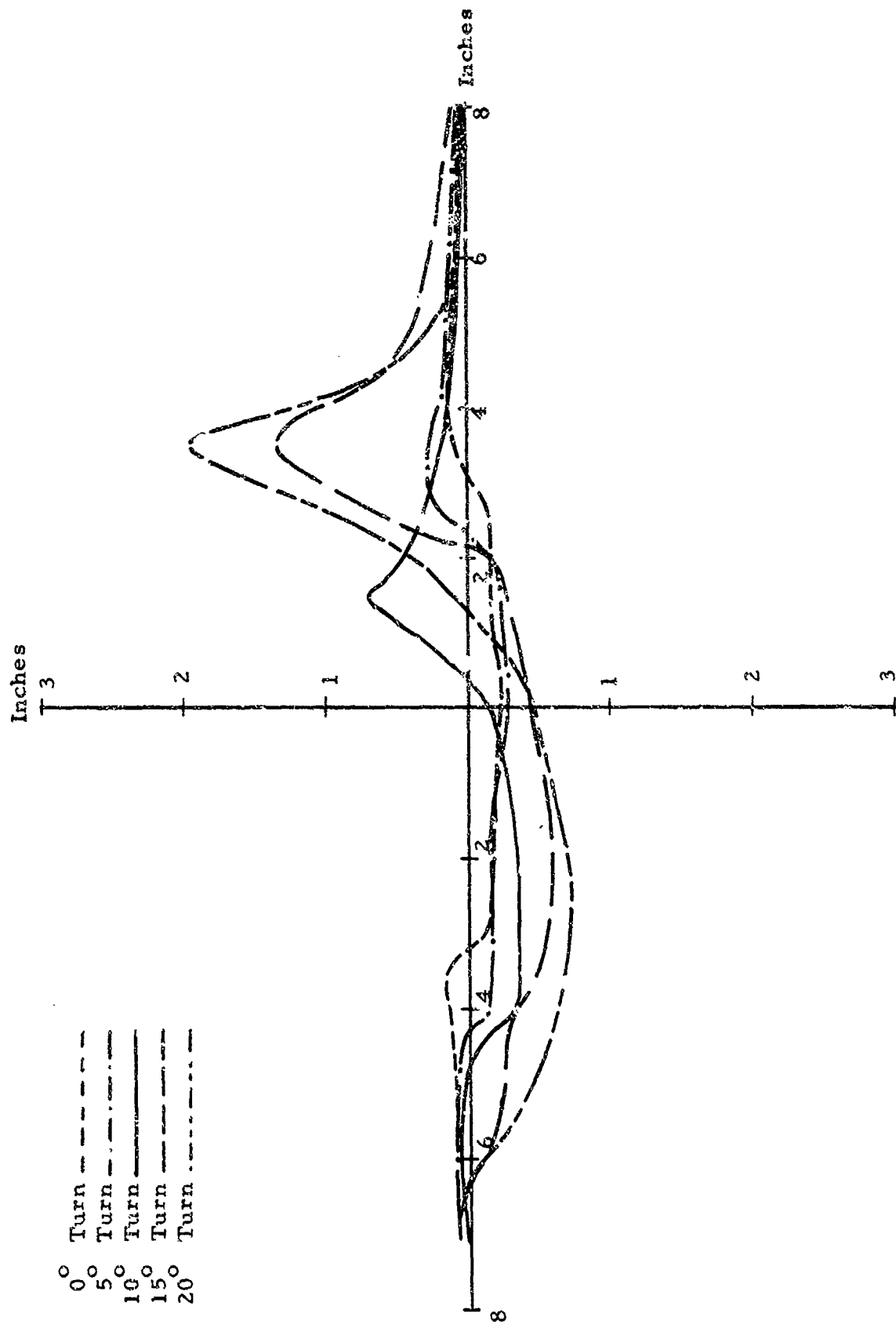


Figure 56. Turned Tire Rut Profile, 7:00 - 6 Tires, d = 35% Clay UD (AEWES).

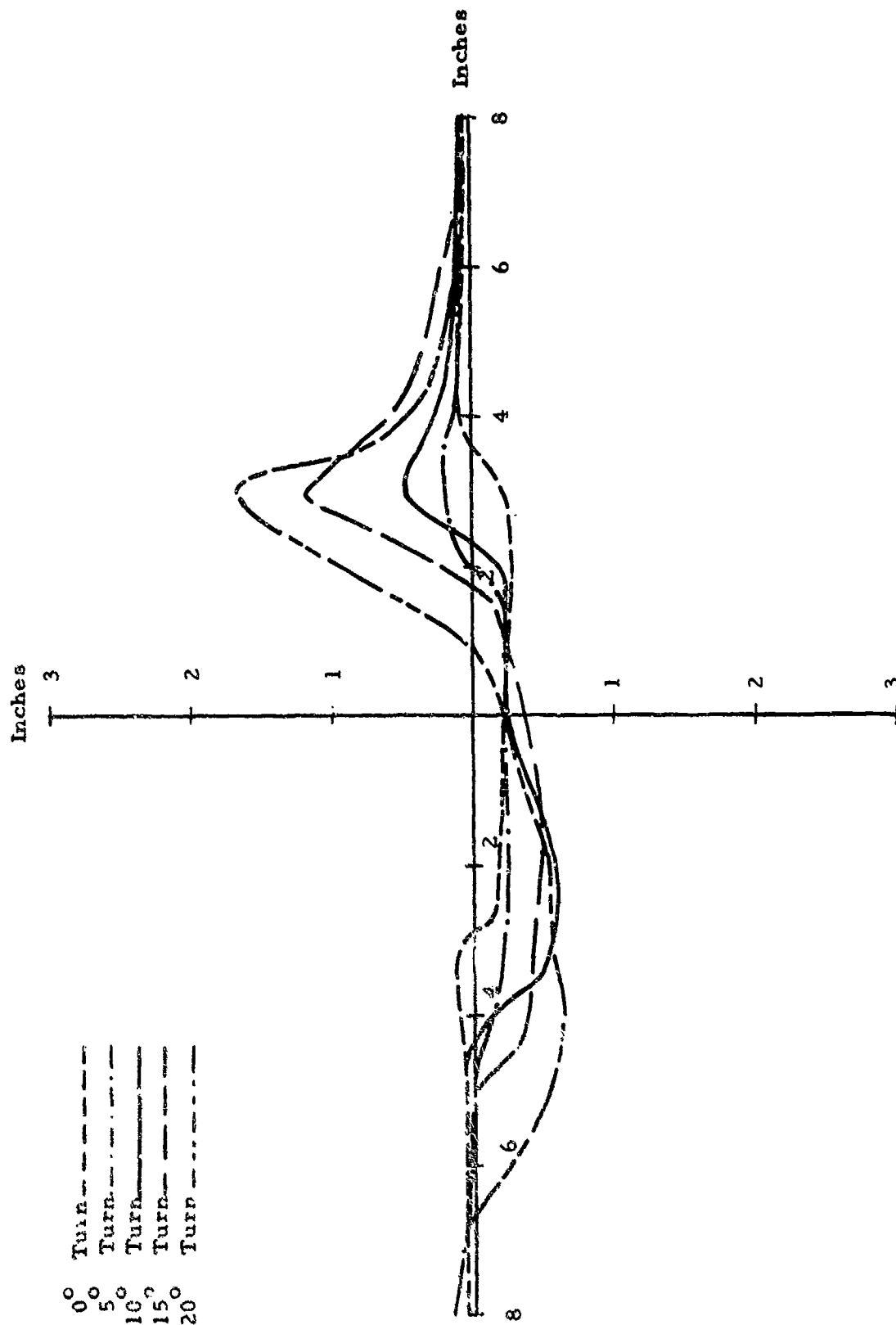


Figure 57. Turned Tire Rut Profile, 7:00 - 6 Tires, d = 40% Clay UD (AEWES).

TURNED TIRE TEST PROGRAM (AEWES) - SAND

Δ $d = 35\%$

\odot $d = 40\%$

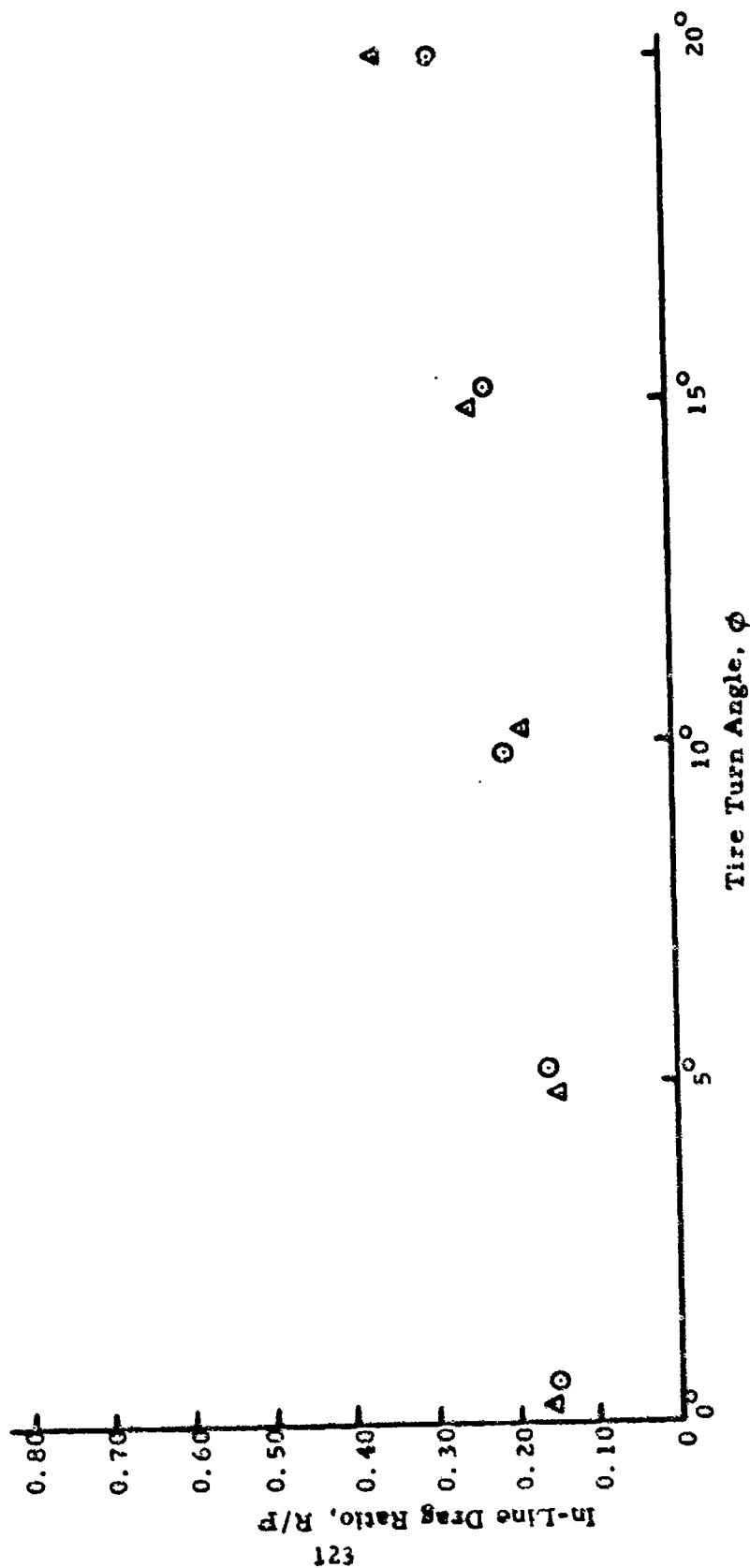


Figure 58. In-Line Drag Ratio (R/P) vs. Turn Angle, ϕ : 50-10 Tire, Sand UD (AEWES)

TURNED TIRE TEST PROGRAM (AEWES) -SAND

Δ $d = 35\%$

\odot $d = 40\%$

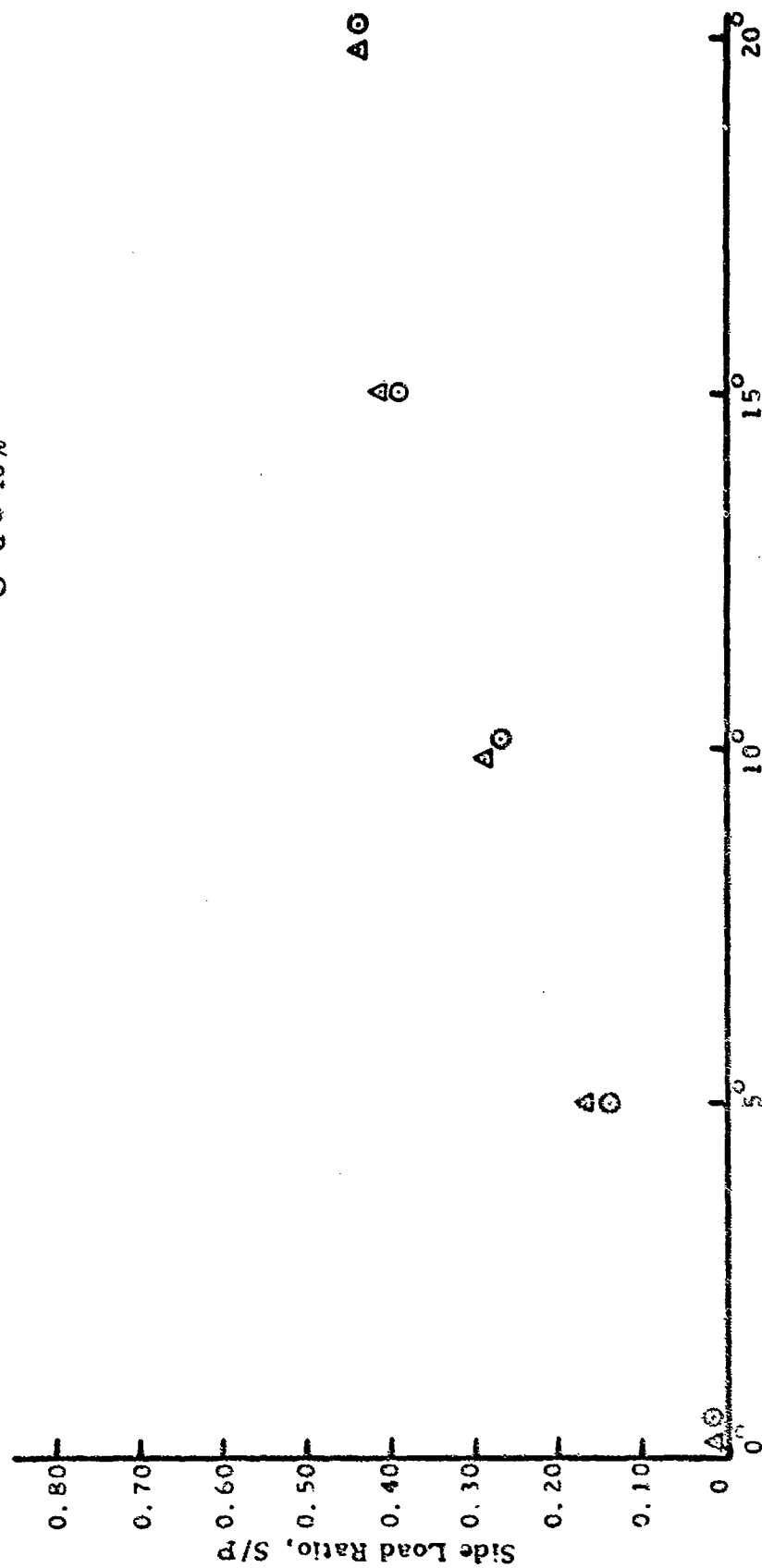


Figure 59. Side Load Ratio (S/P) vs. Turn Angle, 8:50-10 Tire, Sand UD (AEWES)

TURNED TIRE TEST PROGRAM (AEWES) - SAND

Δ $d = 35\%$

\odot $d = 40\%$

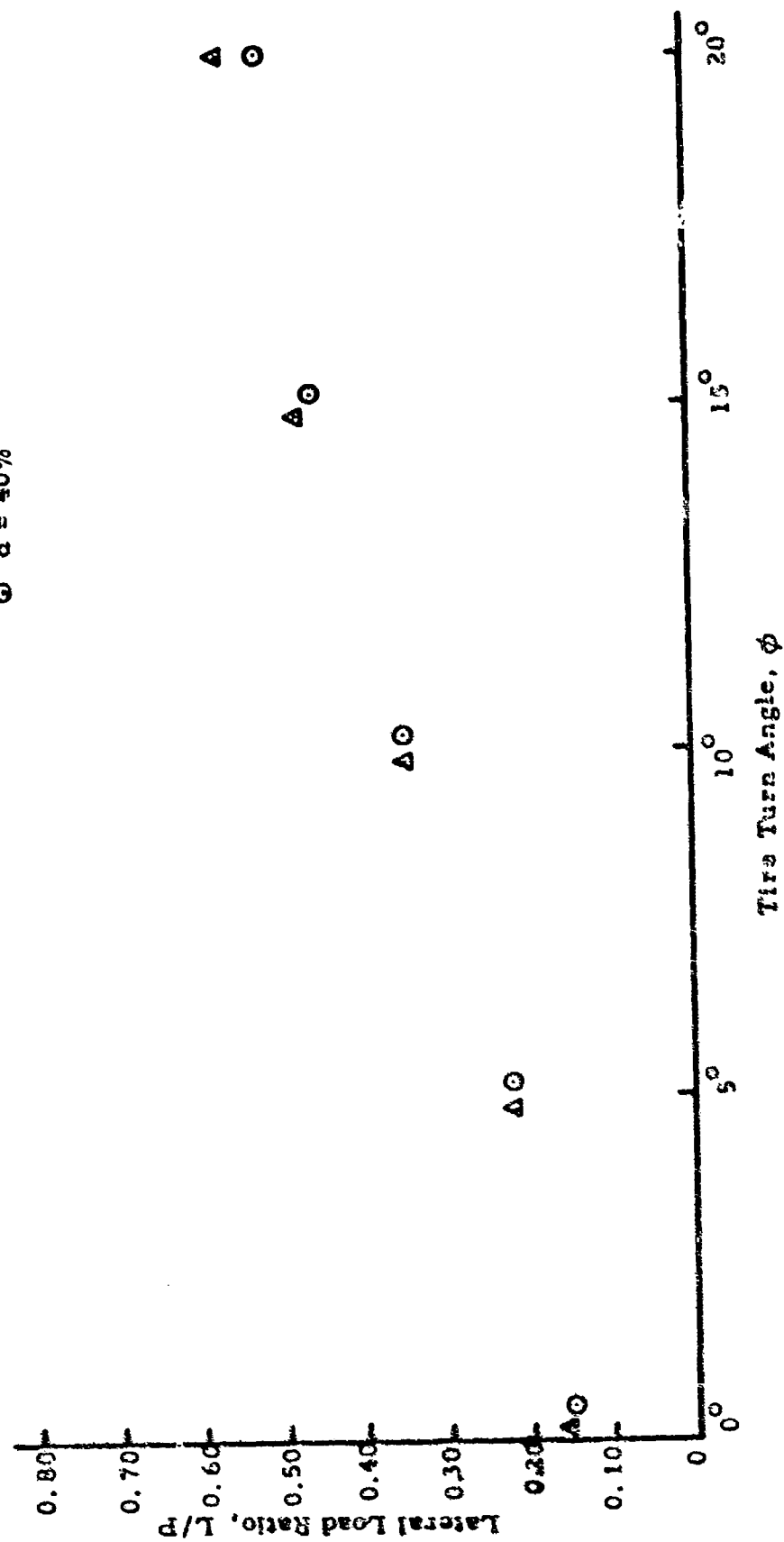


Figure 60. Lateral Load Ratio (L/P) vs. Turn Angle, 8:50-10 Tire, Sand UD (AEWES)

TURNED TIRE TEST PROGRAM (AEWES)-SAND

▲ $d = 35\%$

⊙ $d = 40\%$



Figure 61. In-Line Drag Ratio (R/P) vs. Turn Angle, 7:00-6 Tire, Sand UD (AEWES)

TURNED TIRE TEST PROGRAM (AEWES) -SAND

▲ d = 35%

⊙ d = 40%

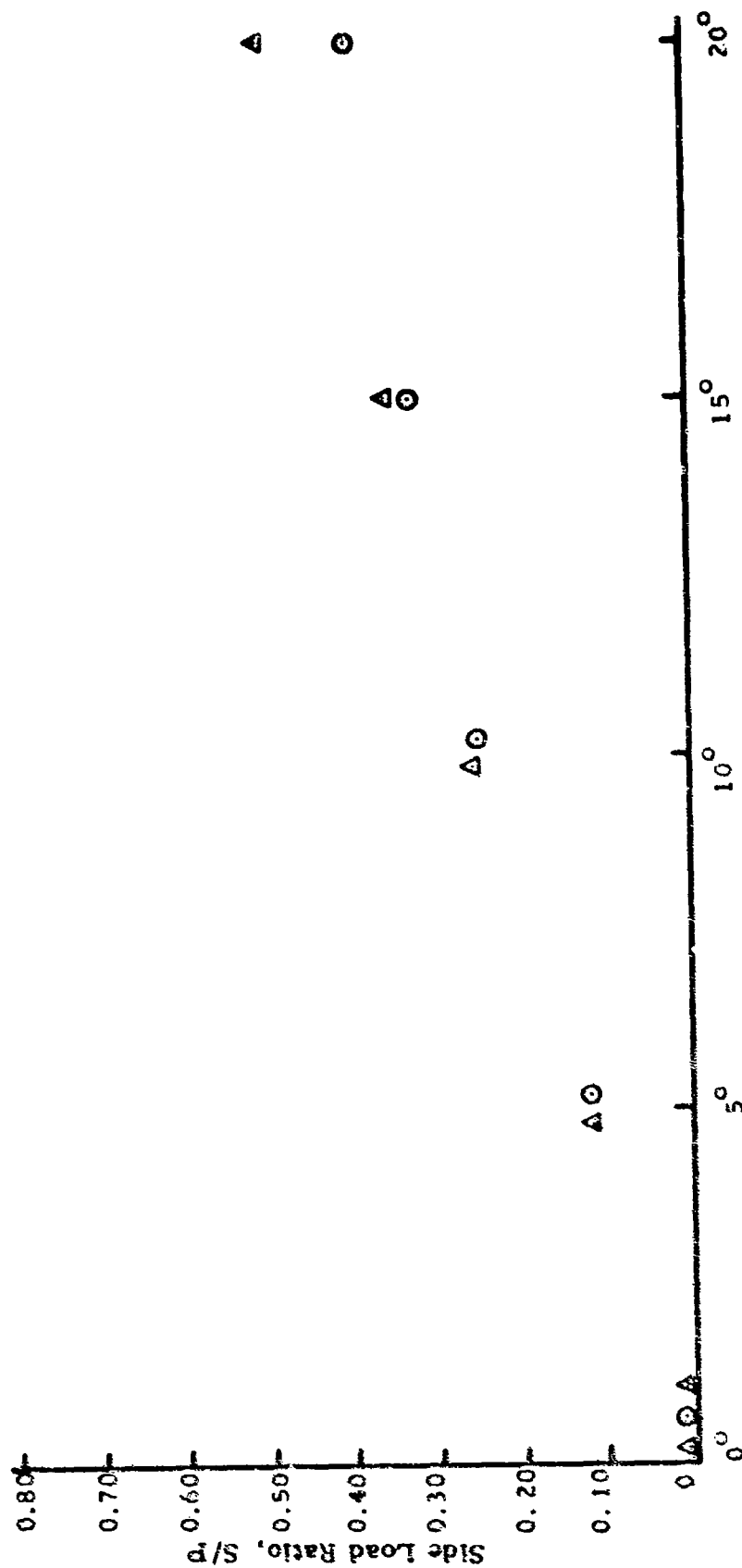


Figure 62. Side Load Ratio (S/P) vs. Turn Angle, 7:00-6 Tire, Sand UD (AEWES)

TURNED TIRE TEST PROGRAM (AEWES) - SAND

Δ $d = 35\%$

\odot $d = 40\%$

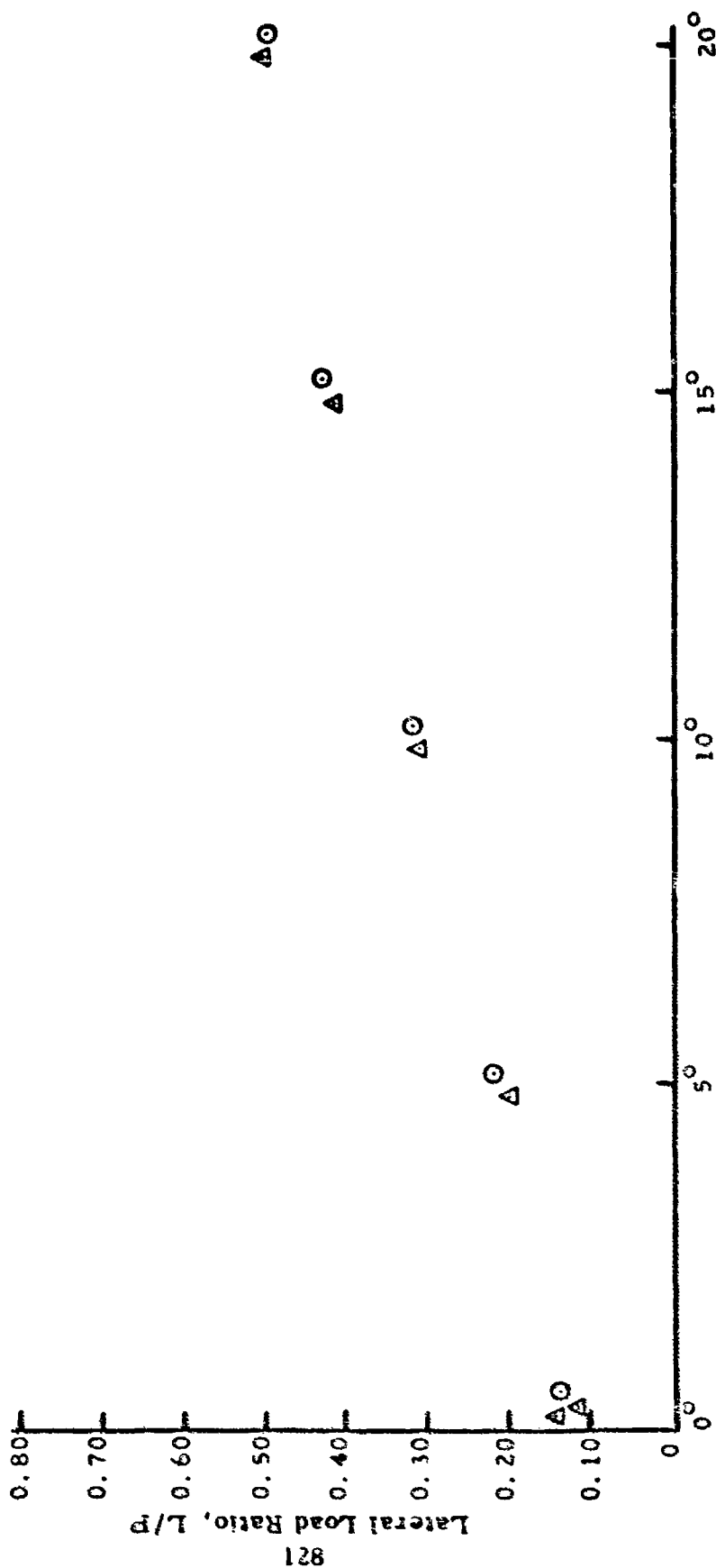


Figure 63. Lateral Load Ratio (L/P) vs. Turn Angle, 7:00-6 Tire, Sand UD (AEWES)

TURNED TIRE TEST PROGRAM (AEWES) - CLAY

Δ d = 35%

⊙ d = 40%

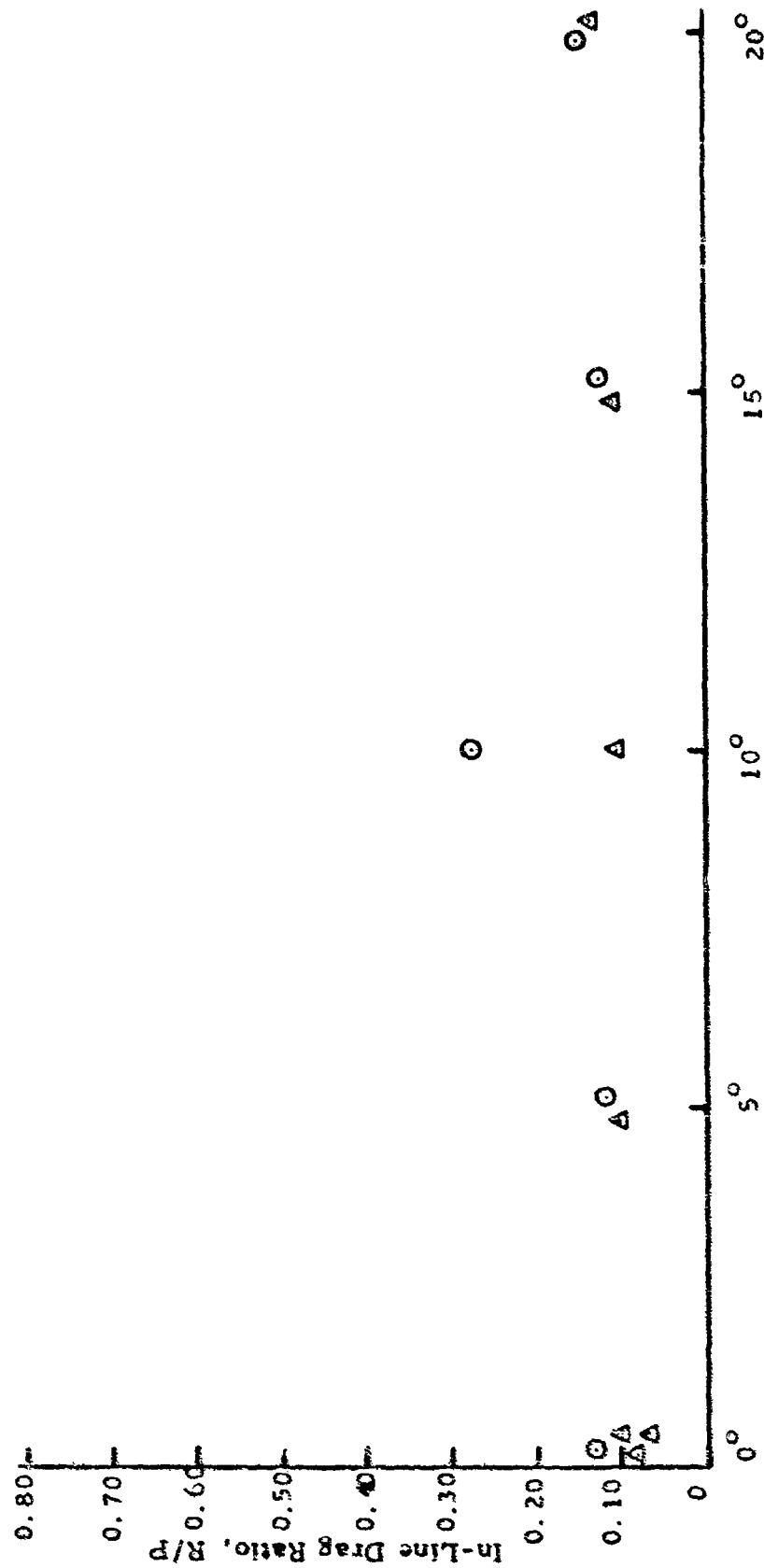


Figure 64. In-Line Drag Ratio (R/P) vs. Turn Angle, 8:50-10 Tire, Clay UD (AEWES)

TURNED TIRE TEST PROGRAM (AEWES) - CLAY

△ d = 35%

○ d = 40%

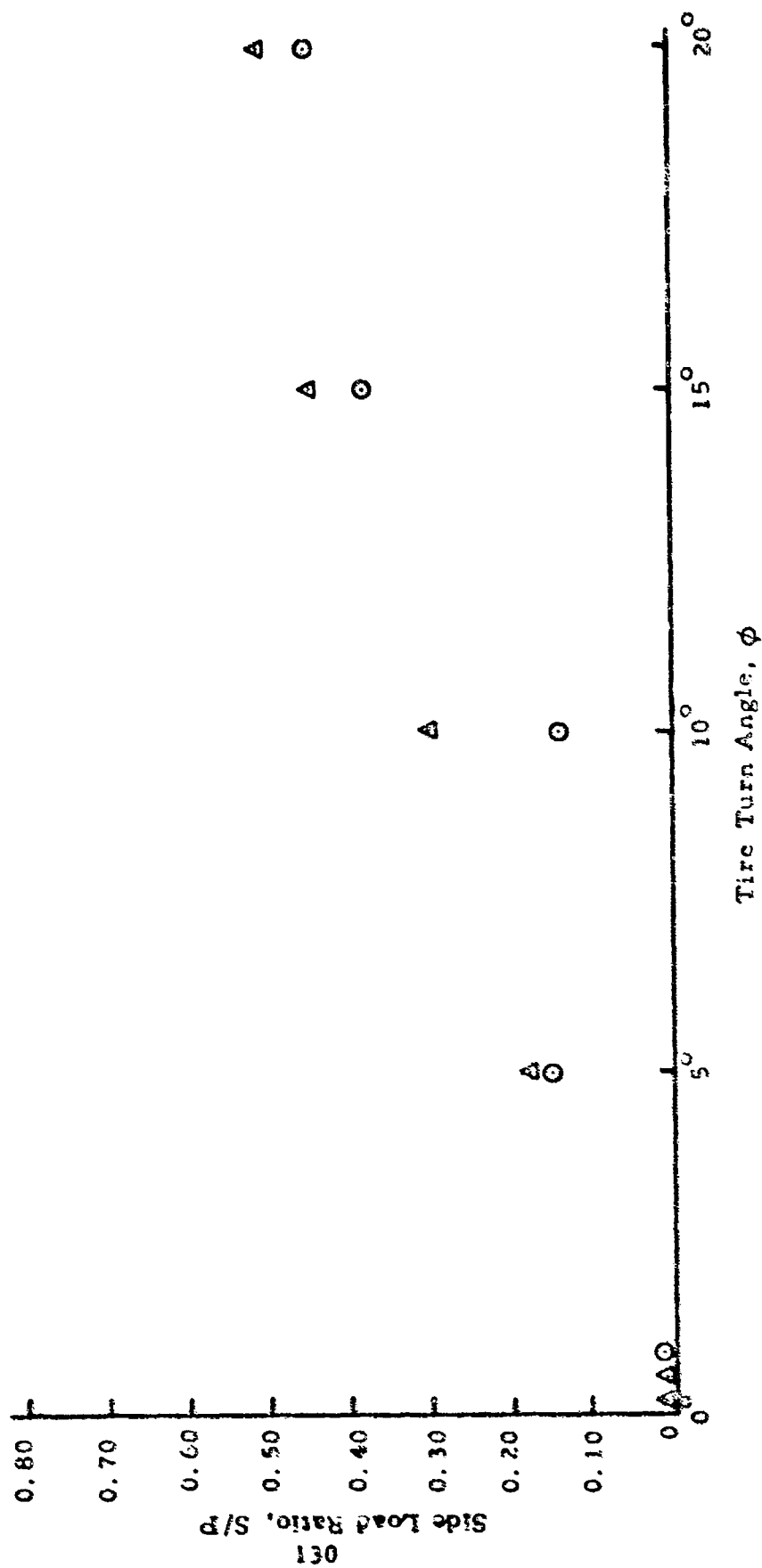


Figure 65. Side Load Ratio (S/P) vs. Turn Angle, 8:50-10 Tire, Clay UD (AEWES)

TURNED TIRE TEST PROGRAM (AEWES) - CLAY

Δ $d = 35\%$

\odot $d = 40\%$

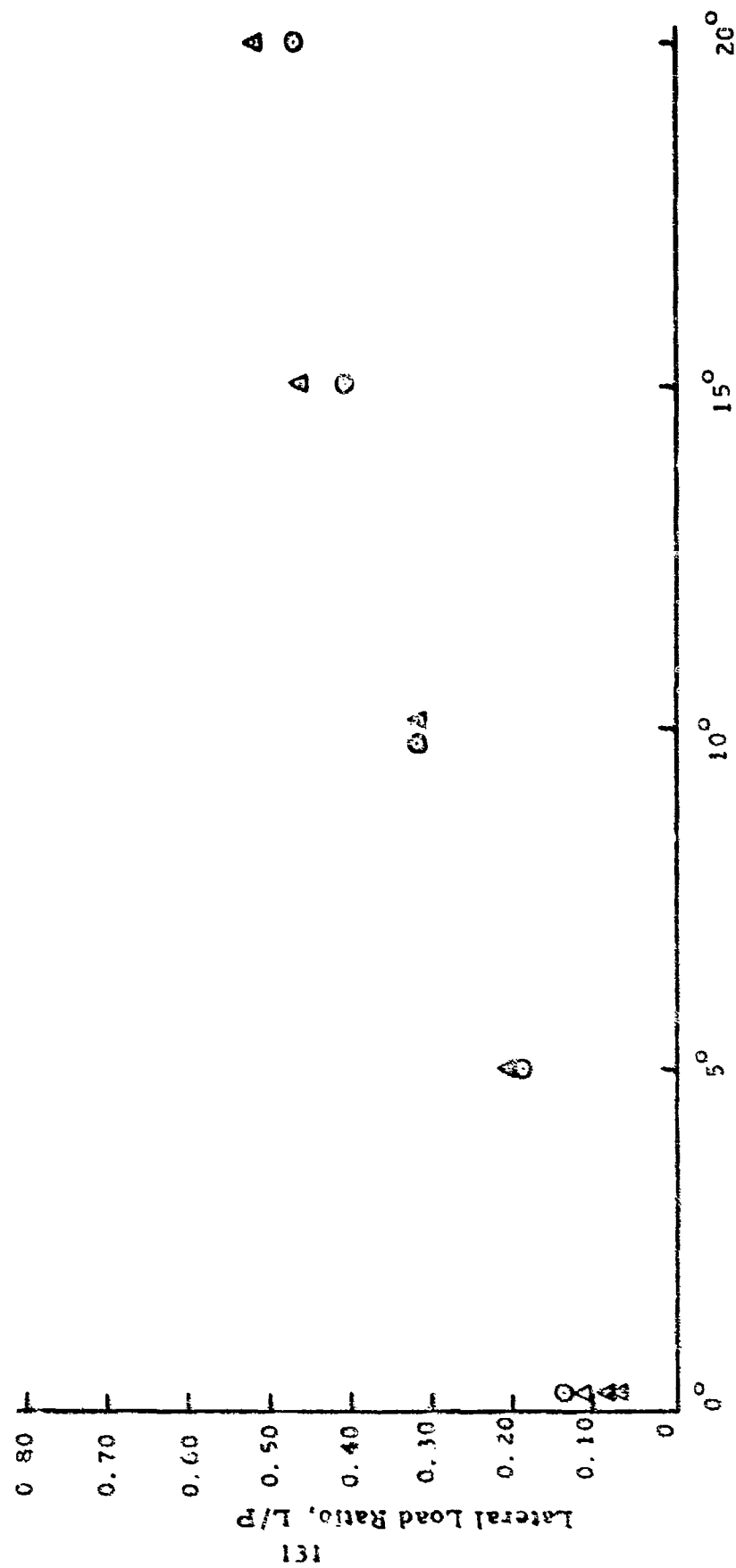
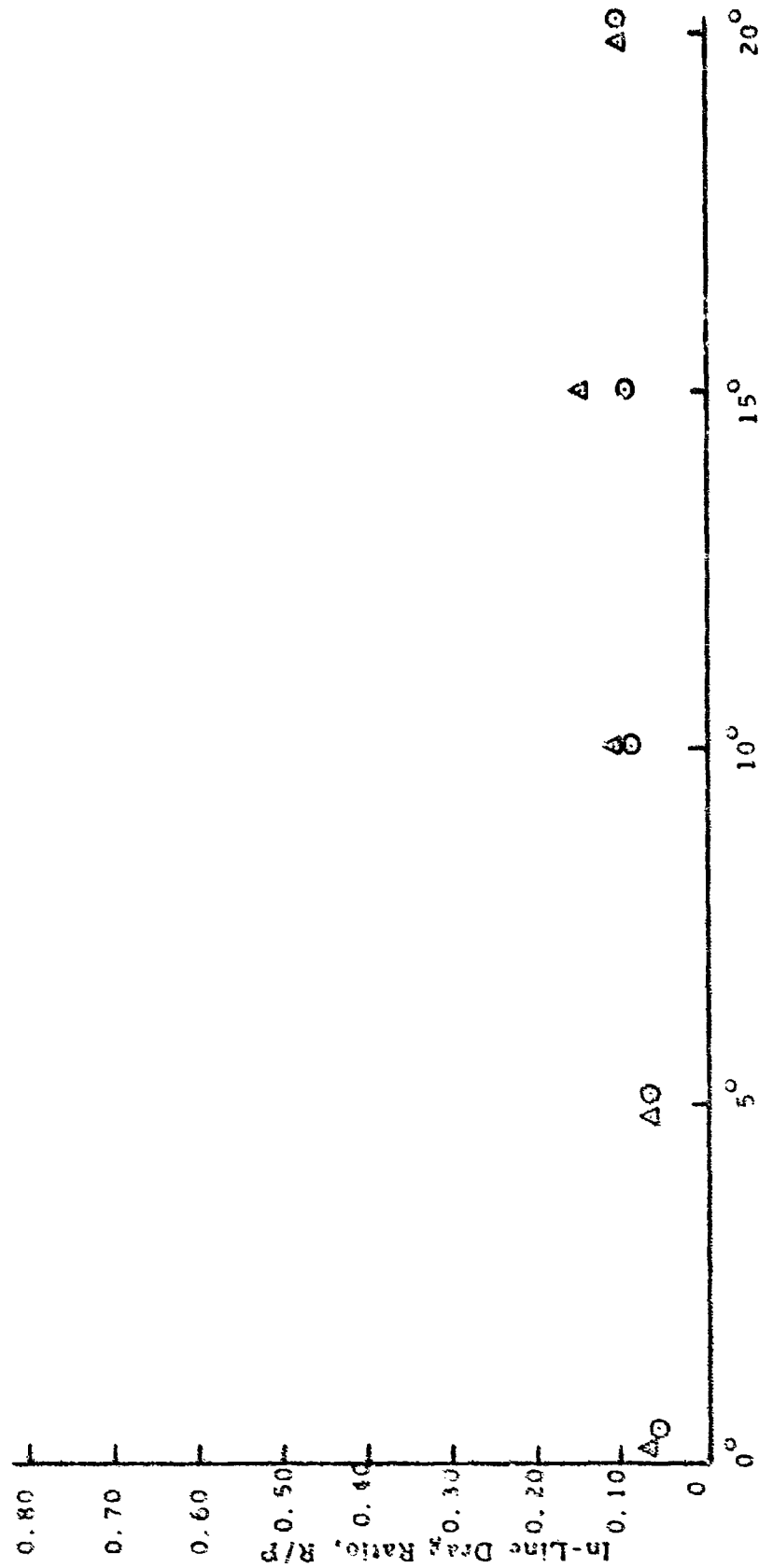


Figure 6b Lateral Load Ratio (L/P) vs. Turn Angle, 8:50-10 Tire, Clay UD (AEWES)

TURNED TIRE TEST PROGRAM (AEWES) - CLAY

Δ $d = 35\%$

\odot $d = 40\%$



Tire Turn Angle, ϕ

Figure 67. In-Line Drag Ratio (R/P) vs. Turn Angle, 7:00:6 Tire, Clay UD (AEWES)

TURNED TIRE TEST PROGRAM (AEWES) - CLAY

△ d = 25%

⊙ d = 40%

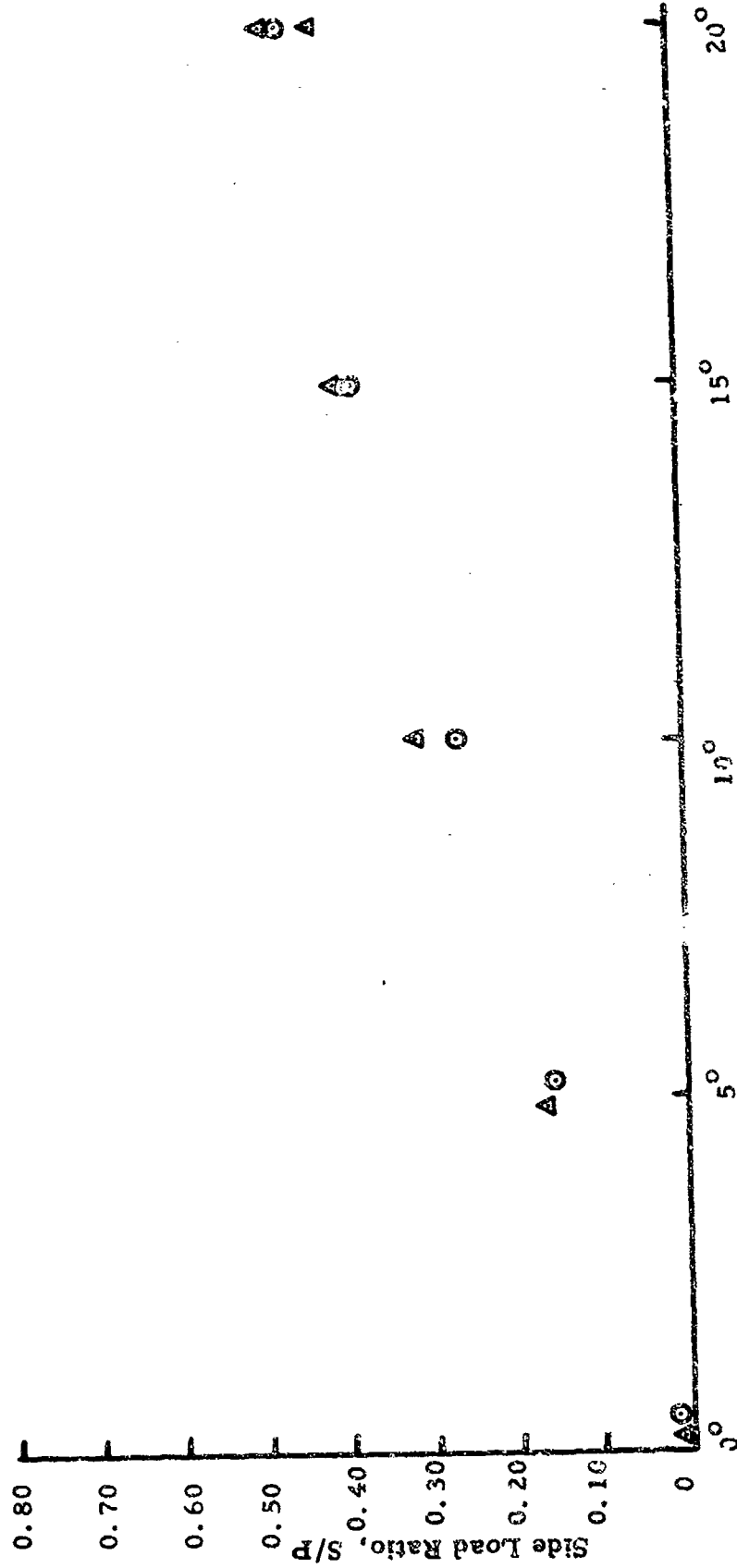


Figure 68. Side Load Ratio (S/P) vs. Turn Angle, 7:00-6 Fire, Clay UD (AEWES)

TURNED TIRE TEST PROGRAM (AEWES) - CLAY

△ d = 35%

○ d = 40%

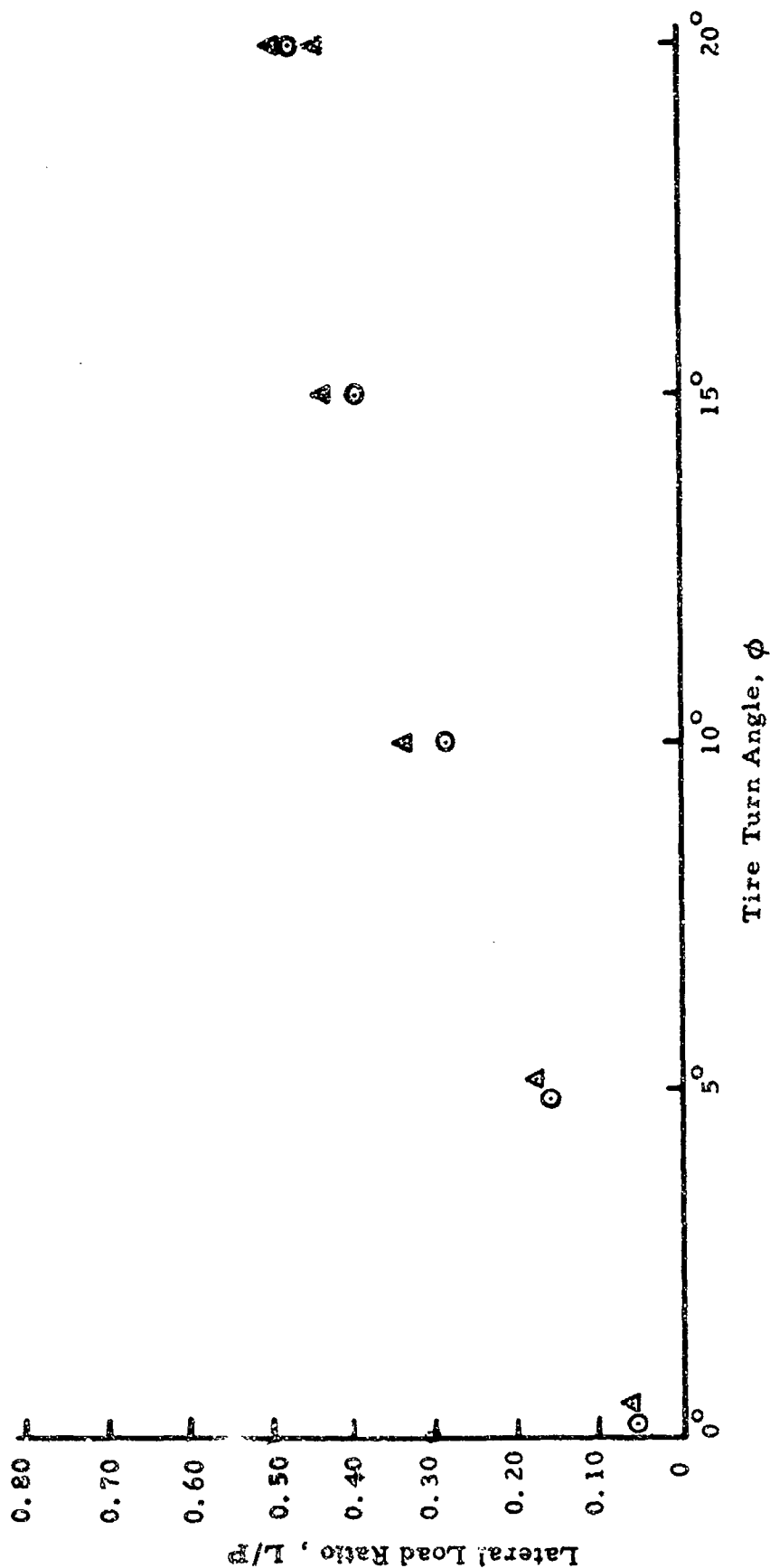


Figure 69. Lateral Load Ratio (L/P) vs. Turn Angle, 7:00-6 Tire, Clay UD (AEWES)

TURNED TIRE TEST PROGRAM (AEWES)

SAND \odot d = 35% CLAY Δ d = 35%
 \bullet d = 40% \blacktriangle d = 40%

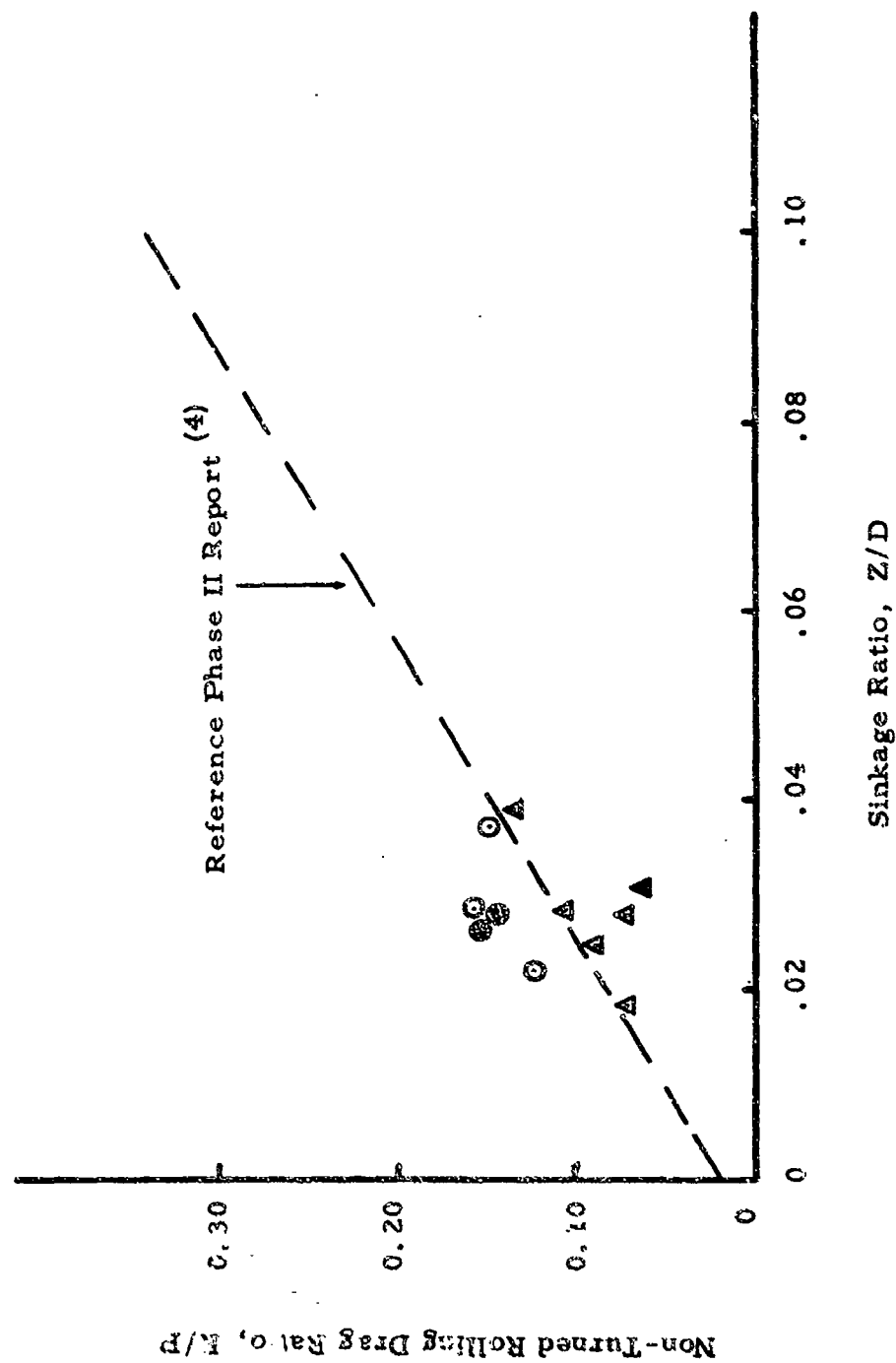


Figure 70. Drag Ratio vs. Sinkage Ratio, 0° Turned Tire Tests UD (AEWES)

APPENDIX II

AIRCRAFT TURNING OPERATION PREDICTIVE
COMPUTER PROGRAM

The "Aircraft Turning Operation Predictive Computer Program" consists of a number of subroutines which calculate the required turning variables leading to both a description of the path of turn and aircraft tire in-line drag and side loads. The program flow chart was previously given in Figure 21. Each subroutine is described below.

Subroutine FAREA and SDRAG

Subroutine FAREA calculates the tire contact area and tire footprint length from the tire input data. These two quantities are needed in the calculation of longitudinal drags. Subroutine SDRAG calculates the longitudinal drag on a tire with or without slip. It uses the load-drag relationships for nonturning single-wheel and multiwheel operation which were reported in previous reports ^(3,4).

Subroutine SIDEF

This subroutine calculates the side force from the cornering angle and the vertical tire load. An approximate relationship between side load and cornering angle was used based on the results of the test program. A fourth degree polynomial equation was fitted to the curve and incorporated into this subroutine.

Subprogram for Determining the Instantaneous Center of Turn

The conditions for determining the location of the instantaneous center of turn of the aircraft are: (a) the summation of forces, including inertia forces, transverse to the aircraft must be zero, and (b) the summation of moments, including inertia moments, about a vertical axis must be zero. These two conditions may be expressed mathematically as:

$$F(x_c, y_c) = 0 \quad (9)$$

$$G(x_c, y_c) = 0 \quad (10)$$

where x_c and y_c are the coordinates of the instantaneous center of turn and are unknowns. F and G are complicated nonlinear functions of x_c and y_c , and are represented by subroutine SUMFM, which will be discussed in the next paragraph. Equations (9) and (10) form a set of nonlinear simultaneous equations for solving x_c and y_c . The Newton-Raphson Method is used for solving the equations. It starts with a trial solution, x_{co} and y_{co} , and iterates toward the solution. The equation for the n^{th} iteration is,

$$x_n = x_{n-1} - \frac{F \frac{\partial G}{\partial y} - G \frac{\partial F}{\partial y}}{J} \quad (11)$$

$$y_n = y_{n-1} + \frac{F \frac{\partial G}{\partial x} - G \frac{\partial F}{\partial x}}{J} \quad (12)$$

where J is the Jacobian

$$J = \begin{vmatrix} \frac{\partial F}{\partial x} & \frac{\partial F}{\partial y} \\ \frac{\partial G}{\partial x} & \frac{\partial G}{\partial y} \end{vmatrix} \quad (13)$$

Subroutine SUMFM

For given x_c and y_c , this subroutine calculates the summation of transverse forces and summation of moments, i.e., $F(x_c, y_c)$ and $G(x_c, y_c)$. They may not be zero, since x_c and y_c may not be the correct

solution. It follows the steps shown below:

- (a) Calculate the cornering angles.
- (b) Calculate the centrifugal forces.
- (c) Using the drags and side forces of the preceding time increment, calculate the thrust required to maintain forward motion.
- (d) Calculate vertical loads on nose and main gears by summation of moments about the roll and pitch axes.
- (e) Calculate new drags and side forces.
- (f) Calculate angular acceleration of the aircraft about its vertical axis.
- (g) Sum transverse forces.
- (h) Sum moments about the vertical axis.

AIRCRAFT TURNING PREDICTIVE COMPUTER PROGRAM

PROGRAM SOURCE LISTING

04/25/738296TFGRS4C.TURN-----22222222222222HENRY LUMING
04/25/738296TFGRS4C.TURN 22222222222222HENRY LUMING

EXTENSION TITLE(5) ,BETA(20),S(20)

REAL L,LL,M

COMMON/ALBC/GW,CI

COMMON/DRGSF/RN,RMR,RML,SFN,SFMR,SFPL

COMMON/VELO/VO,V,AVO,AV,DI

COMMON/TIRE/DA,CP,BN,BP,VN,NI,NMI,NMI,SM,SN,SNM

COMMON/AEL/AN,AP,ELN,ELM

COMMON/CGDIS/AL,F,AVM,U,UE,E

INTEGER IN,IM

READ (5,501) TITLE

501 FORMAT (5A4)

READ (5,502) GW

READ (5,503) CI

503 FORMAT (E13.3)

CI=CI+12.

READ (5,502) CE,DEM

READ (5,502) CM,DFN,BA,AN

READ (5,502) CM,DFM,BM,NM,NMI,NMI

502 FORMAT (3F9.2,4I5)

READ (5,503) IN,IM

503 FORMAT (5I5)

READ (5,504) L,LL,F,M,U,E,SN,SNM,SM

READ (5,504) UE

504 FORMAT (10F6.2)

READ (5,505) VO,DI

505 FORMAT (F10.2,E13.4)

READ (5,506) (BETA(I),I=1,20)

READ (5,506) (S(I),I=1,20)

506 FORMAT (10F7.3)

WRITE (2,551) TITLE

551 FORMAT (1H0,'*****',5A4//)

WRITE (2,552) GW,CI,VC

WRITE (2,553) DL,DEM

WRITE (2,554) DA,DP,DFN,DFM,AN,AP,NI,NMI,NMI,IN,IM

AL=(L+LL)/2.

AVP=F-AL

GO TO 600

WRITE (2,555) L,AL,LL,F,M,AVM,L,UE,L,SN,SNM,SM

WRITE (2,556) DI

DC 2C K=1,2C

AK=K

TIME=AK*DT

2. WRITE (2,557) TIME,BETA(K),S(K)

557 FORMAT (2X,3F7.2)

500 CONTINUE

CALL FAREA (CE,DA,DFN,DA,IN,AN,FLN)

CALL FAREA (DFM,DP,DFM,BM,IP,AP,FLM)

WRITE (2,601) AN,FLN

WRITE (2,601) AM,FLM

601 FORMAT (1H0,6HAREA =,F12.5,18HFCCTPRINT-LENGTH =,F12.5)

VC=VC+1.688

V=VO

AVC=C.

I=1

ITMAX=11

PR=C+3VM/F

PR=(GM-PM)/2.

CALL SERAG (PM,VM,AN,FLN,C,DP,AN,AN,C,SN,D,AN)

CALL SERAG (PM,N1,AM,FLM,C,DM,BM,NMI,NMI,SN,SNM,XML)

RMR=RML

VFA=C.

```

WRITE (2,602) RN,RNR,RML
40 JT=C
XC1=AVP
IT=1
IF (1.GT.1) GO TO 45
B1=BETA(1)/57.29578/2.
GO TO 46
42 B1=(BETA(1)+BETA(1-1))/57.29578/2.
44 YC1=AVP*CCS(B1)/SIN(B1)
WRITE (2,558) XC1,YC1
50 XC2=1.003*XC1
YC2=1.003*YC1
X=XC2-XC1
Y=YC2-YC1
CALL SUMFM (XC1,YC1,SF11,SM11,BETA(1),S(1),1)
CALL SLPFM (XC2,YC1,SF21,SP21,BETA(1),S(1),0)
CALL SUMFM (XC1,YC2,SF12,SM12,BETA(1),S(1),0)
56 AJAC=((SF21-SF11)*(SM12-SM11)-(SF12-SF11)*(SP21-SM11))/DX/DY
XNUM=(SF11*(SF12-SM11)-SM11*(SF12-SF11))/DY
YNUM=(SF11*(SP21-SM11)-SM11*(SF21-SF11))/DX
XC3=XC1-XNUM/AJAC
YC3=YC1+YNUM/AJAC
WRITE (2,603) IT,XC1,YC1
WRITE (2,603) IT,XC3,YC3
IF (JT.EC.1) GO TO 90
CFX=ABS(2.*(XC3-XC1)/(XC3+XC1))
DFY=ABS(2.*(YC3-YC1)/(YC3+YC1))
XC1=XC3
YC1=YC3
IT=IT+1
IF ((CFX.LT.0.003.AND.DFY.LT.C.CC).OR.IT.GT.ITMAX) GO TO 80
GO TO 50
80 JT=1
GO TO 50
90 IF (1.EE.3) GO TO 100
I=I+1
AVC=AV
GO TO 40
100 STOP
END
SUBROUTINE FAREA (DE,C,DF,U,TYPE,A,FL)
INTEGER TYPE
C1=DE*(C-DF)/2CC.
FL=1.2*SCAT(D1*(C-D1))
IF (TYPE.LT.6) GO TO 15
CCFF=1.
GO TO 17
15 IF (TYPE.LT.3) GO TO 16
CCFF=C.93
GO TO 17
16 CCFF=C.94
17 FFA=2.*SCAT(C1*(B-C1))*CCFF
FPA=2.*SCAT(C1*(C-C1))
IF (TYPE.GT.1) GO TO 18
CCFF=C.85
GO TO 19
18 CCFF=C.95
19 A=C.755*FFA*FPA*CCFF
RETURN
END
SUBROUTINE SURAG (P,N,A,FL,SL,D,H,NIN,ATN,STN,STN,DRAG)
C. Determine Rolling SINKAGE
CA=B.
SML=P/CA
CP=SML/A

```

```

20=ZL*PL/D
C. DETERMINE MULTI-MEEL MODIFICATION FACTOR
IF (INT.NE.C) GC TC 10
Y1=C
GC TO 20
10 SP=STW/P
Y1A=C.354336-C.732081*SP-0.0525284*SP**2+0.397306*SP**3
Y1B=-C.405064*SP**4+C.086145*SP**5-C.0031667*SP**6
Y1=Y1A+Y1B
RT1=NT1/N
20 IF (INT.NE.C) GC TC 30
Y2=C
GC TC 40
30 SP=STW/D
Y2A=-0.19264 -C.448567*SP +C.952061 *SP**2
Y2B=-0.53968*SP**3+0.122637*SP**4-C.0098143*SP**5
Y2=Y2A+Y2B
RT1=NT1/N
40 FPM=1.-Y1*RT1-Y2*RT1
C. DETERMINE DRAG
IF (SL.GT.10) GC TC 50
RPS=D.032533+3.37572*ZD
RPM=RPS*FPM
GO TO 60
50 FPM=1.
RPS=10.*ZD+.95.*F**2*SQRT(ZD*SL/100.)/SWL
RPM=RPS*FPM
60 DRAG=RPM*P
RETURN
END
SUBROUTINE SLFPM (XC,YC,SLP,SUPP,PC,SL,JP)
COMMON/AINC/ZN,C1
COMMON/CRGSF/RN,RMR,RML,SFN,SFMR,SFML
COMMON/ZVELD/YC,V,AVC,AV,DI
COMMON/TIRE/DN,DM,BN,BM,N1,NL,NP1,SP,SN,SAM
COMMON/AFEL/AN,AM,FLN,FLM
COMMON/CGOIS/AL,F,AVP,U,UE,C
BP=BC/57.29578
PN=PP-ATAN((F-XC)/YC)
PHL=ATAN(XC/(YC+E/2.))
PMR=ATAN(XC/(YC+E/2.))
RC=SQRT((XC-AM)**2+(YC-FC)**2)
CENT=GK*V*V*12./RC/32.2
CENTY=CENT*YC/RC
CENTX=CENT*(XC-AM)/RC
CL=50.11*1.7
THRI=RPR*RML+RN*CES(BP)+SFN*SI(BP)+CENTA
PDM=THRI*E-CENTX*E
P1=(CW*AVM+PDM)/F
P2=(GK*21-EXCP)/E/2.*CENTY*U/E
PML=PMR-2.*CENTY*U/E
CALL SERAG (PN,N1,AN,FLN,C,AM,BN,BM,C,SN,D,RA1)
CALL SERAG (PMR,N1,AM,FLM,D,DM,BM,A,CL,NM1,SN,SCH,THRI)
CALL SERAG (PML,N1,AM,FLN,SL,CP,PP,RA1,NP1,SP,SMP,RML)
CALL SDEF (PMR,PN,SFN)
CALL SDEF (PDM,PMR,SFMR)
CALL SDEF (PML,PML,SFML)
SLMF=SFM+SFML+SFN*CES(BP)-CENTY-RA*SI(BP)
AV=12.*V/YC
AAC=(AX-AV)/ET
SLMF=(SFM+SFML)*AVP+(RN*SI(BP)-SFN*CES(BP))*AL+(RMR-RML)*E/2.*AAC*G1
(E,11,EC,1) GO TO 645
CSF=ABS((SLMF-SF1)*2./(SLMF+SF1))
DSF=ABS((SLMF-SM1)*2./(SLMF+SF1))
IF (DSF.LT.C.CC1.AND.DSM.LT.C.CC1) GO TO 670

```

```

      SFI=SUMM
630 CONTINUE
670 IF (JP.EC.Q.OR.IT.LE.4) GO TO 690
      WRITE (2,602) PHN,PHPR,PHPL,RC
      WRITE (2,602) CENT,CENTX,CENTY,AAC
      WRITE (2,602) RN,RMR,RML
      WRITE (2,602) SFN,SFMR,SFML
640 WRITE (2,602) II,SUMF-SUMM
640 FORMAT (1HC,12,2E13.6)
670 RETURN
      END
SUBROUTINE SIDEF (PHI,P,SF)
  PF=ABS(PH-1)*57.29576
  SA=C.123045E-01*0.447242E-01*PH-0.227065E-02*PH*PH
  SE=C.815037E-04*PH**3-0.118086E-05*PH**4
  SAB=SA+SU
  SF=P*SAB
  IF (PHI.II.0.) SF=-SF
  RETURN
  END

```

APPENDIX III

ROLLING HIGH SPEED DRAG RATIO PREDICTION TECHNIQUE AND COMPUTER PROGRAM

The computer program developed and used in conducting the high speed rolling drag ratio comparative study as given in Figures 28 through 34, is detailed below. A Fortran IV source program listing of the computer program, a list of definitions of symbols, and some remarks about running the program, and the outputs from the comparative cases are included.

Procedure for Running the Computer Program

1. Specify the first two data cards:

First Card Specify three tire parameters: (D) Tire Diameter, inches; (B) Tire Section Width, inches; (D1) Tire Deflection, inches.

Second Card Specify five parameters: (P) Vertical Load, lbs; (Z01) Initial Sinkage, in.; (CI) Cone Index, psi; (CBR) California Bearing Ratio (optional); Tire Inflation Pressure, psi (optional)

2. All input cards are to be typed in as real values with consistent units.

3. To make more than one continuous run, additional cards with the same format as data cards 1 and 2 must be inserted behind the original set of data

List of Symbols

A	= Contact area
B	= Tire section width
CBR	= California Bearing Ratio
CI	= Cone Index (average over 0" to 6" in psi)
D1	= Tire deflection, inches (rigid surface)
DELTAR	= Incremental change in rolling drag resistance due to inertia effects
DELTZI	= Incremental sinkage due to inertia
DELTZL	= Incremental sinkage due to lift

DRAG	= Rolling drag ratio (R/P) at any velocity
P	= Vertical load
PLIFT	= Hydrodynamic lift
PSI	= Tire inflation pressure
THETAO	= Initial angle of attack, θ , for Region II velocity range
THETAV	= Angle of attack, θ , at any velocity
V	= Velocity in feet per second
V1	= Velocity in knots
ZI	= Instantaneous sinkage at any velocity
ZO1	= Initial tire sinkage in Region II velocity range

Fortran IV Source Program Listing

```

PROGRAM SP      (INPUT,OUTPUT, TAPE 5= INPUT)
REAL TAB(20,7)
REAL K,M,L
DATA ((TA9(J,I),I=1,7),J=1,20)/0.,.01,.02,.03,.04,.06,.08,
AC.,.1.,.1.,.1.,.1.,.1.,.1.,
B10.,.998,.995,.99,.987,.987,.99,
C20.,.995,.99,.98,.975,.975,.985,
D30.,.992,.985,.945,.955,.967,.98,
E40.,.99,.98,.88,.90,.90,.97,
F50.,.98,.95,.86,.87,.855,.93,
G60.,.97,.92,.85,.85,.83,.87,
H70.,.965,.90,.81,.81,.79,.82,
I80.,.96,.87,.785,.785,.75,.78,
J90.,.955,.86,.76,.76,.73,.73,
K100.,.95,.85,.755,.745,.705,.68,
L110.,.945,.795,.72,.73,.682,.655,
M120.,.94,.79,.73,.71,.66,.63,
N130.,.935,.765,.72,.695,.642,.61,
O140.,.93,.77,.71,.68,.625,.59,
P150.,.925,.765,.705,.67,.612,.565,
Q160.,.92,.76,.70,.65,.60,.54,
R170.,.92,.755,.695,.63,.58,.53,
S180.,.92,.75,.69,.61,.57,.52/
99  READ (5,5) D,B,D1
5   FORMAT (3F9.3)
    READ (5,15) P,Z01,CI,CBR,PSI
15  FORMAT (5F9.3)
    PRINT 1,CBR,PSI
1   FORMAT(*1*,*CBR =*,F4.1,*      PSI =*,F5.1)
    PRINT 9
9   FORMAT(*-*,*SOIL TYPE = CLAY*)
    PRINT 2
2   FORMAT (*-*,*VELOCITY*,13X,*THETA*,13X,*DELTA Z*,13X,*DELTA Z*,13X
A,*LIFT*,13X,*DELTA R*,13X,*DRAG*)
    PRINT 3
3   FORMAT (* *,2X,*KNOTS*,15X,*DEG.* ,13X,*LIFT,IN.* ,10X,*INERTIA,IN.*
O,11X,*LBS.*14>,*LES.* ,14X,*RATIO*)
    PRINT 4
4   FORMAT (*J*,*-----
C-----
D-----)
    V=20.
    A1=Z01/D
    H=2*SQRT(D1*(O-D1))
    F=2*SQRT(O1*(B-D1))
    L=0.85*M
    A=5.74575*L*F
    X=(A1**523)/((3.93416 - (5.93297*L/D))*(L/D))
    TANX=ATAN(X)
    THETA0=TANX * 57.296
10  V=V+20
    MW=0
    ZO=Z01
    IF(V.EQ.200.) GO TO 8
    CALL SPEED (A1,V,TAB,C)

```

```

      THETA V = THETA O * C
      Y = THETA V / 57.296
      DC 60 J=1, 10
38    PLIFT = ((110/32.2) * B * Z0 * V * V * COS(Y) * SIN(Y)) / 144
      DELTAR = PLIFT * TAN(Y)
      A2 = (P - PLIFT) / A
      E1 = A2 / CI
      K = 0.23 + (0.13 * E1)
      DELTZL = (K * PLIFT * L) / (A * CI)
      DELTZI = (DELTAR * D) / (3.85 * (P - PLIFT))
      IF (M.EQ.1) GO TO 30
      IF (DELTZL.GT.DELTZI) GO TO 37
      IF (J.EQ.1) GO TO 30
      GO TO 35
37    ZC = ZC + 0.10
60    CONTINUE
30    ME = 1
      IF (DELTZL.GT.DELTZI) GO TO 35
      IF (ABS(ZC1 - ZC).EQ.1.) GO TO 35
      ZC = ZC - 0.10
      GO TO 38
35    ZI = Z0 - DELTZL + DELTZI
      DRAG = (3.85 * ZI / D) + (DELTAR / P)
      V1 = V * 0.5921
      PRINT 70, V1, THETA V, DELTZL, DELTZI, PLIFT, DELTAR, DRAG
70    FORMAT(*J*, F6.1, 15X, F5.1, 12X, F7.3, 11X, F7.2, 13X, F8.1, 9X, F9.1, 11X, F6
D.2)
      PRINT 7, Z0
7    FORMAT(* *, *FINAL Z =*, F5.2)
      GO TO 10
8    PRINT 6, THETA O
6    FORMAT(*-*, *THETA O =*, F5.1)
      GO TO 99
      END

```

```

SUBROUTINE SPEED (A1,V,TAB,C)
REAL TAB(20,7)
DC 8J I=1,20
CK=TAB(I,1)
IF(CK.EQ.V) N=I
IF(CK.EQ.V) GO TO 85
80  CONTINUE
85  IF(A1.GT.0.00) GO TO 95
    DC 9J M=2,7
    CK1=TAB(1,M)
    IF(CK1.GT.A1) N1=M-1
    IF(CK1.GT.A1) GO TO 100
90  CONTINUE
100  C=TAB(N,N1)-((TAB(N,N1)-TAB(N,N1+1))*((A1-TAB(1,N1))/(TAB(1,N1+1)
    D-TAB(1,N1))))
    GO TO 105
95  C=TAB(N,7)
105  RETURN
    END

```

Rolling-High Speed Drag Ratio Prediction - Case I

CBR = 1.5 PSI = 30.0

SCIL TYPE = CLAY

VELOCITY KNOTS	THETA DEG.	DELTA Z LIFT, IN.	DELTA Z INERTIA, IN.	LIFT LBS.	DELTA R LBS.	CRAG RATIO
23.7 FINAL Z = 1.05	21.2	.806	.09	143.7	55.7	.15
35.5 FINAL Z = 1.05	26.3	.186	.19	312.7	115.5	.16
47.4 FINAL Z = 1.35	18.8	.390	.40	568.6	227.4	.23
55.2 FINAL Z = 1.05	12.0	.454	.45	783.3	254.5	.19
71.1 FINAL Z = .85	17.3	.510	.50	883.8	275.9	.17
82.9 FINAL Z = .65	16.8	.516	.50	894.4	289.9	.14
94.7 FINAL Z = .55	16.4	.537	.53	969.2	285.6	.13
106.6 FINAL Z = .45	16.0	.562	.53	979.7	288.6	.11

THETA0 = 23.9

Rolling-High Speed Drag Ratio Prediction - Case II

CBR = 1.5 PSI = 45.0

SOIL TYPE = CLAY

VELOCITY KNOTS	THETA DEG.	DELTA Z LIFT, IN.	DELTA Z INERTIA, IN.	LIFT LOS.	DELTA R LOS.	DRAG RATG.
23.7	22.5	.131	.13	201.0	83.2	.20
FINAL Z = 1.40						
35.5	20.9	.331	.33	516.9	197.8	.27
FINAL Z = 1.70						
47.4	19.0	.562	.57	890.3	388.8	.30
FINAL Z = 1.00						
55.2	17.9	.644	.64	1037.3	334.2	.25
FINAL Z = 1.40						
71.1	16.0	.745	.73	1223.3	368.2	.23
FINAL Z = 1.20						
82.9	15.9	.802	.77	1314.8	378.7	.20
FINAL Z = 1.00						
94.7	15.3	.890	.87	1486.1	407.8	.20
FINAL Z = .90						
106.6	14.5	.956	.91	1593.4	411.6	.18
FINAL Z = .80						
THETA0 = 25.0						

Rolling-High Speed Drag Ratio Prediction - Case III

CBR = 1.5 PSI = 70.0

SOIL TYPE = CLAY

VELOCITY KNOTS	THETA DEG.	DELTA Z LIFT, IN.	DELTA Z INERTIA, IN.	LIFT LBS.	DELTA R LBS.	DRAG RATIO
23.7 FINAL Z = 2.30	24.0	.267	.27	355.3	163.9	.34
35.5 FINAL Z = 2.50	22.2	.502	.59	799.5	326.5	.40
47.4 FINAL Z = 2.20	19.9	.813	.81	1144.5	414.6	.37
59.2 FINAL Z = 2.10	17.4	1.050	1.03	1519.1	474.6	.37
71.1 FINAL Z = 1.80	16.1	1.191	1.17	1751.4	505.8	.34
82.9 FINAL Z = 1.50	15.1	1.262	1.21	1872.0	504.8	.29
94.7 FINAL Z = 1.40	13.8	1.395	1.34	2105.9	516.6	.28
106.6 FINAL Z = 1.20	13.3	1.450	1.40	2205.7	528.4	.26

THETA = 25.5

Rolling-High Speed Drag Ratio Prediction - Case V

CBR = 2.3 PSI = 45.0

SOIL TYPE = CLAY

VELOCITY KNOTS	THETA DEG.	DELTA Z LIFT, IN.	DELTA Z INERTIA, IN.	LIFT LBS.	DELTA F LBS.	DRAG RATIO
23.7 FINAL Z = .40	15.0	.010	.02	42.6	12.0	.06
35.5 FINAL Z = 1.20	15.0	.117	.12	274.1	73.4	.17
47.4 FINAL Z = 1.40	14.0	.225	.23	535.6	134.0	.21
55.2 FINAL Z = 1.10	13.6	.260	.27	640.0	155.3	.19
71.1 FINAL Z = 1.10	12.9	.362	.36	873.5	199.7	.19
82.9 FINAL Z = .90	12.5	.392	.39	949.0	211.1	.16
94.7 FINAL Z = .80	12.4	.446	.46	1008.0	230.7	.16
106.6 FINAL Z = .60	12.2	.419	.42	1019.6	220.5	.12

THETA0 = 16.0

Rolling-High Speed Drag Ratio Prediction - Case VI

CER = 2.3 PSI = 76.6

SOIL TYPE = CLAY

VELOCITY KNOTS	WETA DEG.	DELTA Z LIFT, IN.	DELTA Z INERTIA, IN.	LIFT LBS.	DELTA R LBS.	DRAG RATIO
22.7 FINAL Z = 1.25	17.5	.072	.07	145.0	46.0	.10
35.5 FINAL Z = 1.75	16.4	.210	.21	433.6	127.0	.26
47.4 FINAL Z = 1.05	15.1	.359	.36	754.1	202.3	.29
59.2 FINAL Z = 1.55	14.2	.442	.44	930.6	230.4	.25
71.1 FINAL Z = 1.45	12.9	.559	.57	1203.4	209.0	.25
82.9 FINAL Z = 1.15	12.9	.576	.57	1244.0	204.6	.21
94.7 FINAL Z = .95	12.3	.595	.57	1200.4	261.0	.18
106.6 FINAL Z = .95	11.6	.702	.69	1541.6	317.0	.19
THETA0 = 19.5						

APPENDIX IV

AFFDL/FEM APPROVED LIST OF SYMBOLS ON AIRCRAFT LANDING
GEAR/SURFACE INTERACTION COMPUTER PROGRAMS

The following list is composed of five parts. These are:

- a) Landing Gear Configuration Data
- b) Soil and Runway Data
- c) Aircraft Configuration Data
- d) Initial Conditions Data
- e) Calculated Data

The development of the several digital programs concerned with take-off/landing, turning, high speed, and multipass performance, led to the need for a group of common symbols. All programs developed are to eventually be incorporated into one master predictive program and hence it is necessary to insure compatability of terms. This will also provide a guide for further programs and avoid the use of needless multiple definitions of the same quantity. The symbols provided are not all of those used in the programs developed to date (1973), because they would be of little interest to the user. However, many have been selected as those which the reader would require for an understanding of both the test material and computer input/output data. The list shown is a first attempt at compiling a "useable" list and will require updating with future changing needs.

a) Landing Gear Configuration Data

A	Tire contact area
AL	Mean distance from aircraft center of gravity to nose gear center of gravity
AM	Main tire contact area
AN	Nose tire
AVM	Mean distance from aircraft center of gravity to main gear center of gravity
BM	Section width of main tires

BN	Section width of nose tires
B1	Distance from center of gravity of outer tire to center of gravity of inner tire for main landing gear set
CPM	Main tire contact pressure
CPN	Nose tire contact pressure
DE	Deflection of nose tires
DEM	Deflection of main tires
DFM	Flange diameter of main tires
DFN	Flange diameter of nose tires
DM	Diameter of main tires
DN	Diameter of nose tires
E	Distance from center of gravity of one main gear to center of gravity of the other main gear
F	Distance from center of gravity of nose gear to center of gravity of main gear
FLM	Footprint length of main gear tire
FLN	Footprint length of nose gear tire
L	Distance from center of gravity of nose gear to aircraft forward center of gravity
LL	Distance from center of gravity of nose gear to aircraft aft center of gravity
M	Distance from center of gravity of main gear to aircraft forward center of gravity
NM	Number of main tires

NMG	Total number of main gear units
NM1	Number of tires that are in a tandem-tracking situation - main gear
NN	Number of tires - nose gear
NN1	Number of tires that are in a twin situation - main gear
N1	Number of tires per main landing gear
SM	Spacing of twin tires - main gear
SN	Spacing of nose tires
SNM	Spacing of tandem-tracking tires - main gear
TM	Tire type of main tires
TN	Tire type of nose tires

b) Soil and Runway Data

CBR	California Bearing Ratio
CI	Cone Index
NTYP	Soil type, cohesive or noncohesive
RHOS	Soil density
RRC	Rigid surface friction coefficient
SLOPE	Runway slope

c) Aircraft Configuration Data

AW	Wing reference area
CD	Drag coefficient
CL	Lift coefficient
GW	Gross weight

K	Number of thrust-velocity values for one engine
QI	Yawing moment of inertia
U	Distance from ground level to forward center of gravity
UE	Distance from ground level to point of thrust application

d) Initial Conditions or Controlled Parameters

AO	Initial acceleration
BETA	Steering angle
DT	Time increment
S	Slip in percent
SIG	Air density ratio
SO	Initial displacement
VO	Initial velocity
VTO	Takeoff velocity

e) Calculated Data

ACRPM	Multiwheel rolling drag for main tires
ACRPN	Multiwheel rolling drag for nose tires
ACRPT	Total multiwheel aircraft rolling drag
APM	Number of aircraft passes for main tires
APN	Number of aircraft passes for nose tires
DR/G	Drag force
ESWLM	Equivalent single wheel load for main tires
ESWLN	Equivalent single wheel load for nose tires
FMA	Major axis of footprint

FMI	Minor axis of footprint
P	Vertical force
PCM	Passes per coverage main gear
PCN	Passes per coverage nose gear
PHML	Turn angle of left main gear
PHMR	Turn angle of right main gear
PHN	Turn angle of nose
PM	Total main gear force
PMR	Vertical force on right main gear
PML	Vertical force on left main gear
PN	Vertical force on nose gear
R	Drag force
RBPM	Main gear braked drag ratio
RBPM1	Main braked drag
RBPN	Nose gear braked drag ratio
RBPN1	Nose braked drag
RC	Radius of turn
RML	Drag force on left main gear
RMR	Drag force on right main gear
RN	Drag force on nose gear
RFM	Multiwheel drag ratio -main gear
RPN	Multiwheel drag ratio - nose gear
RPS	Single wheel drag ratio

RPSM	Single wheel rolling drag ratio -main gear
RPSN	Single wheel rolling drag ratio -nose gear
RPSM1	Single wheel rolling drag - main gear
RPSN1	Single wheel rolling drag - nose gear
RPT	Aircraft multiwheel drag ratio
RTN	Ratio of number of tandem tires to total number of tires per landing gear strut
RTW	Ratio of number of twin tires to total number of tires per landing gear strut
S	Slip in percent
SDRAG	Soil drag
SF	Side force
SFML	Side force on left main gear
SFMR	Side force on right main gear
SFN	Side force on nose gear
SP	Multiwheel spacing parameter
SWL	Single wheel vertical load
SWLM	Main gear single wheel load
SWLN	Nose gear single wheel load
SWLN1	Nose gear operational single wheel load
THRT	Total aircraft thrust
TSMGL	Total static main gear load
TSNGL	Total static nose gear load

V	Velocity
XC	Location of center of turn in X direction
YC	Location of center of turn in Y direction
ZD	Sinkage ratio, Z/D
ZL	Sinkage characteristic, Z/l